AD-A185 383 CONDENSATION HEAT-TRANSFER MEASUREMENTS OF REFRIGERANTS ON EXTERNALLY ENHANCED TUBES(U) NAVAL POSTGRADUATE SCHOOL MONTEREY CA D S ZEBROWSKI JUN 87 1/2

UNCLASSIFIED F/G 13/1 NL

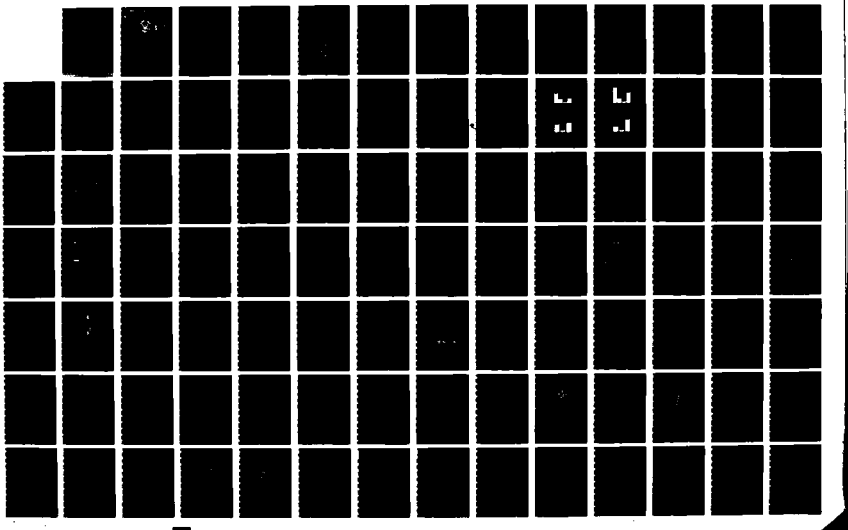

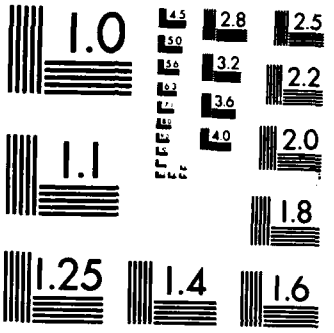

MICROCOPY RESOLUTION TEST CHART
NATIONAL BUREAU OF STANDARDS-1963-A

DTIC FILE COPY

AD-A185 383

NAVAL POSTGRADUATE SCHOOL
Monterey, California

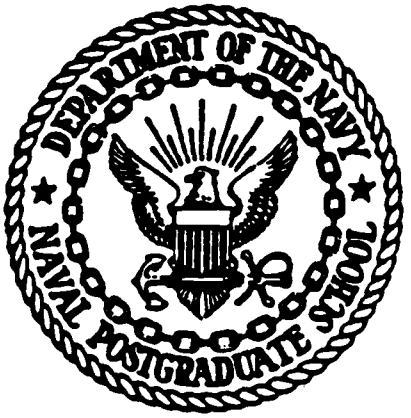

DTIC
ELECTE
OCT 2 0 1987
D

THESIS

CONDENSATION HEAT-TRANSFER MEASUREMENTS OF REFRIGERANTS ON EXTERNALLY ENHANCED TUBES

by

David Stephen Zebrowski

June 1987

Thesis Advisor — P. J. Marto
Co-Advisor — A. J. Wanniarachchi

Approved for public release; distribution is unlimited

87 10 6 187

A185 313

SECURITY CLASSIFICATION OF THIS PAGE

REPORT DOCUMENTATION PAGE

1a REPORT SECURITY CLASSIFICATION Unclassified	1b RESTRICTIVE MARKINGS
2a SECURITY CLASSIFICATION AUTHORITY	3 DISTRIBUTION/AVAILABILITY OF REPORT Approved for public release; distribution unlimited
2b DECLASSIFICATION/DOWNGRADING SCHEDULE	
4 PERFORMING ORGANIZATION REPORT NUMBER(S)	5 MONITORING ORGANIZATION REPORT NUMBER(S)
6a NAME OF PERFORMING ORGANIZATION Naval Postgraduate School 6b OFFICE SYMBOL (If applicable) 69	7a NAME OF MONITORING ORGANIZATION Naval Postgraduate School
6c ADDRESS (City, State, and ZIP Code) Monterey California 93943-5000	7b ADDRESS (City, State, and ZIP Code) Monterey, California 93943-5000
8a NAME OF FUNDING/SPONSORING ORGANIZATION DTNSRDC 8b OFFICE SYMBOL (If applicable)	9 PROCUREMENT INSTRUMENT IDENTIFICATION NUMBER
8c ADDRESS (City, State, and ZIP Code) Annapolis, Maryland 21402	10 SOURCE OF FUNDING NUMBERS PROGRAM ELEMENT NO / PROJECT NO / TASK NO / WORK UNIT ACCESSION NO

11 TITLE (Include Security Classification)
Condensation Heat-Transfer Measurements of Refrigerants on Externally Enhanced Tubes

12 PERSONAL AUTHOR(S)
Zebrowski, David Stephen

13a TYPE OF REPORT	13b TIME COVERED	14 DATE OF REPORT (Year, Month, Day)	15 PAGE COUNT
Engineers Thesis	FROM _____ TO _____	June 1987	149

16 SUPPLEMENTARY NOTATION

17 COSATI CODES			18 SUBJECT TERMS (Continue on reverse if necessary and identify by block number)
FIELD	GROUP	SUB-GROUP	R-113, Refrigerants, Condensation, Heat-Transfer Coefficient, Finned Tubes, Enhancement Ratio, Film-wise, Condensate Retention, Tube Bundle

19 ABSTRACT (Continue on reverse if necessary and identify by block number)

An apparatus was designed and fabricated for testing of a horizontal bundle of five tubes in a vertical row with R-114 as the working fluid.

Twenty-four tubes with rectangular-section fins and a smooth tube were tested in a single-tube apparatus using R-113 as the working fluid. An enhancement ratio (based on constant vapor-side temperature drop) of about 7.0 was obtained for the best-performing tube.

Among the tubes tested, the optimum fin spacing was found to be between 0.25 mm to 0.5 mm. The optimum fin thickness for tubes with a 1.0 mm fin height was found to be 0.5 mm. The vapor-side enhancement ratio increased with increasing fin height. However, the rate of increase in the vapor-side enhancement was found to be smaller with increasing fin ehight compared to the rate of area increase.

20 DISTRIBUTION/AVAILABILITY OF ABSTRACT	21 ABSTRACT SECURITY CLASSIFICATION	
☒ UNCLASSIFIED/UNLIMITED ☐ SAME AS RPT ☐ DTIC USERS	Unclassified	
22a NAME OF RESPONSIBLE INDIVIDUAL P. J. Marto	22b TELEPHONE (Include Area Code) 408-646-2586	22c OFFICE SYMBOL 69Mx

DD FORM 1473, 84 MAR 83 APR edition may be used until exhausted
All other editions are obsolete

SECURITY CLASSIFICATION OF THIS PAGE

19 Abstract (Continued)

The indirect measurement of the local condensing heat-transfer coefficient around a finned tube showed a local value at the top of each of the two tubes tested that is approximately twice the average value for the entire tube.

Approved for public release; distribution is unlimited.

Condensation Heat-Transfer Measurements of Refrigerants on Externally Enhanced Tubes

by

David Stephen Zebrowski
Lieutenant Commander, United States Navy
B.S.N.E., Purdue University, 1976

DTIC COPY INSPECTED

Submitted in partial fulfillment of the requirements for the degrees of

MASTER OF SCIENCE IN MECHANICAL ENGINEERING
and
MECHANICAL ENGINEER

from the

NAVAL POSTGRADUATE SCHOOL
June 1987

Accesion For
NTIS CRA&I
DTIC TAB
Unannounced
Justification
By
Distribution/
Availability Codes
Dist | Avail and/or Special
A-1

Author: _____
D. S. Zebrowski

Approved by: _____
P. J. Marto, Thesis Advisor

_____
A. S. Wanniarachchi, Co-Advisor

_____
A. J. Healey, Chairman,
Department of Mechanical Engineering

_____
G. E. Schacher,
Dean of Science and Engineering

ABSTRACT

An apparatus was designed and fabricated for testing of a horizontal bundle of five tubes in a vertical row with R-114 as the working fluid.

Twenty-four tubes with rectangular-section fins and a smooth tube were tested in a single-tube apparatus using R-113 as the working fluid. An enhancement ratio (based on constant vapor-side temperature drop) of about 7.0 was obtained for the best-performing tube.

Among the tubes tested, the optimum fin spacing was found to be between 0.25 mm to 0.5 mm. The optimum fin thickness for tubes with a 1.0 mm fin height was found to be 0.5 mm. The vapor-side enhancement ratio increased with increasing fin height. However, the rate of increase in the vapor-side enhancement was found to be smaller with increasing fin height compared to the rate of area increase.

The indirect measurement of the local condensing heat-transfer coefficient around a finned tube showed a local value at the top of each of the two tubes tested that is approximately twice the average value for the entire tube.

TABLE OF CONTENTS

LIST OF TABLES

LIST OF FIGURES

NOMENCLATURE

A_{ef}	Effective outside area of finned tube (eqn. 2.10) (m^2)
A_f	Actual area of finned tube (m^2)
a_f	Coefficient used in eqn. 5.5
A_o	Smooth tube outside area ($= \pi D_o L$) (m^2)
A_p	Profile area of fin (m^2)
A_r	Surface area of tube at base of fins (m^2)
a_s	Coefficient used in eqn. 5.6
A_t	Area of smooth tube (same as A_o) (m^2)
c_b	Fraction of tube surface flooded
C_i	Sieder-Tate-type coefficient used in eqn. 4.6
c_p	Specific heat of cooling water (J/kg·K)
D_{eq}	Equivalent diameter of finned tube (eqn. 2.8) (m)
D_f	Diameter of tube at tip of fins (m^2)
D_i	Inside diameter of test tube (m)
D_o	Root diameter of fin tubes or outside diameter of smooth tube (m)
e	Fin height (mm or m)
g	Acceleration due to gravity (m/s^2)
h	Condensing heat-transfer coefficient ($W/m^2 \cdot K$)
h_b	Condensing coefficient of flooded region based on A_r ($W/m^2 \cdot K$)

h_f	Condensing coefficient of fin based on A_f ($W/m^2 \cdot K$)
h_{fg}	Specific enthalpy of vaporization of R-113 (J/kg)
h_h	Condensing coefficient for plain tube based on A_o ($W/m^2 \cdot K$)
h_i	Inside heat-transfer coefficient ($W/m^2 \cdot K$)
h_o	Outside condensing heat-transfer coefficient based on A_o ($W/m^2 \cdot K$)
k_b	Thermal conductivity of cooling water at T_b ($W/m \cdot K$)
k_f	Thermal conductivity of R-113 at T_f ($W/m \cdot K$)
k_m	Thermal conductivity of tube metal ($W/m \cdot K$)
L	Length of condenser test tube (m)
L_1	Length of tube portion (not exposed to vapor) inside nylon bushing at the inlet (m)
L_2	Length of tube portion (not exposed to vapor) inside nylon bushing at the outlet (m)
LMTD	Log-mean-temperature difference (eqn. 4.5)
$\dot{m}$	Mass flow rate of cooling water (kg/s)
P	Wetted perimeter (m)
P_f	Fin pitch (m)
Pr	Prandtl Number of cooling water
Q	Heat-transfer rate (W)
q	Heat flux (W/m^2)
q_f	Heat flux of finned tube based on A_o (W/m^2)
q_s	Heat flux of smooth tube based on A_o (W/m^2)

Re	Cooling water-side Reynolds Number
Re_f	Reynolds Number of condensate film
r_t	Radius of tube to tip of fin (m)
R_w	Tube-wall thermal resistance (eqn. 4.2)
s	Fin spacing (mm or m)
S_m	Length of convex surface over $0<\theta<\theta_m$ (m)
s_t	Fin spacing at tip of fin (m)
t	Fin thickness (mm or m)
T_b	Bulk mean temperature of cooling water (K)
t_b	Fin thickness at base (m)
T_{ci}	Cooling water inlet temperature (K)
T_{co}	Cooling water outlet temperature (K)
T_f	Film temperature of liquid R-113 $\left(=\frac{T_{sat}}{3}+\frac{2}{3}T_{wo}\right)$ (K)
T_{sat}	Saturation temperature of the R-113 at system pressure
T_{wo}	Outside average wall temperature (K)
U_o	Overall heat-transfer coefficient based on smooth tube outside area ($m^2 \cdot K/W$)
μ_b	Dynamic viscosity of cooling water at T_b ($N \cdot s/m^2$)
μ_f	Dynamic viscosity of liquid R-113 at T_f ($N \cdot s/m^2$)
μ_w	Dynamic viscosity of cooling water at inside wall temperature ($N \cdot s/m^2$)
β	Fin tip half angle

ψ	Condensate retention angle; i.e., angle measured from the bottom of the tube to the position at which the condensate first fills the interfin space
ϕ	Insulated half angle
ΔT	Average temperature drop across the condensate film ($= T_{sat} - T_{wo}$) (K)
ΔT_{cw}	Temperature rise of cooling water across test tube ($= T_{co} - T_{ci}$) (K)
ϵ_q	Enhancement ratio based on constant q (eqn. 5.8)
$\epsilon_{\Delta T}$	Enhancement ratio based on constant ΔT (eqn. 5.12)
ρ_f	Density of condensate at T_f (kg/m^3)
θ	Insulated angle
θ_m	Rotation angle of normal to fin surface
σ_f	Surface tension of condensate (N/m)
α	Nusselt-type coefficient used in eqn. 4.8
ζ	Parameter in eqn, 2.14
η	Surface efficiency
η_1	Fin efficiency of the portion of the tube L_1
η_2	Fin efficiency of the portion of the tube L_2
η_f	Fin efficiency

ACKNOWLEDGEMENTS

The author would like to express his appreciation to Professor P. J. Marto and Professor A. S. Wanniarachchi for their guidance and support in completing this work. The author would also like to express his thanks to Mr. T. McCord and his machine shop for their invaluable help in manufacturing the tube bundle apparatus.

Lastly, the author would like to express his thanks to his family and friends.

I. INTRODUCTION

A. BACKGROUND

The U.S. Navy has a continued interest in reducing the size and weight of various components on board its vessels. The Navy is carrying out research in many different areas to achieve this goal. For example, the David Taylor Naval Ship Research and Development Center, in collaboration with the Naval Postgraduate School (NPS), has been engaged in a research program that will contribute to achieving the Navy's goal by reducing the size and weight of refrigeration systems on board naval vessels. This thesis effort concentrates on one component of these air-conditioning systems: the condenser.

Condenser designers must deal with a large number of design variables, such as the tube diameter, tube pitch, number of tubes, tube length, cooling water velocity, external fin density, internal enhancement, tube material, etc.. While all of these parameters must be considered in arriving at the optimum design (i.e., minimum size and weight), the tube material seems to be the one single parameter that has the largest influence. For example, if copper-nickel tubes are replaced with titanium tubes, a significant saving in weight can be realized. The advantages offered by titanium over copper-nickel are: (1) it has a higher strength-to-weight ratio, thus requiring a smaller wall thickness,

and (2) it is less susceptible to erosion and corrosion, thus enabling the use of higher water velocities through the tubes. Notice that these features lead to smaller and lighter condenser designs. On the other hand, titanium has three disadvantages: (1) it has a thermal conductivity that is three times lower than that of copper-nickel, (2) titanium is relatively more costly than copper-nickel, and (3) titanium is more susceptible to bio-fouling than Cu-Ni.

While industry mainly uses R-11 and R-22 as the working fluids for large refrigeration systems, the Navy has been using R-114 as the working fluid for air-conditioning systems, requiring a cooling capacity of 100 tons or more on board its vessels. The Navy's decision to use R-114 over other refrigerants has been based on the following major advantages offered by this refrigerant: (1) it is a moderate-pressure refrigerant, (2) it is more stable with temperature, (3) it is more stable when exposed to water vapor, and (4) it belongs to the group of refrigerants with the least toxicity [Ref. 1].

The Navy has achieved significant success in reducing the size and weight of its air-conditioning and refrigeration (AC&R) systems. For example, such units being developed for the DDG-51 class ships are approximately 25% smaller in size and weight than similar units such as those on the CG-47 class ships. This reduction was achieved primarily by using titanium tubes with enhanced heat-transfer surfaces in the refrigerant condenser and evaporator on the DDG-51. The design and operating parameters, together with some computed

parameters, for the CG-47 and DDG-51 condensers are listed in Tables 1.1 and 1.2, respectively. Since almost all parameters are different between these two units, a direct comparison of the size and weight is not desirable. Therefore, the ratios U_oA_o/M (i.e., the overall thermal conductance per unit mass of tube material) and U_oA_o/V (i.e., the overall thermal conductance per unit volume of condenser shell) have been listed in Tables 1.1 and 1.2 to enable a more meaningful comparison. Based on these numbers, the DDG-51 condenser represents no reduction in size but a 70% reduction in weight of tubes when compared to the CG-47 condenser.

Figures 1.1 and 1.2 show a comparison of inside, wall and outside resistances on absolute and relative bases, respectively, for the CG-47 condenser. Figures 1.3 and 1.4 show similar comparisons for the DDG-51 condenser. Comparing Figures 1.1 and 1.3, it is seen that the total thermal resistance has increased in the DDG-51 condenser. As mentioned above, there are many design variables involved in a condenser design. The increase in thermal resistance in this case is overcome by changes in the operating conditions. Notice that, however, in both condensers, the outside represents the dominant thermal resistance: 50 percent and 67 percent for the CG-47 and DDG-51 condensers, respectively. Therefore, any successful attempt at decreasing the outside thermal resistance is highly desirable and will result in further reducing the size and weight of condensers in future designs.

TABLE 1.1
DESIGN, OPERATING, AND COMPUTED PARAMETERS
FOR CG-47 CONDENSER

Design Parameters [Ref. 2]	
Tube material	90-10 Cu-Ni
Fin density	748 fins/m
Tube inside diameter	15.9 mm
Tube outside diameter	19.0 mm
Tube wall thickness	1.24 mm
Tube length	3.61 m
Number of tubes per pass	147
Number of passes	2
Operating Parameters [Ref. 2]	
Cooling water inlet temperature	31.1 °C
Cooling water outlet temperature	37.1 °C
Saturation temperature	40.6 °C
Cooling water flow rate	38.75 kg/s
Computed Parameters	
Total cooling load	906 kW
Total outside surface area	207 m^2
Cooling water velocity	1.80 m/s
Overall thermal conductance (U_oA_o)	151 kW/K
Mass of tubes (M)	993 kg
Condenser volume (V)	1.14 m^3
U_oA_o/M	0.152 kW/K·kg
U_oA_o/V	132 kW/K·m^3

TABLE 1.2
DESIGN, OPERATING, AND COMPUTED PARAMETERS
FOR DDG-51 CONDENSER

Design Parameters [Ref. 2]	
Tube material	Titanium
Fin density	1026 fins/m
Tube inside diameter	12.7 mm
Tube outside diameter	13.5 mm
Tube wall thickness	0.71 mm
Tube length	2.56 m
Number of tubes per pass	165
Number of passes	2
Operating Parameters [Ref. 2]	
Cooling water inlet temperature	31.1 °C
Cooling water outlet temperature	35.2 °C
Saturation temperature	42.1 °C
Cooling water flow rate	51.75 kg/s
Computed Parameters	
Total cooling load	826 kW
Total outside surface area	106 m^2
Cooling water velocity	2.41 m/s
Overall thermal conductance (U_oA_o)	93.7 kW/K
Mass of tubes (M)	186 kg
Condenser volume (V)	0.722 m^3
U_oA_o/M	0.504 kW/K·kg
U_oA_o/V	130 kW/K·m^3

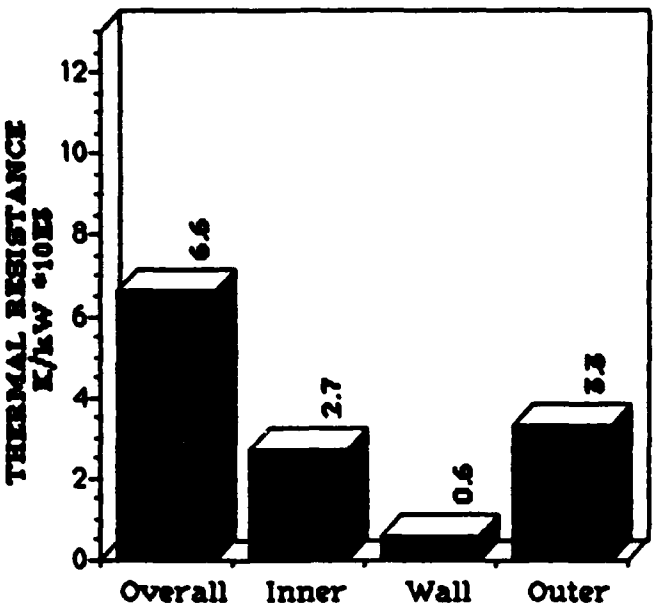

Figure 1.1 Comparison of Inside, Wall, and Outside Thermal Resistances for CG-47 Condenser.

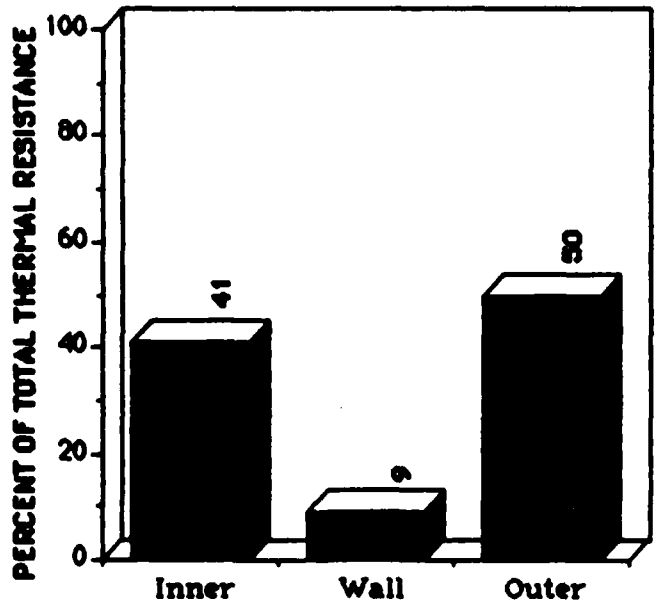

Figure 1.2 Relative Thermal Resistances for CG-47 Condenser.

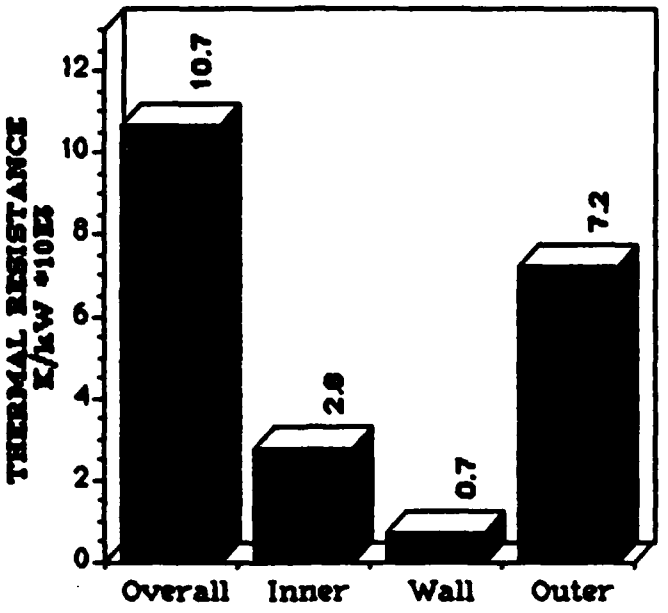

Figure 1.3 Comparison of Inside, Wall, and Outside Thermal Resistances for DDG-51 Condenser.

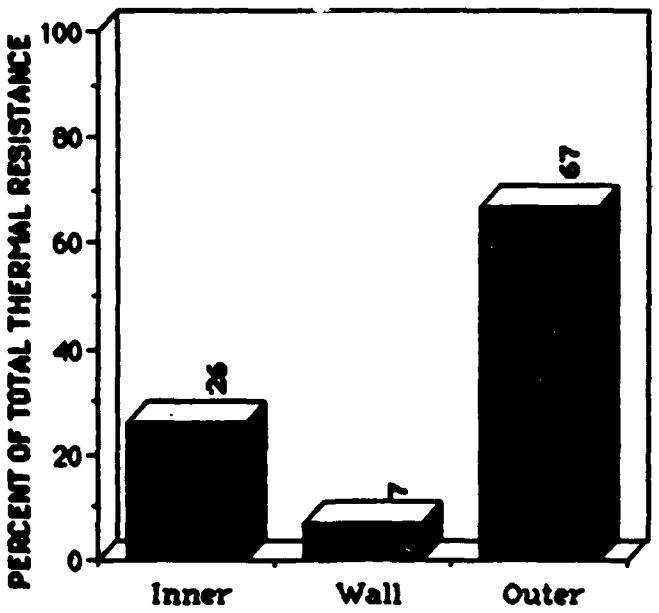

Figure 1.4 Relative Thermal Resistances for DDG-51 Condenser.

Film condensation on finned tubes is an extremely complex process. In fact, as it will be discussed in Chapter II, theoretical prediction of the condensing heat-transfer coefficient on externally finned tubes in a bundle still cannot be achieved with sufficient reliability despite the availability of about ten theoretical models. For this reason, it is imperative to perform careful heat-transfer measurements covering the important design and operating parameters. In fact, a large pool of reliable data, systematically covering relevant parameters (for example, the fin dimensions such as fin spacing, thickness, and height), would be extremely important in verifying theoretical models or in developing a successful empirical correlation.

B. OBJECTIVES

Based on the foregoing discussion, the major objectives of this thesis are:

1. Design, build, and operate an apparatus for the testing of a condenser tube bundle with up to five tubes in a vertical row using R-114 as the working fluid.[1]

---

[1]Initially, the primary objective of this study was to test a five-tube bundle of smooth and externally enhanced (such as finned) tubes in an attempt to obtain the best performing tubes for the conditions of the Navy's interest. For example, the testing of titanium finned tubes was essential. Unfortunately, owing to considerable delays experienced in receiving funding for this project and further delays with the installation of a large refrigeration unit, it was not possible to complete this objective. Therefore, two new objectives were added to provide supplementary information toward the primary goal. Notice that the tubes discussed in the second and third objectives are made of copper and no titanium tubes were available for testing on the single-tube apparatus.

2. Using a single-tube apparatus, with R-113 as the working fluid, test a series of 24 finned tubes with rectangular-section fins and a smooth tube in an attempt to obtain the optimum fin dimensions through a systematic study of these dimensions.

3. Make indirect measurements of the local heat-transfer coefficient around the periphery of two finned tubes with rectangular-section fins in an attempt to study the complex mechanisms involved during condensation on finned tubes.

II. LITERATURE SURVEY

A. GENERAL OBSERVATIONS

Condensation is the process by which a vapor is converted to a liquid by removing the latent heat of condensation from the vapor. The most common mode of condensation is filmwise in which individual drops of condensate coalesce to form a stable, continuous film on the cooled heat-transfer surface. This condensate film adds an additional thermal resistance to the heat-transfer process. As the thickness of the condensate film increases, the thermal resistance increases. When a vapor condenses on a smooth horizontal tube, this condensate film is relatively thin at the top when compared to other locations on the tube. The further from the top of the tube, the thicker the condensate film becomes and thus the thermal resistance increases. It is the thermal resistance of the condensate film that limits the heat-transfer performance of the tube. Therefore, to enhance the heat-transfer characteristics of a tube, it is necessary to reduce the condensate film thickness. For horizontal tubes, thinning of the condensate film may be achieved by using finned surfaces, drainage strips, or other enhanced heat-transfer surfaces, such as wire-wrapped tubes or roped tubes.

When examining a finned tube during condensation, there exist two regions: a flooded region and an unflooded region. The flow of condensate between the fins depends on the ratio of surface

tension forces to gravitational forces. The effect of surface tension on the behavior of the condensate is twofold. The first effect is a reduction of the condensate film thickness on the fin flanks in the unflooded region of the tube, which leads to enhanced heat transfer. In this region, the condensate on the fin surface is driven by the combined effects of surface tension and gravitational forces into the fin root where it is drained by gravity. The second effect is the retention of condensate between the fins on the lower, flooded portion of the tube, which leads to a decrease in the effective heat-transfer area and thus reduced heat transfer.

The flooded portion of a finned tube is defined by the retention angle (ψ) (i.e., the angle from the bottom of the tube to the highest position on the tube where the interfin space is filled with condensate as shown schematically in Figure 2.1). Decreasing the retention angle increases the heat-transfer performance. Therefore, any means of reducing the retention angle is beneficial.

B. EXPERIMENTAL STUDIES

1. Condensate Retention Angle

Measurements of the condensate retention angle, ψ, were first made in 1946 by Katz et al. [Ref. 3]. These measurements were made for water, aniline, acetone, and carbon tetrachloride under static conditions (i.e., no condensation taking place) on tubes with fin densities ranging from 276 to 984 fins/m and fin heights of 1.2 to 5.7 mm. It was shown that condensate retention depended

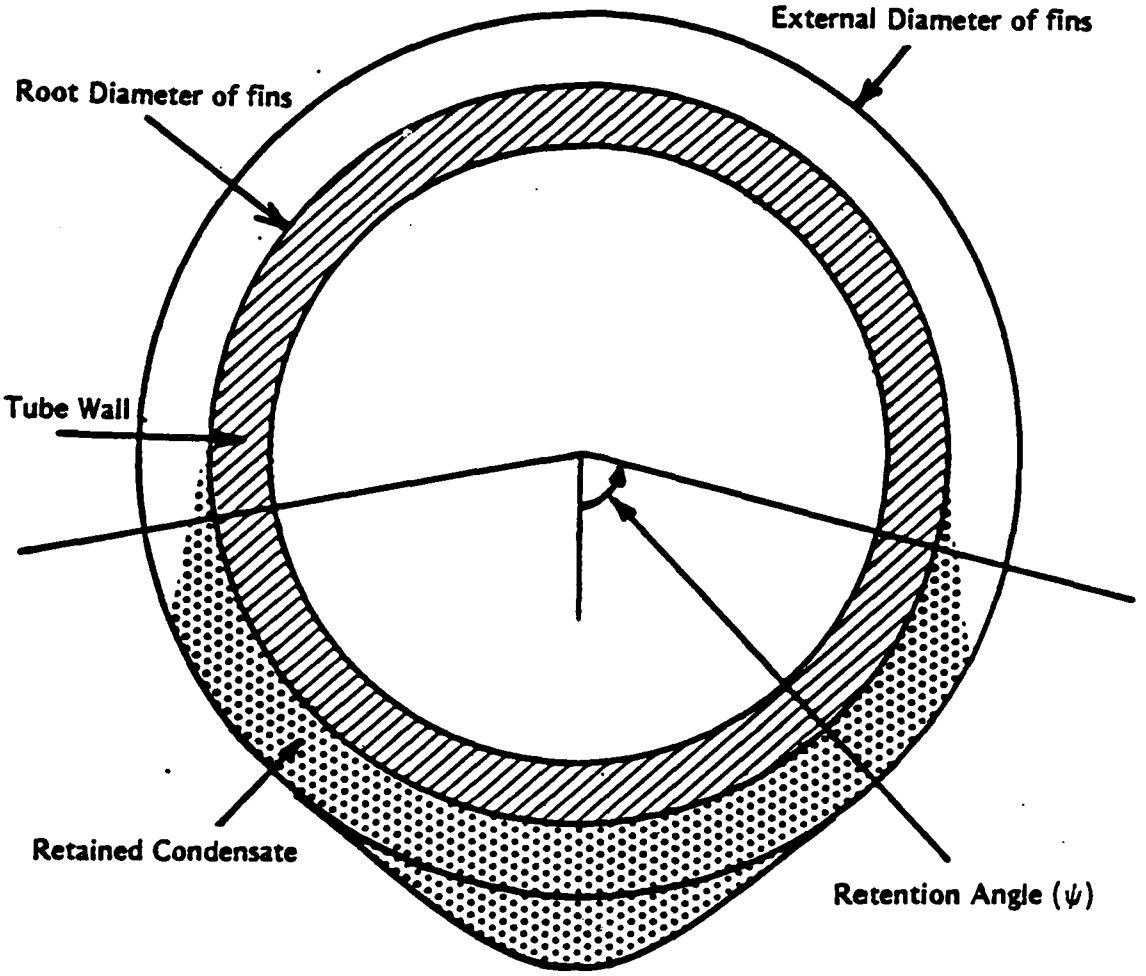

Figure 2.1 Schematic of Condensate Retention Angle on a Finned Tube.

mainly on the ratio of surface tension to liquid density and on the fin spacing. In some circumstances, condensate could completely flood the tubes.

More recently, measurements of the condensate retention angle have been made for both static and dynamic conditions. In 1981, Rudy and Webb [Ref. 4] made measurements of condensate retention angles on finned tubes with three different fin densities (748, 1024, 1378 fins/m) for water, R-11, and n-pentane under static conditions and for R-11 and n-pentane under condensing conditions. Their results showed that the retention angle increases with an increase in the ratio of surface tension to density (σ_f/ρ_f). It was further concluded that the retention angle did not differ significantly between the static and dynamic conditions for integral-finned tubes. Honda et al. [Ref. 5], in 1983, reported measurements on finned tubes with ethanol and R-113 for both static and condensing conditions and found essentially the same results. The use of porous drainage strips significantly reduced the retention angle, and, again, there was little difference between static and dynamic tests. Yau et al. [Ref. 6] also made measurements under static conditions for a range of fin densities using water, ethylene glycol, and R-113. They used an apparatus to simulate condensation on finned tubes with and without drainage strips. They concluded that a drainage strip attached edgewise to the bottom of the tube can significantly reduce the condensate retention angle.

2. Heat-Transfer Measurements

Beatty and Katz, [Ref. 7], in 1948, performed experimental measurements of the heat-transfer enhancement of finned tubes for various test fluids (methyl chloride, sulfur dioxide, R-22, propane, and n-pentane) on a 15.9 mm diameter copper tube having 630 fins per meter, and for R-22 for copper tubes of various other fin geometries and on a nickel tube. They reported enhancements in the overall heat-transfer coefficient of up to 2.3 over that of the smooth tube for R-22. A direct comparison of the enhancement in the outside heat-transfer coefficient was not made.

In 1971, Palen et al. [Ref. 8] measured the overall heat-transfer coefficients for steam condensing on spirally grooved tubes with a deep groove configuration in a baffled multi-tube shell-and-tube condenser and compared the results to those for a smooth tube. The tube tested had a groove depth of 4.8 mm deep, a pitch length of 57 mm with four groove starts. It should be noted that enhancements were obtained on both sides of this tube. An increase in the overall heat-transfer coefficient of 2.2 was obtained after correcting for tube wall thickness. A Wilson plot technique was used to separate shell-side and tube-side film coefficients. The enhancement in the condensing heat-transfer coefficient was 120 percent over the corresponding smooth tube.

Karkhu and Borovkov [Ref. 9], in 1971, performed experiments by condensing steam and R-113 on four different tubes with trapezoidal fins. They reported heat-transfer coefficients 50 to

100 percent higher than for a smooth tube. Unfortunately, they did not report enhancement separately for these two fluids. In 1980, Carnavos [Ref. 10] tested a wide variety of finned tubes using R-11 and obtained improvements in the heat-transfer coefficient up to 5 times that of a smooth tube. Honda et al. [Ref. 5], in 1983, tested four low-fin tubes with different fin geometries using methanol and R-113. Enhancements (based on constant ΔT) of the vapor-side coefficient of 6 for methanol and 9 for R-113 were obtained. In 1984, Yau et al. [Ref. 6] tested thirteen tubes with rectangular-section fins, where the only variable was fin spacing. An enhancement based on constant ΔT of 4 was obtained for steam condensing at atmospheric pressure.

During the past four years, a wide variety of data has been obtained at the Naval Postgraduate School (NPS) by Poole [Ref. 11], Georgiadis [Ref. 12], Flook [Ref. 13], and Mitrou [Ref. 14] for filmwise condensation of steam on horizontal finned tubes of rectangular cross-section. Tests were run at both 85 mmHg and atmospheric pressure on these tubes. The results showed optimum enhancement for a fin spacing of 1.5 mm for both pressure conditions. Also, the optimum fin thickness was found to be from 0.75 mm to 1.0 mm. Further, the enhancement increased with increasing fin height, but the rate of increase was smaller than the rate of area increase with fin height values greater than 1.0 mm. Thus, a value of 1.0 mm was found to be an economical fin height.

In 1985, Masuda and Rose [Ref. 15] made measurements of the condensing coefficient of R-113 on rectangular-section fins with a height of 1.59 mm and a thickness of 0.5 mm. Fourteen fin spacings between 0.25 mm and 20 mm were used. They obtained a maximum enhancement of 7.3 (at constant ΔT) at a fin spacing of 0.5 mm.

Union Carbide [Ref. 16], in 1982, reported that test data for single tube tests of steam, ammonia, R-12, and propylene condensing on wire-wrapped tubes of aluminum, copper-nickel, and copper generally showed condensing performance that was 2 to 3 times better than a bare tube. In 1984, Marto and Wanniarachchi [Ref. 17] reported data for the condensation of steam at near atmospheric pressure on smooth tubes and roped tubes with and without a helical, external wrap of a 1.5-mm-diameter titanium wire. Measurements were made on five tubes arranged vertically to simulate a tube bundle. A perforated tube above the test section simulated a tube bundle of up to 25 additional tubes above the tubes under test. It was estimated that increases in the average condensing heat-transfer coefficient for tube bundles of 50 percent (over that for the smooth tubes) can be achieved by wire wrapping of condenser tubes. Sethumadhavan and Rao [Ref. 18], in 1985, condensed steam on one smooth tube and nine spirally wire-wrapped horizontal tubes having varying pitch of the wire-wrap and various wire diameters. Enhancements in the condensing film coefficient for steam ranged from 10 to 45 percent. They reported

that the maximum improvement was achieved when 21% of the tube surface was covered by wire.

C. THEORETICAL MODELS

1. Condensate Retention Angle

The first model for the condensate retention angle was presented in 1946 by Katz et al. [Ref. 3]. The retention angle was given by:

$$\frac{\psi}{\sin\psi} = C\,\frac{\sigma_f}{\rho_f}\left[\frac{(4D_f - 2D_o + 2s)}{\frac{\pi}{4}(D_f^2 - D_o^2)t}\,\frac{180}{980}\right] = C\,\frac{\sigma_f}{\rho_f} \quad , \qquad (2.1)$$

where C is a function of the tube dimensions only. It was shown that condensate retention depends mainly on the ratio of surface tension to liquid density for any given tube.

In 1982, Rifert [Ref. 19], using a model of the capillary rise height of a fluid on a vertical plate, reported the following equation for the retention angle:

$$\psi = \cos^{-1}\left[1 - \frac{2\sigma_f(P - P_f)}{\rho_f g D_o A_p}\right] \qquad (2.2)$$

Rudy and Webb [Ref. 20], in 1983, developed a theoretical model for condensate retention on tubes with rectangular fins, based on capillary equations for condensate rise of a liquid in a vertical U-shaped channel. The expression they developed was

$$\psi = \cos^{-1}\left[1-\frac{2\sigma_f(2e-t)}{\rho_f g e s r_t}\right] \quad . \tag{2.3}$$

The model did not take into account vapor shear or condensate loading. They were able to predict measured condensate retention angles within ± 10 percent of their previous experimental work. The model showed that the important parameters that determined the condensate retention angle were the fin density and the surface tension to density ratio of the condensate. As either the fin density or surface tension to density ratio increase, the condensate retention angle increases. The fin height was shown to play a secondary role.

Also, in 1983, Honda et al. [Ref. 5] presented a theory for the condensate retention angle. Their experimental work suggested that the meniscus profile in the flooded region of the tube was determined primarily by a balance of surface tension and body forces acting on the condensate. In their model, they assumed that the meniscus went from fin tip to fin tip. The final form for the retention angle was given by:

$$\psi = \cos^{-1}\left[1-\frac{2\sigma_f \cos\beta}{\rho_f g s_t r_t}\right] \quad . \tag{2.4}$$

They obtained good agreement with their own experimental measurements and those of Rudy and Webb [Ref. 4].

In 1985, Rudy and Webb [Ref. 21] modified their earlier model for predicting the condensate retention angle (eqn. 2.3) [Ref. 20] to allow for fins of arbitrary shape. As in their previous model, this model was based on capillary rise in a vertical U-shaped channel. The effects of vapor shear and condensate loading were not considered. The following equation was recommended to predict the condensate retention angle:

$$\psi = \cos^{-1}\left[1 - \frac{2\sigma_f(P-t_b)}{D_f \rho_f g (P_f e - A_p)}\right] \quad . \qquad (2.5)$$

Notice that this equation reduces to equation 2.4 for tubes with rectangular-section fins.

Masuda and Rose [Ref. 22], in 1985, considered four separate "flooding" conditions. These different conditions were based by the actual meniscus profile at various locations around the tube. The cases identified were: when the interfin space is just filled by the meniscus but the fin flanks are not fully wetted, when the fin flanks are fully wetted but the interfin space is not, when the entire interfin space is just wet and the contact angle of the meniscus at the fin tip is non-zero, and when the flanks of the fins are just wetted with a finite film thickness at the center of the interfin space. Separate expressions were developed for each of these conditions. The last condition given is that which corresponds to the condensate retention angle. The retention angle is then given by:

$$\cos \psi = \frac{2\sigma_f}{\rho_f g s t r_t} \cos \beta - 1 \quad . \tag{2.6}$$

2. Heat-Transfer Models

The most widely used model for condensation on horizontal finned tubes is that developed by Beatty and Katz [Ref. 7]. Their model, a Nusselt-type equation based on the equivalent diameter of the finned tube, gives the average condensing coefficient by the following equation:

$$h_{BK} = 0.689 \left[\frac{k_f^3 \rho_f^2 g h_{fg}}{\mu_f}\right]^{1/4} \left[\frac{1}{\Delta T}\right]^{1/4} \left[\frac{1}{D_{eq}}\right]^{1/4} , \tag{2.7}$$

where

$$\left[\frac{1}{D_{eq}}\right]^{1/4} = 1.30\, \eta_f \frac{A_f}{A_{ef}} \frac{1}{\bar{L}^{1/4}} + \frac{A_o}{A_{ef}} \frac{1}{D_o^{1/4}} , \tag{2.8}$$

$$\bar{L} = \frac{\pi \left[D_f^2 - D_o^2\right]}{4 D_f} , \text{ and} \tag{2.9}$$

$$A_{ef} = A_o + \eta_f A_f \quad . \tag{2.10}$$

The model assumed gravity-dependent flow and did not take into account surface tension or the effects of condensate retention. The leading coefficient of the Nusselt equation was modified to fit their experimental data. The equivalent diameter, D_{eq}, accounts for the

fin efficiency and includes the term $\bar{L}$ which is the mean effective height of the fins. The resulting equivalent diameter is smaller than the smooth tube diameter. As the fin density increases, the predicted heat-transfer coefficient increases faster than the area ratio of the finned tube to the smooth tube. This is a direct result of the smaller equivalent diameter. They reported a maximum error of +7.2 percent and -10.2 percent with their experimental data for low-surface-tension fluids. The model tends to overpredict the heat-transfer coefficient as surface tension or fin density increases.

In 1954, Gregorig [Ref. 23] noted that surface tension effects can lead to large pressure gradients in the condensate film. These pressure gradients can be many times larger than those due to gravity alone. The result is to accelerate the condensate flow and therefore thin the condensate film giving larger heat-transfer coefficients.

Karkhu and Borovkov [Ref. 9], in 1971, developed a model for the condensing coefficient of steam on horizontal tubes with fins of trapezoidal cross section. Their analysis assumed: the thin condensate film on the fin is a laminar boundary layer with the pressure gradient due to surface tension only, the motion of the condensate is laminar and is produced by gravity, condensation in the condensate-filled space can be neglected, and the fin temperature is constant over its entire height. The final expression they obtained for the average condensing coefficient was related to the condensate flow rate.

In 1981, Rudy and Webb [Ref. 4] proposed correcting the Beatty and Katz model to account for flooding. They assumed that the flooded portion of the tube was ineffective. Therefore, they multiplied the heat-transfer coefficient predicted by the Beatty and Katz correlation [Ref. 7] (eqn. 2.7) by the ratio of the unflooded area of the tube to the total area, as shown below:

$$h_{BK}^{*} = h_{BK}\left[\frac{\pi-\psi}{\pi}\right] \quad . \tag{2.11}$$

They found that this model underpredicted the condensing coefficient by 10 to 50 percent.

In 1985, Webb, Kedzierski, and Rudy [Ref. 24] developed a new model which included surface tension effects on film drainage and on condensate retention. Their new model took the form:

$$h\,\eta = (1 - c_b)\left[h_h \frac{A_r}{A} + h_{fs}\,\eta_f \frac{A_f}{A}\right] + c_b\, h_b \tag{2.12}$$

where:

$$h_h = 1.514\left[\frac{\mu_f^2}{k_f^3\,\rho_f^2\,g}Re_f\right]^{-1/3} \quad , \tag{2.13}$$

$$h_{fs} = 2.149^{*}\frac{k_f}{S_m}\left[\frac{\sigma_f\,\rho_f\,h_{fg}\,\Theta_m\,S_m}{\mu_f\,k_f\,\Delta T}\frac{(\zeta+1)}{(\zeta+2)^3}\right]^{1/4} \quad , \tag{2.14}$$

$$h_b = \frac{q_{b2}}{q_{b1}} \frac{k_f}{e} \quad , \text{ and} \tag{2.15}$$

$$c_b = \frac{1}{\pi} \cos^{-1}\left[1 - \frac{2\sigma_f (P - t_b)}{\rho_f g D_o (P_f e - A_p)}\right] \quad . \tag{2.16}$$

This new model was able to predict condensing coefficients within ± 20 percent of experimental values for R-11.

Recently, Wanniarachchi et al. [Ref 25] compared their steam data on six tubes with rectangular-section fins against the Webb et al. model. They showed that their data agreed to within ± 20 percent with the predictions, except for the fully flooded tube (i.e., a tube with a fin spacing of 0.5 mm), both under near-atmospheric and low-pressure conditions. Notice that Webb et al. used a two-dimensional conduction model to express heat transfer in the flooded region of the tube. As discussed by Wanniarachchi et al., the fully flooded tube showed a two to three times greater heat-transfer coefficient than that predicted by one- or two-dimensional heat conduction. This unexpected performance may be attributed to significant thinning of the condensate film at the fin tips and edges even when the tube is fully flooded. The Webb et al. model combined with a more realistic model to express the heat-transfer performance through the flooded region appears to show considerable promise.

Honda and Nozu [Ref. 26], in 1985, developed a comprehensive numerical model to predict the heat-transfer

performance on finned tubes. In their model, they included a pressure-gradient term arising from surface-tension forces in the momentum equation. They numerically solved their fourth-order differential equation for the condensate film thickness. This model predicted within ± 20% most of the data for 11 fluids and 22 tubes. In 1987, Honda et al. [Ref. 27] improved the model of Honda and Nozu to include the case of relatively large fin spacings in comparison to fin height. Their model shows agreement within ± 20% between their model and most of the experimental data for 12 fluids and 31 tubes. However, their model underpredicts the data on a fully flooded tube (i.e., when condensing steam on a finned tube with a fin spacing of 0.5 mm) by about 40%, indicative of the very complex mechanisms involved. Despite the considerable success shown by this model, it appears impractical to use it as a design tool owing to its complexity.

III. DESCRIPTION OF APPARATUS

A. MULTI-TUBE TEST APPARATUS

1. Description of Apparatus

A basic schematic of the apparatus is shown in Figure 3.1. The apparatus was designed to support two different lines of research: the condensation of R-114 on enhanced heat-transfer surfaces in a tube bundle and the study of the effects of oil on the tube bundle performance when boiling R-114. The requirements of the boiling research lead to the heater selection and design of the power distribution to be described later, while the evaporator section will be described by Murphy [Ref. 28], the present thesis deals only with the condenser unit of this overall apparatus. The operating pressure was slightly above atmospheric, which corresponds to a saturation temperature of 2.2 °C. This low condensing temperature requires a coolant maintained at about -18 °C necessitating a refrigeration system. While the boiling experiments should be performed at 2.2 °C, which is the actual evaporating temperature used by Navy chillers, condensing experiments may be separately carried out at a slightly higher (up to 20 °C) temperature. Notice that the actual condensing temperature is about 41 °C (see Tables 1.1 and 1.2).

Both the condenser and the evaporator were designed as pressure vessels. It was decided that it would be highly desirable to

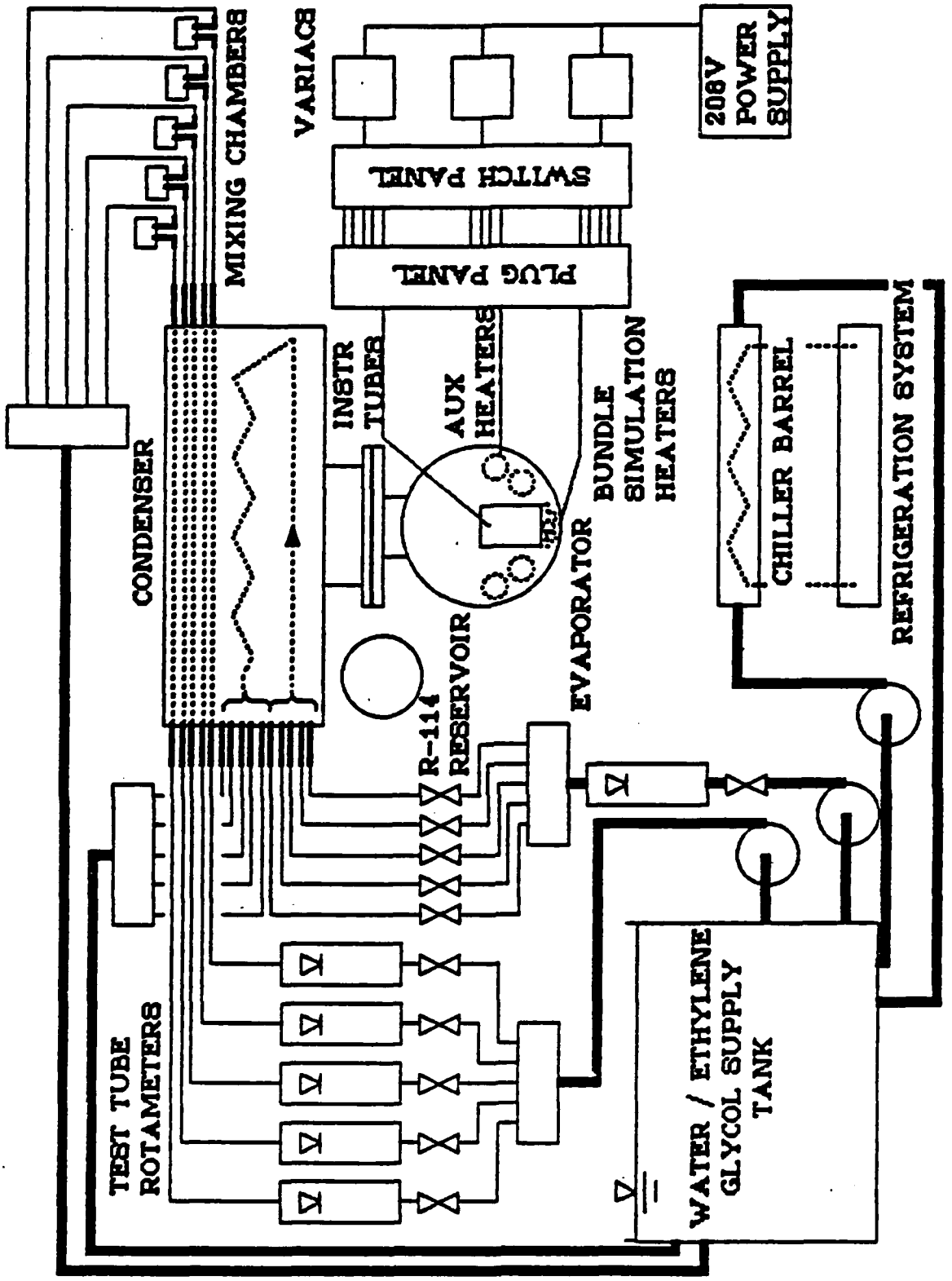

Figure 3.1 Schematic of Multi-Tube Apparatus.

have the system remained charged with R-114 when at room temperature (26 °C). The saturation pressure (absolute) of R-114 corresponding to this temperature is about 220 kPa (32 psi). The design pressure (absolute) was therefore 276 kPa (40 psi) (this corresponds to atmospheric pressure plus 150 percent of the pressure differential at room temperature).

Figure 3.2 shows a side view of the condenser shell. The shell was made of 6.4-mm-thick 304 stainless steel with an outside diameter of 610 mm and a length of 1.2 m. The seam as well as all other joints were double-welded (i.e., welded from both sides) to increase strength and to ensure against any possibility of leaks at the welds. Five viewports were provided on one side of the shell to allow observations and photographing during operation. The viewports have an inner diameter of 102 mm. R-114 causes crazing of Plexiglas and other similar products; therefore, each viewport uses a 12.7-mm-thick Pyrex glass backed by 12.7-mm-thick Plexiglas for safety. The bolting flange on either end of the condenser as well as both end plates were made of a 12.7-mm-thick stainless steel plate. This is to prevent flexing of the endplate when the internal pressure increases from operating conditions to shutdown conditions at room temperature with R-114 charged. Such movement of the endplates may cause the O-rings sealing the test tubes to unseat and allow leakage of R-114 to the atmosphere to result. To further reduce deformations of the

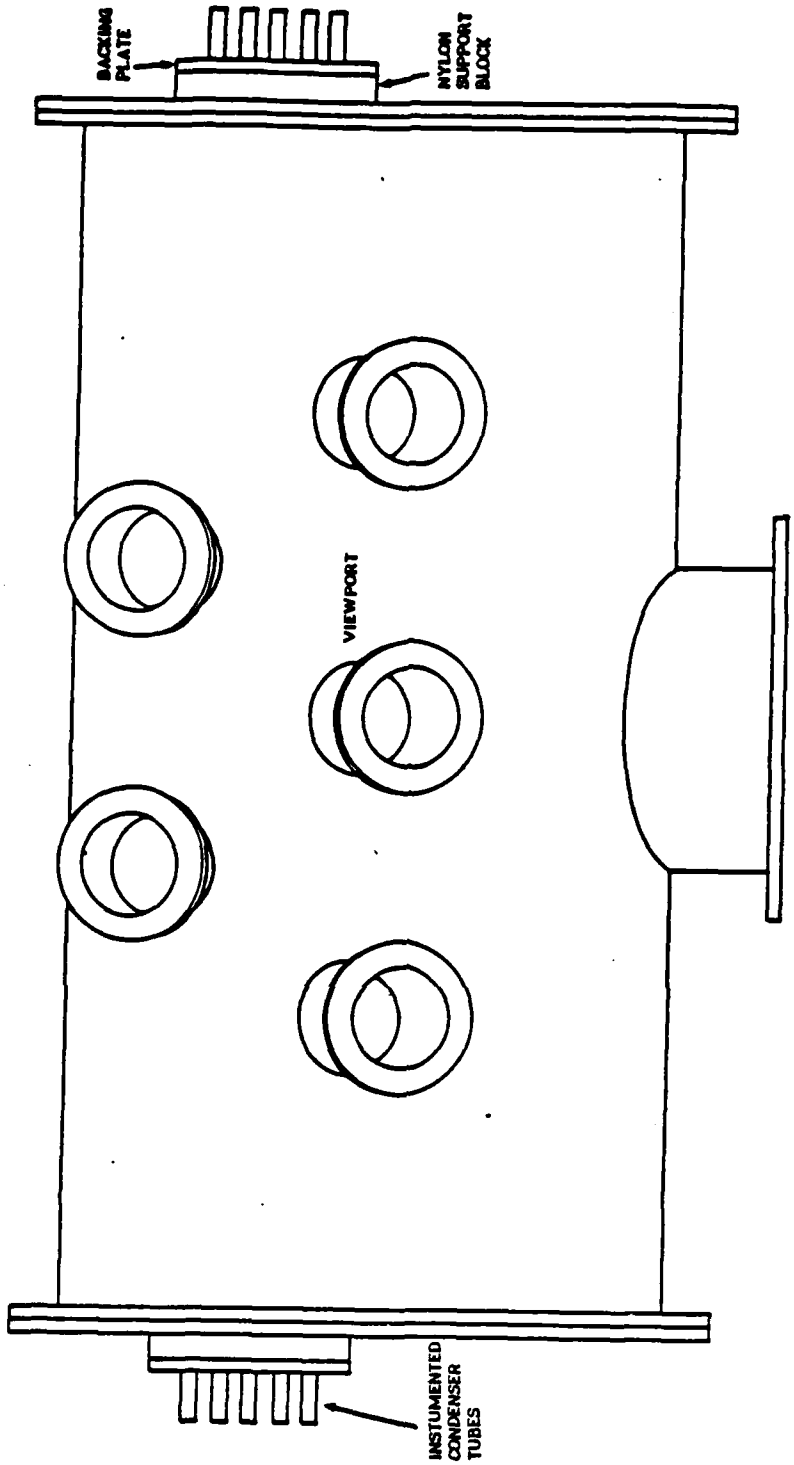

3.2 Side View of Multi-Tube Apparatus Condenser.

endplates, 12.7 mm x 38.1 mm reinforcing bars were welded to the outside of both endplates.

The condenser will allow testing of a bundle simulation of up to five individually-instrumented tubes. The tubes are supported at each end by a 25.4-mm-thick nylon block which is bolted in place. A 12.7-mm-thick stainless steel block is then bolted in place to compress the O-rings. The condenser is attached to the evaporator via a 305-mm-diameter pipe having a wall thickness of 9.5 mm.

Figure 3.3 shows an end view of the condenser with the nylon support block and stainless steel backing plate removed. The opening for the instrumented tubes as well as the inlet and outlet lines for the auxiliary condenser will be discussed later.

Figure 3.4 shows the internal arrangement of the condenser. Inside the condenser shell itself is a shroud to direct the flow of vapor. The shroud is made of a 1.6-mm-thick stainless steel plate and has a glass plate on the side facing the viewports. Vapor will flow up from the evaporator and when it reaches the shroud, it will spread out axially as well as radially. The vapor will continue flowing upward till it reaches the top, and then it will flow downward past the test section into the auxiliary condenser. There is a 102-mm lead-in section before the first test tube is reached. This is to allow for a uniform flow past the test tubes. A portion of the vapor will condense on the five instrumented tubes and the excess vapor will then flow into the auxiliary condenser. The

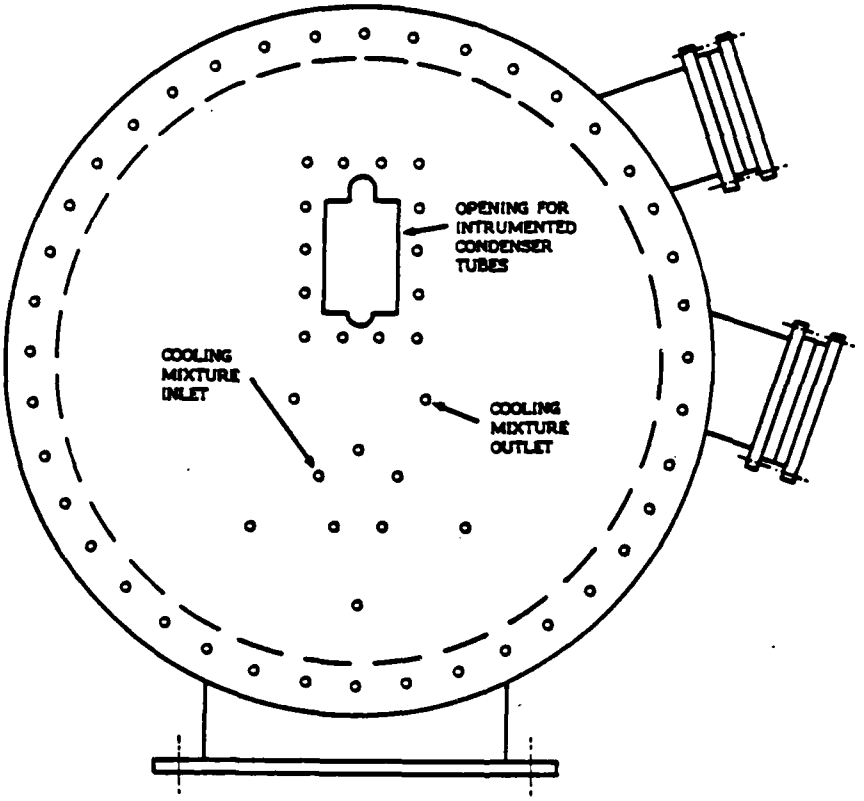

Figure 3.3 End View of Multi-Tube Apparatus Condenser.

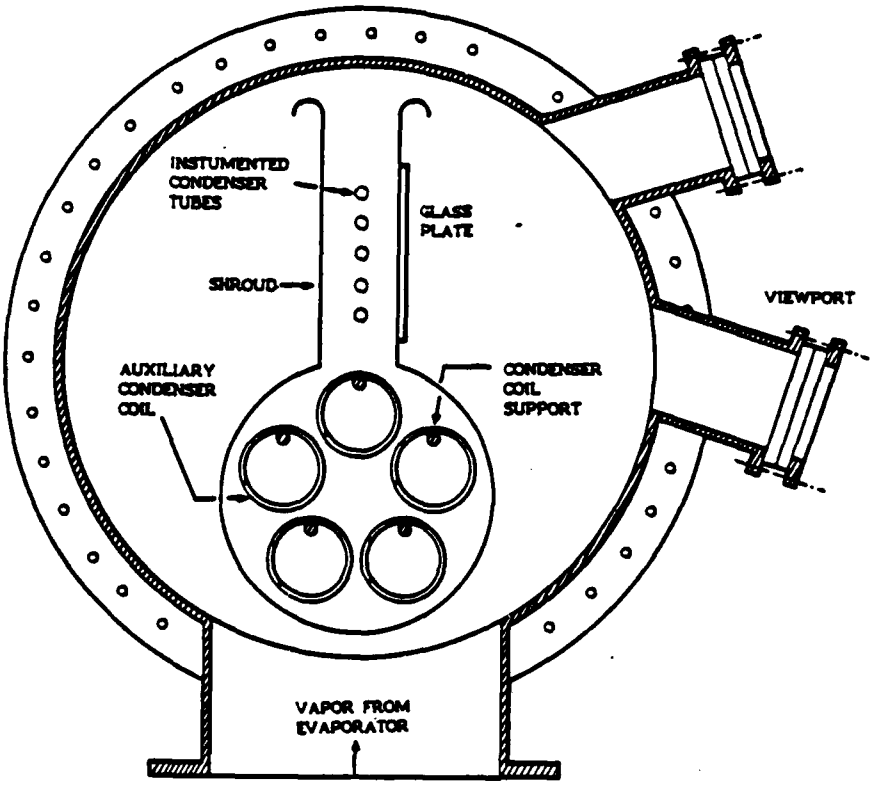

Figure 3.4 Section View of Multi-Tube Apparatus Condenser.

auxiliary condenser is filled with five copper coils, each made from a 9.5-mm-diameter soft-copper tubing having a length of about 12 m. The coils had an outside diameter of approximately 70 mm.

The evaporator was designed to supply a constant output of 15 kW. A constant total heat input to the evaporator is extremely important in maintaining system pressure and temperature and the vapor velocity in the condenser. The heater arrangement was designed to support testing of boiling heat-transfer surfaces. For tube bundle testing of R-114 with oil present, there are five instrumented heated tubes in a vertical row and ten uninstrumented tubes with heaters. Located at the very bottom of the evaporator are the bundle simulation heaters. These heaters are used to simulate varying numbers of rows of tubes below the instrumented tubes. The last bank of heaters are the auxiliary heaters located on either side of the bundle test section. When operating the system, the total output of 15 kW may be obtained by varying the voltage to these various groups of heaters through three individual variacs.

The next item in the overall design to be discussed is the refrigeration system. Unlike R-113 discussed in Section B below, which has a saturation temperature of 47.5 °C at atmospheric pressure, R-114 has a saturation temperature of 2.2 °C. To provide an adequate temperature drop for condensing R-114 vapor, a 40-60 mixture of water and ethylene-glycol at a temperature of -18 °C is used. This mixture is stored in a sump having a capacity

of approximately 1.5 m^3. A refrigeration system having a cooling capacity of 28 kW (8 tons) with a 30-gpm pump takes a suction on the sump and returns the cooled mixture to the sump at the desired temperature of -18 °C. The refrigeration system is provided with a hot gas bypass for continuous operation. It is also provided with the following protective devices to prevent damage to the chiller barrel: low-flow cutout, low-temperature cutout, and high-pressure cutout. Two separate pumps supply coolant to the instrumented condenser tubes and to the auxiliary condenser.

The first pump provides coolant flow to the condenser test tubes. After leaving the pump, the mixture enters a manifold, which distributes the flow equally to each of the five test tubes. The flow then enters individual flowmeters. The coolant then enters the once-through condenser test tube. After leaving the condenser, the mixture enters a mixing chamber to ensure complete mixing of the fluid before exit temperatures are carefully measured. The five individual flow circuits then merge again with a second manifold and finally return to the top of the sump.

The second pump provides flow through a single flowmeter and through a manifold to distribute the flow into the five coils of the auxiliary condenser. There are, however, individual cutout valves for each coil. Flow through the auxiliary condenser coils enters and leaves through the same end of the condenser. As with the test tubes, the five individual circuits are combined and then flows back into the top of the sump.

Wherever possible, the apparatus described above was insulated with foam-rubber thermal insulation to minimize superheating of R-114 vapor and to minimize the load on the refrigeration system.

2. **Instrumentation**

Power to the heaters is controlled by the three variacs as described above. The voltage and current to each group of heaters are measured with in-line sensors and recorded by the data-acquisition system. These sensors provide a linear output of 0-5 Vdc for both AC current and voltage. A pressure gage was installed to measure system pressure. In addition, a vacuum breaker and a pressure relief valve are installed.

Vapor and condensate temperatures are measured using calibrated copper-constantan thermocouples with an accuracy of ± 0.1 K. Thermocouples are also used to measure the cooling mixture inlet temperature to each of the five test tubes. The temperature rise of the cooling mixture across each test tube is measured with a separate 10-junction, series-connected copper-constantan thermopile with a resolution of 0.003 K for each condenser test tube. The cooling mixture flow to each test tube is measured using a calibrated rotameter and the value is manually fed into the computer for computations.

3. **System Integrity**

Initial leak tests will be carried out at positive pressure prior to filling the system with R-114. After filling the system with

a small amount of R-114, an automatic halogen leak detector will be used to detect leaks. After all leaks are corrected the system will be filled with R-114. Each time a connection is broken and remade, it will be tested with only a small amount of R-114 in the system with the automatic halogen detector and any leaks detected will be corrected immediately.

4. Data Acquisition System

An HP-9826A computer will be used to control an HP-3497A Data Acquisition System, which will monitor system temperatures and evaporator power input. Raw data will be processed immediately and also be stored on diskette for later reprocessing. After all data sets are completed, they will be reprocessed using a modified Wilson method.

B. SINGLE-TUBE TEST APPARATUS

1. Description of Apparatus

The construction of the single-tube test apparatus, shown in Figure 3.5, was accomplished by Krohn [Ref. 29] and was modified and improved by Graber [Ref. 30] and Poole [Ref. 11]. The test apparatus was originally designed and built for use in investigating the condensation of steam and has been used extensively for this purpose by Poole [Ref. 11], Georgiadis [Ref. 12], Flook [Ref. 13], and Mitrou [Ref. 14]. Since R-113 is a low-pressure refrigerant with a normal boiling point of 47.5 °C, no modifications of the apparatus were required.

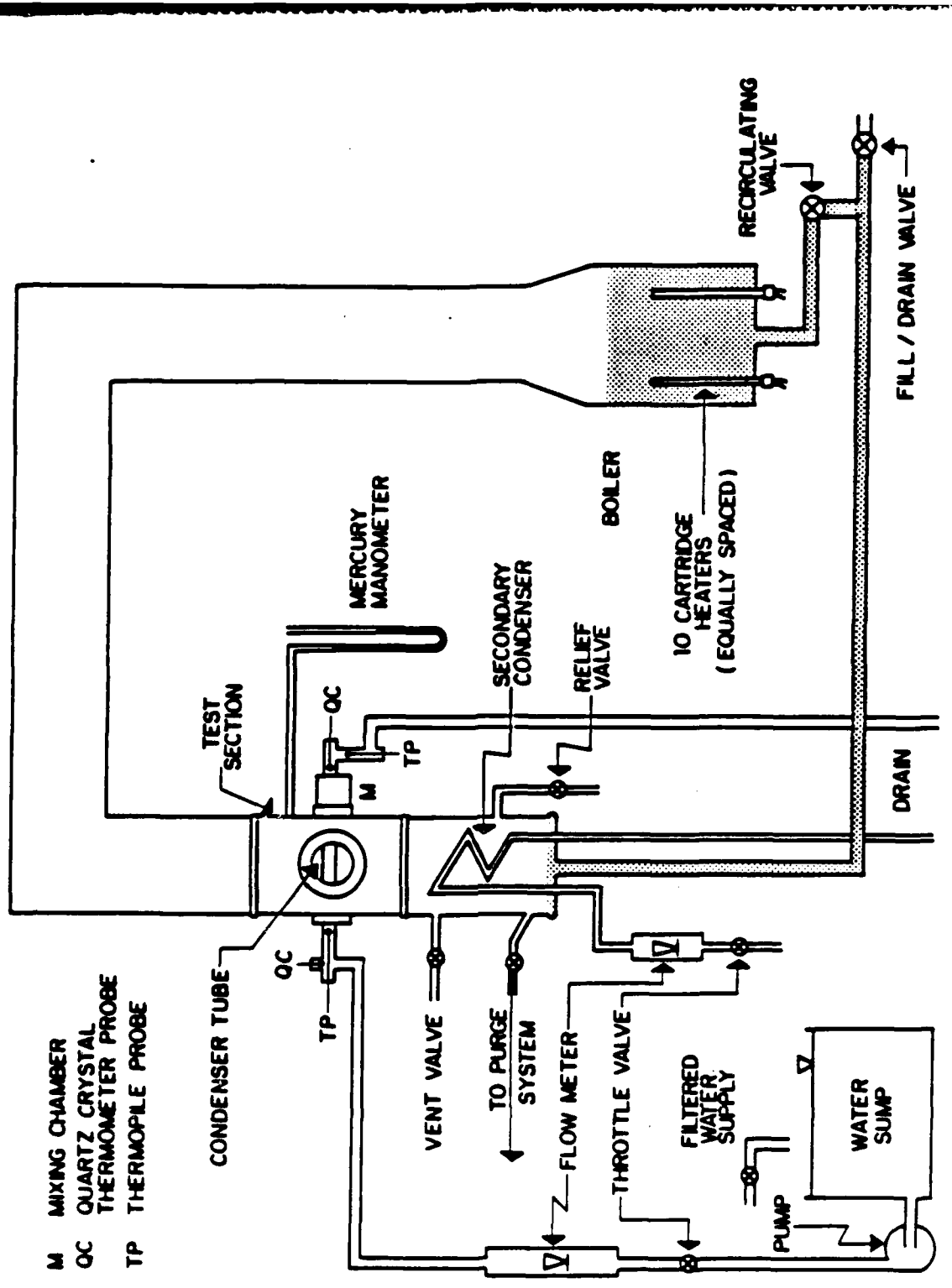

Figure 3.5 Schematic of Single-Tube Apparatus.

The test apparatus was a closed-loop system consisting of a condenser and a boiler. The R-113 was evaporated in a 0.3048 m (12 inch) diameter Pyrex glass section that was fitted with ten 4-kW, 440-V, Watlow immersion heaters. The vapor flowed upward through a 305 mm to 152 mm reducing section, through a 2.44-m-long section of glass piping, and into a 180-degree bend. Upon exiting the 180-degree bend, the vapor then flowed downward through a 1.52-m-long section before entering the stainless-steel test section, shown in Figure 3.6. The tube under test was mounted horizontally in the test section. A portion of the vapor condensed on the test tube, while the remainder was condensed in the auxiliary condenser located below the test tube. The liquid R-113 was gravity drained back to the boiler completing the closed-loop operation of the apparatus.

A viewport was provided in the initial design to enable observation of the mode of steam condensation on the test tube. As noted by Poole [Ref. 11], it is generally fairly difficult to obtain complete filmwise condensation on copper surfaces when condensing steam. However, owing to the very high wetting characteristics of refrigerants, filmwise condensation is the only mode possible. During this investigation, the viewport was used mainly to ensure uniform condensation over the length of the test tube and to take photographs of the tubes during condensation.

The auxiliary condenser was a once-through system consisting of two helically coiled copper tubes 9.5 of mm in diameter

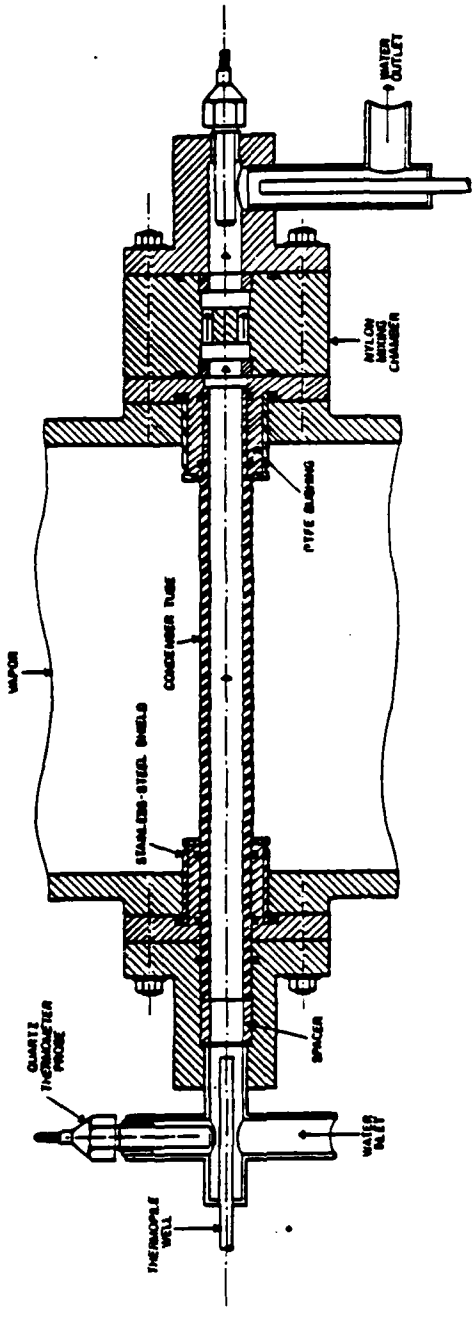

Figure 3.6 Schematic of Single-Tube Apparatus Test Section.

and coiled to a height of 0.457 m. A continuous flow of tap water was provided to the auxiliary condenser through a flowmeter. A throttle valve controlled the water flow rate through the auxiliary condenser to maintain the desired system pressure. A separate source of cooling water was provided for the test tube. A continuous flow of tap water was sent to a water sump with a capacity of 0.4 m^3 that provided the suction head for the two cooling water circulating pumps which were connected in series. The flow was controlled by a throttle valve to control the system pressure and, thereby, the saturation temperature. The discharge of the second pump was throttled and then sent through a flowmeter prior to entering the test tube. Water velocities through the test tube could be varied from 0 to 4.4 m/s. At the exit of the test tube, a mixing chamber was provided to ensure accurate measurement of the water outlet temperature. The water flow was then directed to a drain.

A vacuum pump was used to evacuate the system prior to initial filling with R-113 or after installing a new condenser test tube to remove non-condensing gases. The system used for this purpose is shown in Figure 3.7. The small condenser was provided to reduce the amount of vapor drawn into the vacuum pump by condensing it. The condensate was collected in a cylinder and was drained into a collection bottle after each use of the vacuum pump. The condensate was then reused to replace itself in the system. The operation of the apparatus was commenced by allowing a heat load

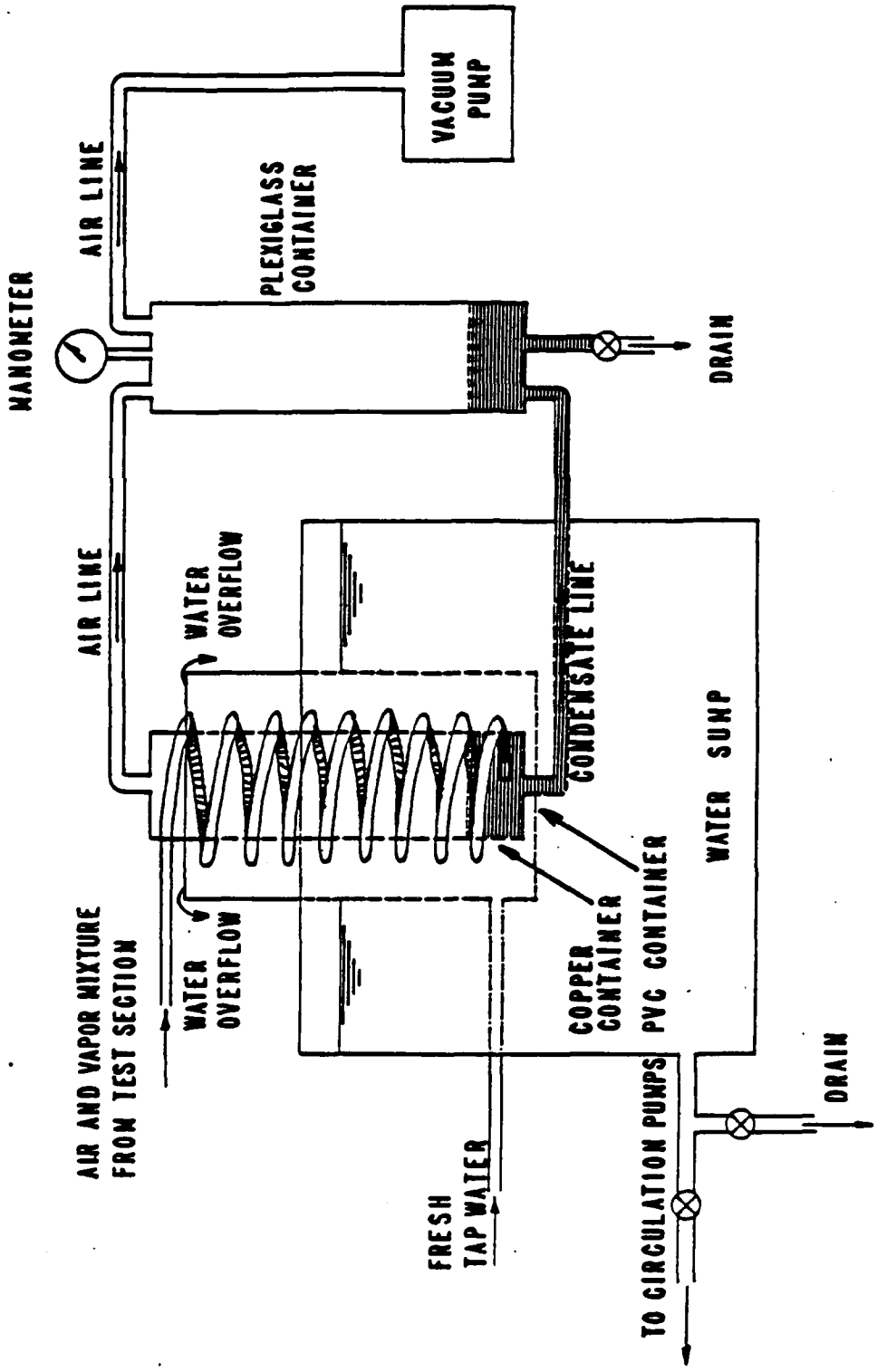

Figure 3.7 Schematic of Single-Tube Apparatus Vacuum System and Cooling Water Sump.

of about 8.4 kW to the boiler heaters. The vacuum pump was energized intermittently, for a period of about one minute each time, to remove air from the system. Care was exercised not to release excessive amounts of R-113 vapor to the surroundings. Initial purging was carried out until no air pockets (i.e., areas of the condenser coil where condensation was inhibited) were seen in the auxiliary condenser (see Figure 3.4). Once the system was operating at near steady-state condition, further purging was carried out for about 60 seconds each time until no further improvement in the measured condensing coefficient was observed. After successful purging using this procedure, air could not be leaked in as the system was operated at a slightly positive pressure. Therefore, continuous purging as performed by previous investigators, when condensing steam at an absolute pressure as low as 85 mmHg, was not required during this investigation.

2. Instrumentation

A panel-mounted potentiometer controlled electrical power to the immersion heaters in the evaporator section. Input power to the evaporator was fed to the data-acquisition system by a root-mean-square converter with an input voltage of 440 VAC. A detailed description of the power supply system is provided by Poole [Ref. 11]. The absolute pressure of the system was measured using a U-tube, mercury-in-glass, manometer graduated in millimeters, connected above the test section.

Vapor, condensate, and ambient temperatures were measured using calibrated copper-constantan thermocouples with an accuracy of ± 0.1 K, when compared to a platinum-resistance thermometer. Two thermocouples were used for vapor temperature measurements, one for condensate return temperature, and one for ambient temperature. The most critical measurement in this experiment was the temperature rise of the coolant through the test tube. Therefore, considerable attention was paid to obtaining the best possible accuracy of this measurement. For this purpose, two independent means of measurement were used: a Hewlett-Packard (HP) 2804A quartz thermometer with two probes having a resolution of up to ± 0.0001 K, and a 10-junction, series-connected copper-constantan thermopile with a resolution of 0.003 K. These two techniques resulted in temperature-rise measurements to within ± 0.03 K about 90% of the time. The thermopile reading was found to fluctuate up to ± 0.05 K as a result of the radio frequency interference discussed by Poole [Ref. 11]. On the other hand, the reading of the quartz thermometer was very stable and this reading was used for calculation of the heat-transfer performance of all tubes tested.

Cooling water flow was measured using a calibrated rotameter and the value was manually fed into the computer for computations. A second rotameter was provided to allow for adjusting water flow though the auxiliary condenser.

3. System Integrity

Leak tests were carried out both under vacuum and at positive pressure prior to filling the system with R-113. The leak rate at an absolute pressure of 45 mmHg was estimated to be less than that corresponding to a pressure rise of 6 mmHg in 24 hours. Also, an automatic halogen leak detector was used when the system was at a positive pressure, and no leaks were detected. Once the system was filled with R-113, no further vacuum tests were performed. Instead, each time a connection was broken and remade, it was tested with the system operating at a slight pressure (as discussed earlier) with the automatic halogen detector and any leaks detected were corrected immediately.

4. Data Acquisition System

An HP-9826A computer was used to control an HP-3497A Data Acquisition System to monitor system temperatures and boiler power input (using the converter signal). Raw data were processed immediately and also stored on diskette for later reprocessing. After all data sets were completed, they were reprocessed using a modified Wilson method.

5. Tubes Tested

A total of twenty-four finned tubes and a smooth tube were tested. All tubes were made of copper and had the following dimensions: an inner diameter (D_i) of 12.7 mm, a smooth tube outer diameter (D_o) or finned tube root diameter (D_o) of 19.05 mm, a test length (L) of 133.3 mm, a length (L_1) unexposed to vapor on the

inlet side of 60.3 mm, and a length (L_2) not exposed to vapor of 34.9 mm on the cooling water outlet side. A summary of tubes tested and their fin dimensions is given in Table 3.1.

6. Insulation of Tubes for Local Measurements

Two of the tubes listed in Table 3.1 (tubes F04 and F15) were tested to determine the variation of the local heat-transfer coefficient. To accomplish this, the inner and outer surfaces were insulated as shown in Figure 3.8. The insulation was applied between the fins and across the tips of the fins over a given total angle. This insulation was held in place by an additional insulating strip which was fastened in place by a piece of fine stainless steel wire. The inner insulating strip was held in place by a T-shaped stainless steel insert as shown in Figure 3.9.

TABLE 3.1
GEOMETRY OF TUBES TESTED

Tube No.	Fin Height e (mm)	Fin Thickness t (mm)	Fin Spacing s (mm)
S01	-	-	-
D02	1.0	1.0	0.25
F04			0.5
F05			1.0
F06			1.5
F07			2.0
F08			4.0
F10	1.0	0.75	0.5
F11			1.0
F12			1.5
F13			2.0
D01	1.0	0.5	0.25
F15			0.5
F16			1.0
F17			1.5
F18			2.0
F22	2.0	1.0	1.0
F23			1.5
F24			2.0
F26	0.5	1.0	1.0
F27			1.5
F28			2.0
F30	1.5	1.0	1.0
F31			1.5
F32			2.0

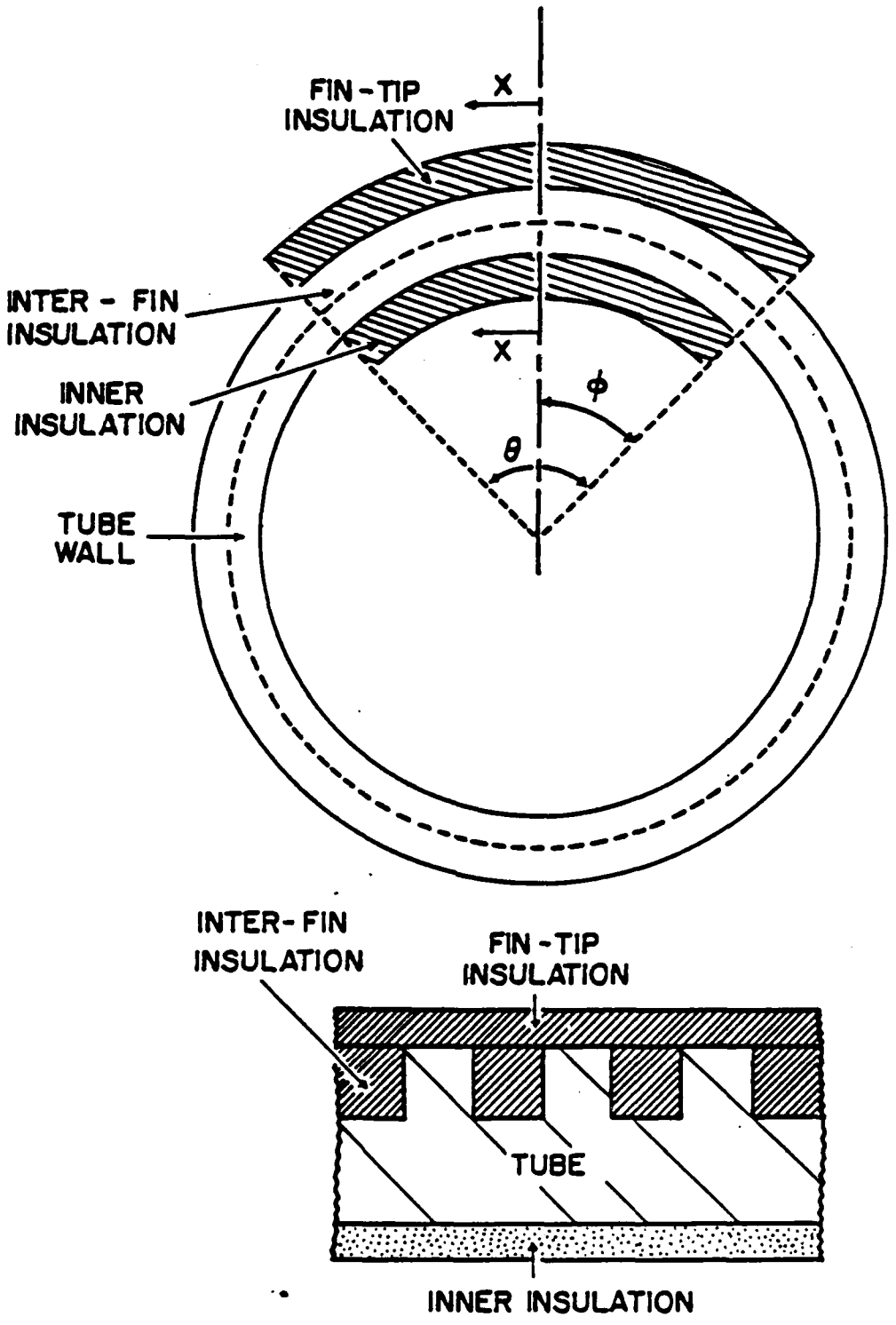

Figure 3.8 Schematic of Insulation Used for Indirect Measurement of Heat-Transfer Performance.

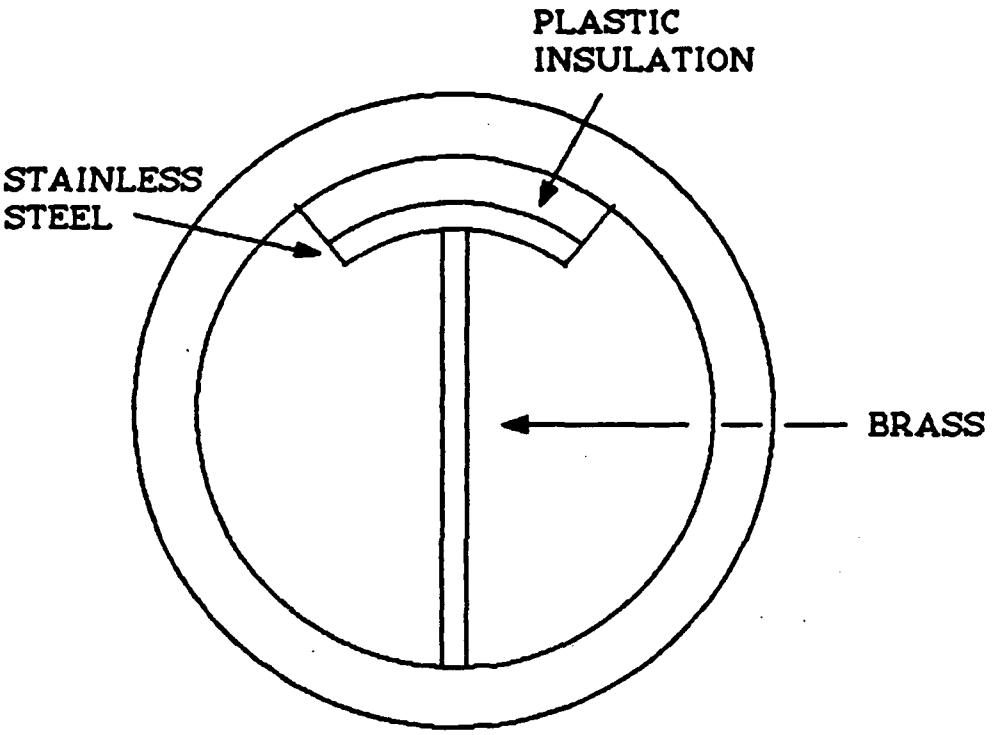

Figure 3.9 Schematic of Retaining Device for Inner Insulation.

IV. SYSTEM OPERATION AND DATA REDUCTION

A. PROPOSED PLAN FOR OPERATING MULTI-TUBE TEST APPARATUS

1. System Operation

Following the installation of condenser test tubes and after ensuring that all studs and any other connections that were broken are assembled and tight, a small amount of R-114 will be introduced into the system. The system will then be checked for leaks with the portable halogen detector. After any leaks that are discovered are fixed, the system will then be fully charged with R-114. After the system is fully charged, the pumps for the coolant mixture will be started and flow through the condenser test tubes and the auxiliary condenser will be started. Flow through the condenser will be used to control the saturation temperature, and therefore the pressure of the system. When the temperature is near the desired operating value of 2.2 °C, the heaters will be energized and adjusted to 15 kW. Periodically, the vacuum pump which takes a suction at the center of the auxiliary condenser will be operated to remove non-condensing gases. At all times, care will be taken not to allow system pressure from falling below 700 mmHg or from exceeding 248 kPa (36 psi). These precautions are necessary to prevent opening the vacuum breaker and reintroducing non-condensing gases or lifting the pressure relief valve.

When steady-state conditions at 2.2 °C are reached, sample data sets will be taken and the outside condensing heat-transfer coefficient for the test tubes will be calculated. After collecting each data set, the vacuum system will be operated to remove any remaining non-condensing gases. This procedure will be repeated until three consecutive data sets show no increase in the calculated condensing coefficient on any of the five test tubes at which time it will be assumed that all non-condensing gases have been removed. Since the system operates at slightly above-atmospheric pressure, once non-condensing gases have been removed, the vacuum pump will be secured.

Data will be taken at different flow rates through the test tubes at values to be determined after the initial test runs. Flow rates will be selected to provide approximately even-spaced heat-flux values. After data are taken at a selected flow rate, flow through the test tubes will be adjusted to the next value. The flow to the auxiliary condenser will be adjusted as necessary to correct for any drift from the desired operating pressure.

The system will be secured to one of two states. The first is shutdown state while remaining charged with R-114. This is the condition that may exist when securing for the night and it is desired to retest the installed tubes the next day. This shutdown condition would also be desired when taking data on the effects of various oil concentrations of boiling surfaces and it is desired to increase the oil concentration. This shutdown condition requires

that the heaters in the evaporator and flow through the condenser be secured. As the system slowly heats up to 26 °C, pressure will increase to about 220 kPa (32 psi).

The second shutdown condition is the one required to change tubes. This condition requires as much R-114 as possible be removed from the system. This is accomplished by securing all heaters except the bundle-simulation heaters at the bottom of the evaporator. The flow through the condenser will be maintained; however, the return condensate will be diverted to the R-114 reservoir. The bundle-simulation heaters will be run until the R-114 level barely uncovers the heaters. The heaters will then be secured and the thermal insulation at the bottom of the evaporator will be removed and a hot air gun will be used to evaporate the remaining R-114 as observed through the glass ports in the evaporator. When all the R-114 has been evaporated, the coolant flow to the condenser will be secured and the system be opened to the atmosphere.

Care will be taken when changing condenser test tubes to prevent contaminating the R-114 with the water and ethylene-glycol mixture. After the lines connecting the coolant supply and return lines have been removed, they will be capped to prevent spilling the cooling mixture. The test tubes will then be blown out with air into a container. Each tube will then be plugged to prevent any coolant still remaining to drip out.

2. Data Reduction

Data Reduction will be accomplished using the a similar method as described in Section B.2 below.

B. SINGLE-TUBE APPARATUS

1. System Operation

Following installation of a test tube, the operation of the apparatus was started by evacuating the system to the saturation pressure of the R-113 in the boiler. This was indicated by observing the sudden generation of bubbles forming in the liquid. The evacuation system was then secured. Cooling water to the auxiliary condenser and to the test tube was turned on and the heaters were then energized to a previously determined setting to achieve the desired 2 m/s vapor velocity. As soon as condensation was observed in the auxiliary condenser, the evacuation system was operated again to remove non-condensing gases. The test apparatus was brought to operating temperature and pressure by adjusting the cooling water flow through the auxiliary condenser. Steady-state conditions were assumed when the operating conditions were stabilized with fluctuations of less than ± 2 μV (i.e., ± 0.05 K) for the vapor thermocouple and ± 0.005 K for the cooling-water temperature-rise measurements. When steady-state conditions were reached, the cooling water flow rate through the test tube was manually entered into the computer. All other required data were gathered automatically by the data-acquisition system. Sample

data sets were taken initially to verify that no non-condensing gases were present. After taking each sample data set, the vacuum system was operated for about 60 seconds. When no increase in the calculated condensing heat-transfer coefficient was observed, it was assumed that all non-condensing gases had been removed. For each tube, data were taken at cooling water flow rates of 20 percent (1.16 m/s), 26, 35, 45, 54, 62, 70, 80 percent (4.4 m/s), and again at 20 percent. Two data sets were taken at each of these flow rates to demonstrate repeatability. These cooling water flow rates were selected to provide approximately even-spaced heat-flux values. After each change in cooling water flow rate through the tube, the system temperature and pressure experienced a slow drift, and the flow rate to the auxiliary condenser was adjusted to maintain the desired operating conditions. All data were taken in a band of 1955 ± 5 μV (i.e., 48.0 ± 0.2 °C) on the vapor temperature thermocouple.

2. Data Reduction

The program used for data reduction was the same as that used by Mitrou [Ref. 14] and other previous investigators. This program included property functions of the cooling water, calibration curves for the cooling water flowmeter and for the thermocouples, and calibration curves for the temperature rise due to frictional heating across the mixing chamber. Modifications were made to the program to include property functions of R-113 and ethylene glycol on the vapor side. In addition, a new calibration run was

performed for frictional heating (i.e., the temperature rise) across the mixing chamber, and was included in the program.

The separation of individual thermal resistances (water-side, wall and vapor-side) properly from the overall thermal resistance ($1/U_oA_o$) is very important to obtain the condensing heat-transfer coefficient (h_o). The condensing coefficient was based on the smooth tube outside surface area (A_o). The overall thermal resistance is given by:

$$\frac{1}{U_o A_o} = \frac{1}{h_i A_i} + \frac{R_w}{A_o} + \frac{1}{h_o A_o} \quad , \tag{4.1}$$

where

$$R_w = \frac{D_o \ln\left[\frac{D_o}{D_i}\right]}{2 k_m} \quad , \text{ and} \tag{4.2}$$

$$A_i = \pi D_i (L + L_1\eta_1 + L_2\eta_2) \quad . \tag{4.3}$$

Further, the overall thermal resistance could be computed using the following equations:

$$Q = \dot{m} c_p \Delta T_{cw} = U_o A_o \text{ LMTD} \quad , \tag{4.4}$$

where

$$LMTD = \frac{T_{co} - T_{ci}}{\ln\left[\frac{T_{sat} - T_{ci}}{T_{sat} - T_{co}}\right]} \quad . \tag{4.5}$$

The inside heat-transfer coefficient is given by a Sieder-Tate-type equation:

$$h_i = C_i \frac{k_b}{D_i} Re^{0.8} Pr^{1/3} \left[\frac{\mu_b}{\mu_w}\right]^{0.14} = C_i \Omega \quad , \tag{4.6}$$

where

$$\Omega = \frac{k_b}{D_i} Re^{0.8} Pr^{1/3} \left[\frac{\mu_b}{\mu_w}\right]^{0.14} \quad . \tag{4.7}$$

The inside heat-transfer coefficient was obtained using a modified Wilson plot method.

a. Modified Wilson Plot

A modified Wilson plot method was used to process all data. The Sieder-Tate-type equation (eqn. 4.6) was used for the inside heat-transfer coefficient. A Nusselt-type equation was used for the outside condensing coefficient as given by:

$$h_o = \alpha \left[\frac{k_f^3 \rho_f^2 g h_{fg}}{\mu_f D_o \Delta T}\right]^{1/4} = \alpha F \quad , \tag{4.8}$$

where

$$F = \left[\frac{k_f^3 \rho_f^2 g h_{fg}}{\mu_f D_o \Delta T} \right]^{1/4} \quad . \tag{4.9}$$

Substituting h_i (eqn. 4.6) and h_o (eqn 4.8), into equation (4.1) and rearranging, the following expression can be obtained:

$$\left[\frac{1}{U_o} - R_w \right] F = \frac{A_o F}{C_i \Omega A_i} + \frac{1}{\alpha} \quad . \tag{4.10}$$

This is a linear equation of the form:

$$Y = m X + b \quad , \tag{4.11}$$

where

$$Y = \left[\frac{1}{U_o} - R_w \right] F \quad , \tag{4.12}$$

$$X = \frac{A_o F}{A_i \Omega} \quad , \tag{4.13}$$

$$C_i = \frac{1}{m} \quad , \text{ and} \tag{4.14}$$

$$\alpha = \frac{1}{b} \quad . \tag{4.15}$$

Equation 4.10 has two unknowns: α and C_i. An iterative process was used to obtain values of these unknowns while fitting a least-squares line to the data points. The initial values used to start the iterations were $\alpha = 2.5$ and $C_i = 0.031$. The iterative process was repeated until the assumed and computed values of α and C_i both agreed within $\pm$ 0.1 percent.

After all data for the tubes were initially processed and the calculated value of C_i obtained, the average value of C_i was computed. This value was found to be 0.028 ± 0.002. Since all tubes had identical inner diameters, it is expected that the Sieder-Tate-type coefficient C_i should be the same. Therefore, all data were reprocessed using the average value of C_i.

b. Determination of Local Heat-Transfer Coefficient

The method for determining the local heat-transfer coefficient was developed by Lester [Ref. 31]. The form of the local enhancement ratio was assumed to be:

$$\epsilon_\phi = a_0 + a_1 \phi + a_2 \phi^2 + a_3 \phi^3 \quad , \qquad (4.16)$$

where ϕ is the angle measured from the top of the tube. Notice that ϵ can be based on constant ΔT or constant q as defined in Chapter V. During this study, ϵ based on constant ΔT was used. This assumed form for the local enhancement ratio has four unknown coefficients: a_0, a_1, a_2, and a_3. Two of the unknowns can be formed by the boundary condition as shown below:

$$\frac{d\epsilon_\phi}{d\phi} = 0 \text{ at } \phi = 0 \quad \text{and,} \tag{4.17}$$

$$\epsilon_\phi = 0 \text{ at } \phi = \pi \quad . \tag{4.18}$$

A third unknown can be found by the following condition:

$$\bar{\epsilon}_\pi = \frac{1}{\pi} \int_0^\pi \epsilon_\phi \, d\phi \quad . \tag{4.19}$$

Notice that $\bar{\epsilon}_\pi$ represents the experimentally measured enhancement ratio for the tube without any insulation.

When the upper portion of the tube is insulated, the experimentally measured enhancement ratio represents the value for the lower, uninsulated portion of the tube. However, the analysis requires that the average enhancement be expressed for the upper portion (i.e., $\bar{\epsilon}_\phi$). For this purpose, the following expression was used:

$$\bar{\epsilon}_\phi = \frac{\pi}{\phi}\left[\bar{\epsilon}_\pi - \bar{\epsilon}_{\pi-\phi}\frac{(\pi-\phi)}{\pi}\right] \tag{4.20}$$

To compute the final unknown, a least-squares technique was performed as described by Lester [Ref. 31] by minimizing the errors

between the computed and measured $\bar{\varepsilon}_\phi$ values as shown below:

$$\min \quad \Sigma(\bar{\varepsilon}_\phi - \bar{\varepsilon}_p)^2 \quad , \tag{4.21}$$

where $\bar{\varepsilon}_p$ represents the value from the polynomial.

V. RESULTS AND DISCUSSION

A. INTRODUCTION

Data were taken with extreme care as described in Chapter IV. Initially, the data were taken on a few tubes on different days to demonstrate repeatability. Since non-condensing gases were removed effectively before collecting data and filmwise condensation was the only possible mode with R-113, data were highly repeatable. Notice that, as mentioned in Chapter II, Poole [Ref. 11], Georgiadis [Ref. 12], and Mitrou [Ref. 14] had to perform a number of runs for each tube to verify filmwise condensation as they used steam, which tends to undergo partial dropwise condensation on copper tubes in the presence of even a minute contamination. During the present study, the condensing coefficient was repeatable within about 3 percent on different days.

All of the data were taken with a nominal vapor velocity of 2 m/s, at a pressure slightly above-atmospheric (~ 765 mmHg), which corresponds to a nominal saturation temperature of 48 °C. As discussed in the next section, most of the tubes were tested without an insert to enhance the water-side coefficient, while one series of tubes were tested both with and without an insert.

The vapor-side heat-transfer coefficients presented in this chapter are based on the outside area of the corresponding smooth

tube (A_o). Thus, the computed h_o includes the area enhancement and the fin efficiency.

B. EFFECT OF FIN DIMENSIONS ON CONDENSING HEAT-TRANSFER PERFORMANCE

1. Inside Heat-Transfer Coefficient

The data presented in this section are for a series of 24 finned tubes and a smooth tube. All these tubes had identical inside geometry and nearly identical flow conditions. Therefore, it was expected that all of these tubes would result in nearly the same inside heat-transfer coefficients or C_i as defined by equation (4.14). As discussed earlier in Chapter IV, data were taken using an assumed value of 0.031 for C_i. Immediately after completing a data run, these data were reprocessed to find a new, more reasonable C_i using the modified Wilson plot as discussed in Section 4.2.a. The C_i values thus computed produced an average value of 0.028 $\pm$ 0.002. Since the C_i value should be identical for all tubes, all the data were reprocessed using a value of 0.028 for the C_i.

During previous investigations with steam at the Naval Postgraduate School [Ref. 11, 12, 13, and 14], data were taken with an insert installed in the test tube to enhance the inside coefficient. This was necessary due to the high outside heat-transfer coefficient when condensing steam. For example, for tube F06, the vapor-side condensing coefficient was approximately 40 $kW/m^2 \cdot K$, whereas when condensing R-113 the vapor-side coefficient was

approximately 6 $kW/m^2 \cdot K$. Figure 5.1 shows the effect of water-side enhancement on the condensing heat-transfer coefficient for R-113. Data were taken on a set of tubes with a fin height of 1.0 mm and a fin thickness of 1.0 mm both with an insert to enhance the inside coefficient and without an insert. As can be seen, the agreement between the two sets of data is very good. Since a wider range of ΔT was achieved without the insert installed, it was decided that all further data would be taken without the insert.

For comparison purposes, data for the smooth tube as well as a curve representing the Nusselt theory are also plotted on this figure. Notice that the data for the smooth tube lie about 10% higher than the Nusselt curve. This is attributed to the moderate vapor velocity (2 m/s) used during the experiment.

2. Vapor-Side Heat-Transfer Performance

The figures presented in this section showing the variation of the vapor-side coefficient with the temperature drop across the condensate film are provided with curves representing least-squares fits based on the following equations:

$$q_f = a_f \, \Delta T_f^{0.75} \text{ (finned tube)}, \qquad (5.1)$$

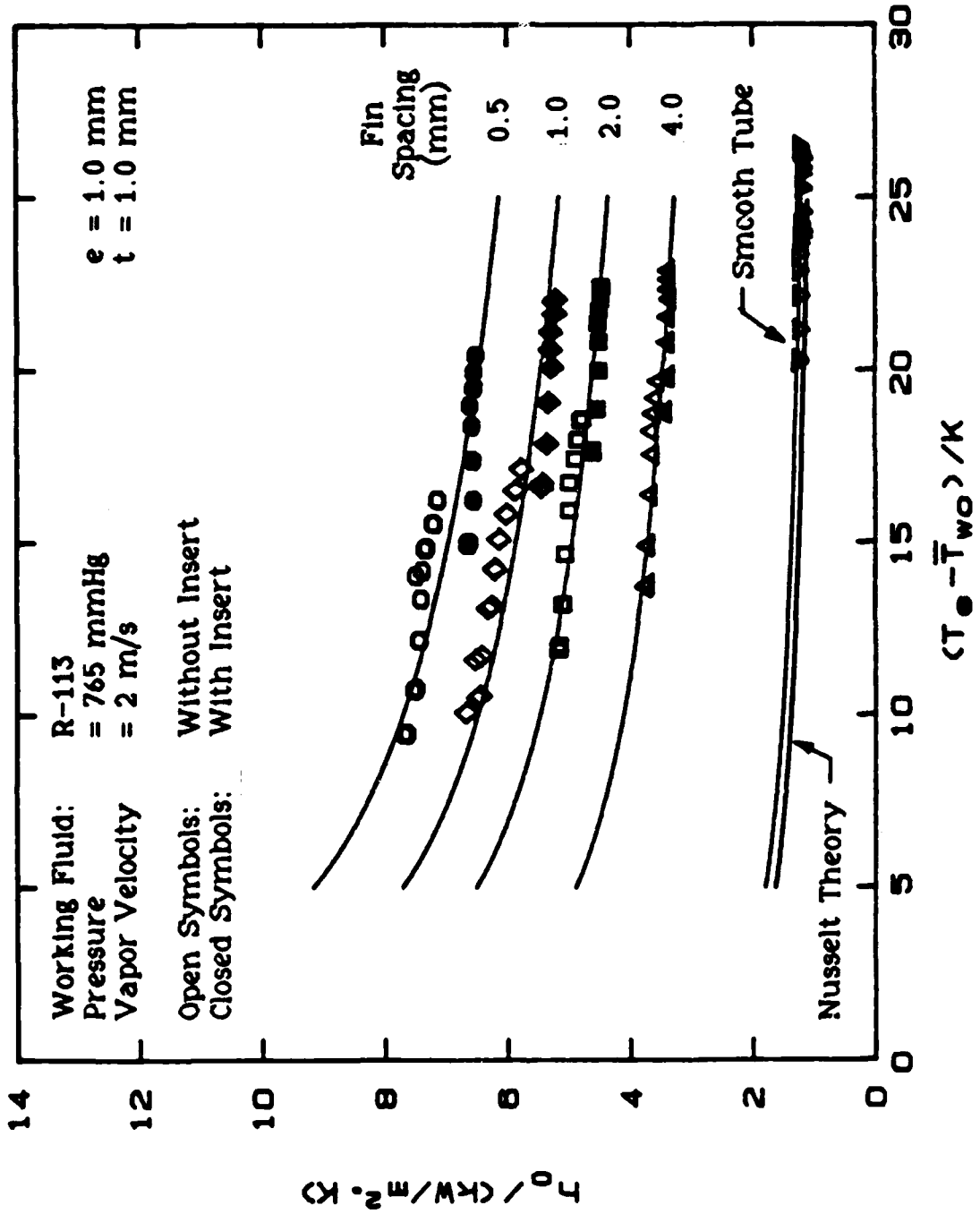

Figure 5.1 Effect of Water-Side Enhancement on Condensing Heat-Transfer Coefficient.

and

$$q_s = a_s \Delta T_s^{0.75} \text{ (smooth tube)} \quad . \qquad (5.2)$$

Even though slightly better least-squares fits were possible by allowing the exponent of ΔT (i.e., 0.75) to be a variable, as it will be discussed later in this section, an exponent value of 0.75 is highly desirable in presenting the data in a compact form.

Figure 5.2 shows the variation of the condensing heat-transfer coefficient with the temperature drop across the condensate film for a series of tubes with a fin height and thickness of 1.0 mm and for fin spacings of 0.25, 0.5, 1.0, 1.5, 2.0, and 4.0 mm. This figure also shows computed typical uncertainties associated with the vapor-side coefficient. The procedure for calculating the uncertainties are discussed in Appendix B. Notice that, while the typical uncertainties for h_o are around ± 7 percent, data were repeatable within ± 3 percent. As can be seen, the vapor-side coefficient increases with decreasing fin spacing up to a value of 0.5 mm. This is, of course, due to the considerable fin area increase associated with decreasing fin spacing. However, the tube with fin spacing of 0.25 mm (tube D02, see Table 5.1) shows a slightly poorer heat-transfer performance than the tube with a 0.5 mm fin spacing (tube F04). This is attributed to increased flooding of the lower portion of the tube. Notice that equation (2.5) predicts condensate retention angles of 77 degrees and 52 degrees for tubes with fin

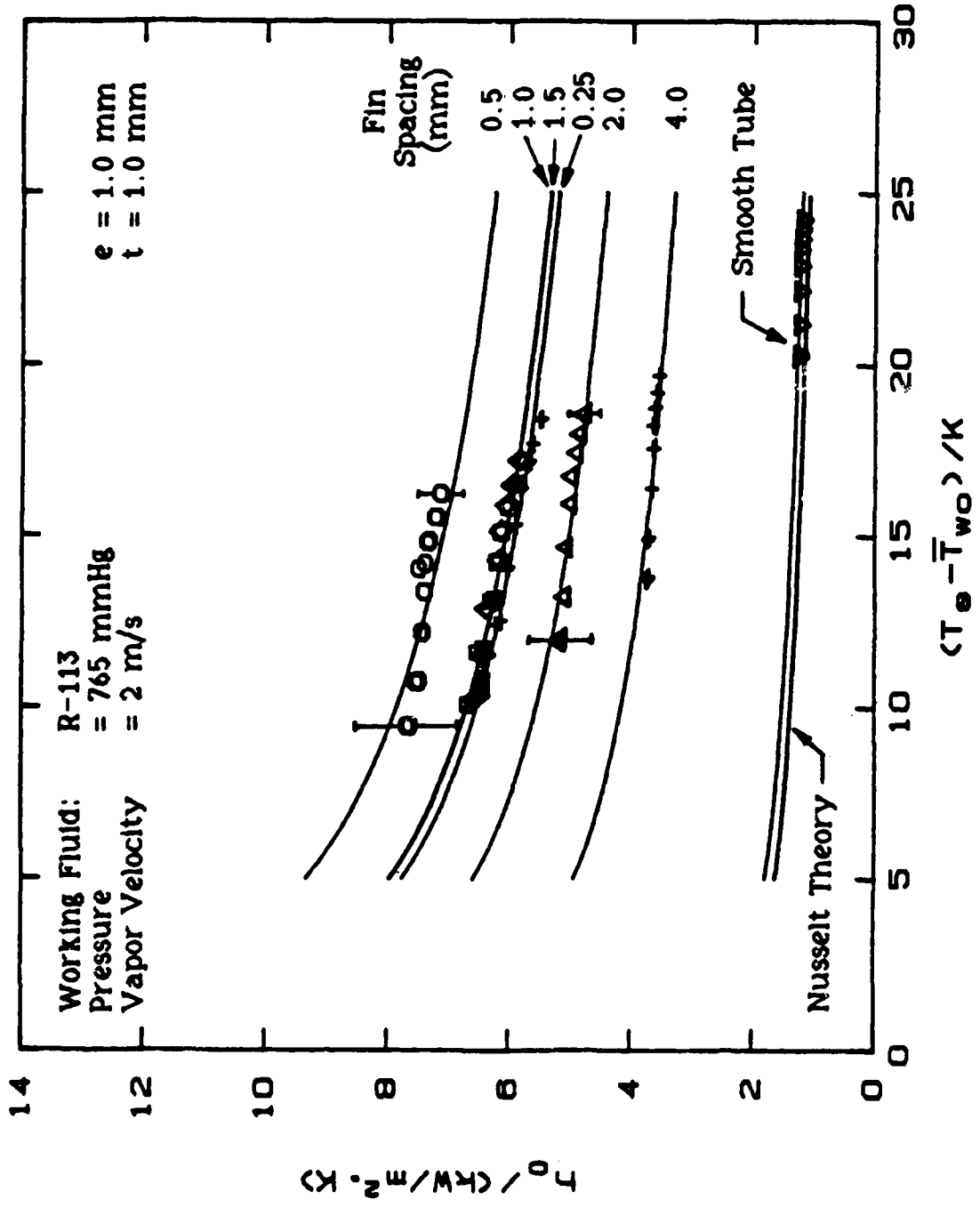

Figure 5.2 Effect of Fin Spacing on Vapor-Side Coefficient for Tubes with Fin Height of 1.0 mm and Fin Thickness of 1.0 mm.

TABLE 5.1
ENHANCEMENT RATIOS OF TUBES TESTED

Tube No.	Fin Height e (mm)	Fin Thickness t (mm)	Fin Spacing s (mm)	Area Ratio A_f/A_o	Enhancement Ratios $\epsilon_{\Delta T}$	ϵ_q
S01	-	-	-	1.00	1.00	1.00
D02	1.0	1.0	0.25	2.77	4.37	7.15
F04			0.5	2.47	5.28	9.19
F05			1.0	2.10	4.49	7.40
F06			1.5	1.88	4.50	7.43
F07			2.0	1.74	3.70	5.73
F08			4.0	1.44	2.76	2.84
F10	1.0	0.75	0.5	2.25	6.10	11.15
F11			1.0	1.97	6.08	11.09
F12			1.5	1.97	4.90	8.32
F13			2.0	1.79	4.85	8.21
D01	1.0	0.5	0.25	3.88	6.96	13.30
F15			0.5	3.16	6.67	12.55
F16			1.0	2.44	5.23	9.07
F17			1.5	2.08	4.71	7.90
F18			2.0	1.86	4.21	6.79
F22	2.0	1.0	1.0	3.31	5.95	10.72
F23			1.5	2.85	5.78	10.36
F24			2.0	2.54	5.22	9.05
F26	0.5	1.0	1.0	1.54	3.47	5.26
F27			1.5	1.43	3.21	8.79
F28			2.0	1.36	2.93	7.72
F30	1.5	1.0	1.0	2.70	5.25	9.13
F31			1.5	2.36	5.11	8.79
F32			2.0	2.13	4.63	7.72

spacings of 0.25 mm and 0.5 mm, respectively, for a tube with a fin height of 1.0 mm.

Figure 5.3 shows data similar to Figure 5.2 but for a series of tubes having a fin height of 1.0 mm, a fin thickness of 0.75 mm, and fin spacings of 0.5, 1.0, 1.5, and 2.0 mm. As can be seen, the tube with a fin spacing of 0.5 mm shows the best performance.

Figure 5.4 shows similar data for finned tubes having a fin height of 1.0 mm, a fin thickness of 0.5 mm, and fin spacings of 0.25, 0.5, 1.0, 1.5, and 2.0 mm. Unlike in the first set of tubes, the tube with a fin spacing of 0.25 mm shows a similar heat-transfer performance to the tube with a 0.5 mm spacing. The effect of fin thickness on the heat-transfer performance will be discussed later in this section.

Similar data are shown in Figure 5.5 for a set of tubes having a fin thickness of 1.0 mm, a fin height of of 2.0 mm, and fin spacings of 1.0, 1.5, and 2.0.[1] The tube with a fin spacing of 1.0 mm shows the best heat-transfer performance, as it provides the largest area enhancement in this set of tubes. Figures 5.6 and 5.7 show similar data for fin heights of 0.5 mm and 1.5 mm, respectively. Notice that, once again, the tubes with a fin spacing of 1.0 mm show the best performance in each of these sets of tubes.

---

[1]Notice that these tubes were originally manufactured for testing with steam, which has an optimum fin spacing of 1.5 mm as reported by Georgiadis [Ref. 12]; thus, a tube of 0.5 mm fin spacing had not been manufactured for these tube sets.

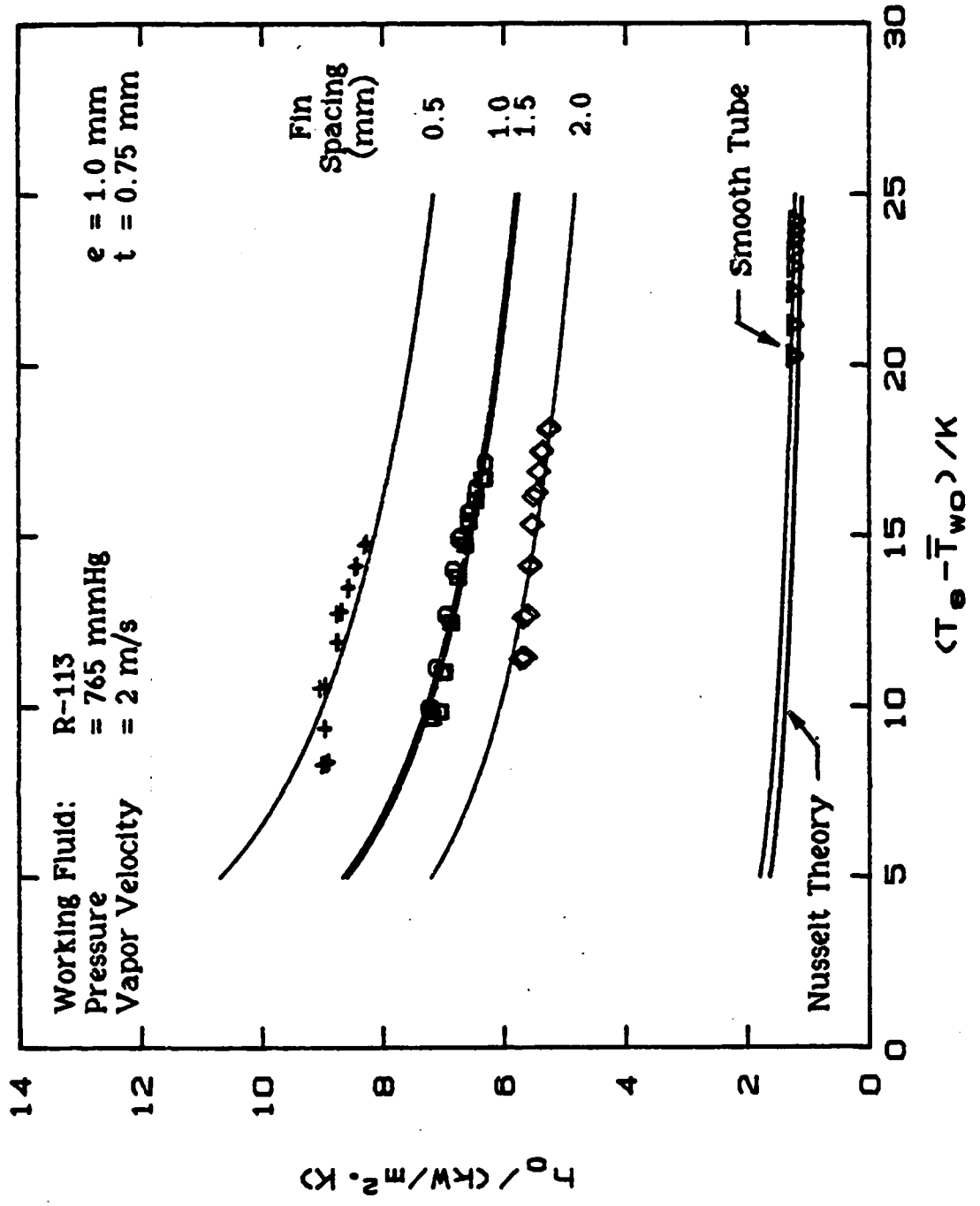

Figure 5.3 Effect of Fin Spacing on Vapor-Side Coefficient for Tubes with Fin Height of 1.0 mm and Fin Thickness of 0.75 mm.

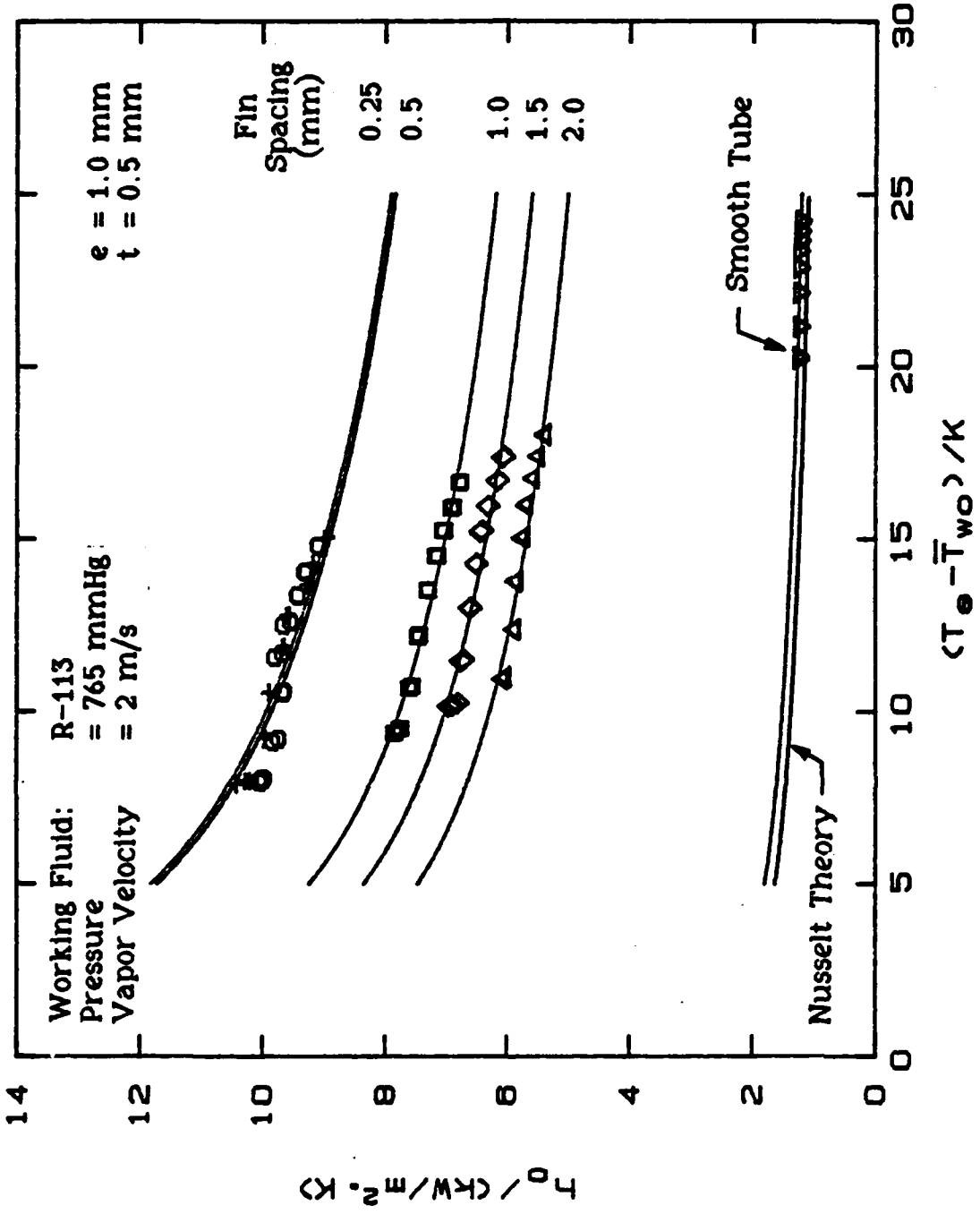

Figure 5.4 Effect of Fin Spacing on Vapor-Side Coefficient for Tubes with Fin Height of 1.0 mm and Fin Thickness of 0.5 mm.

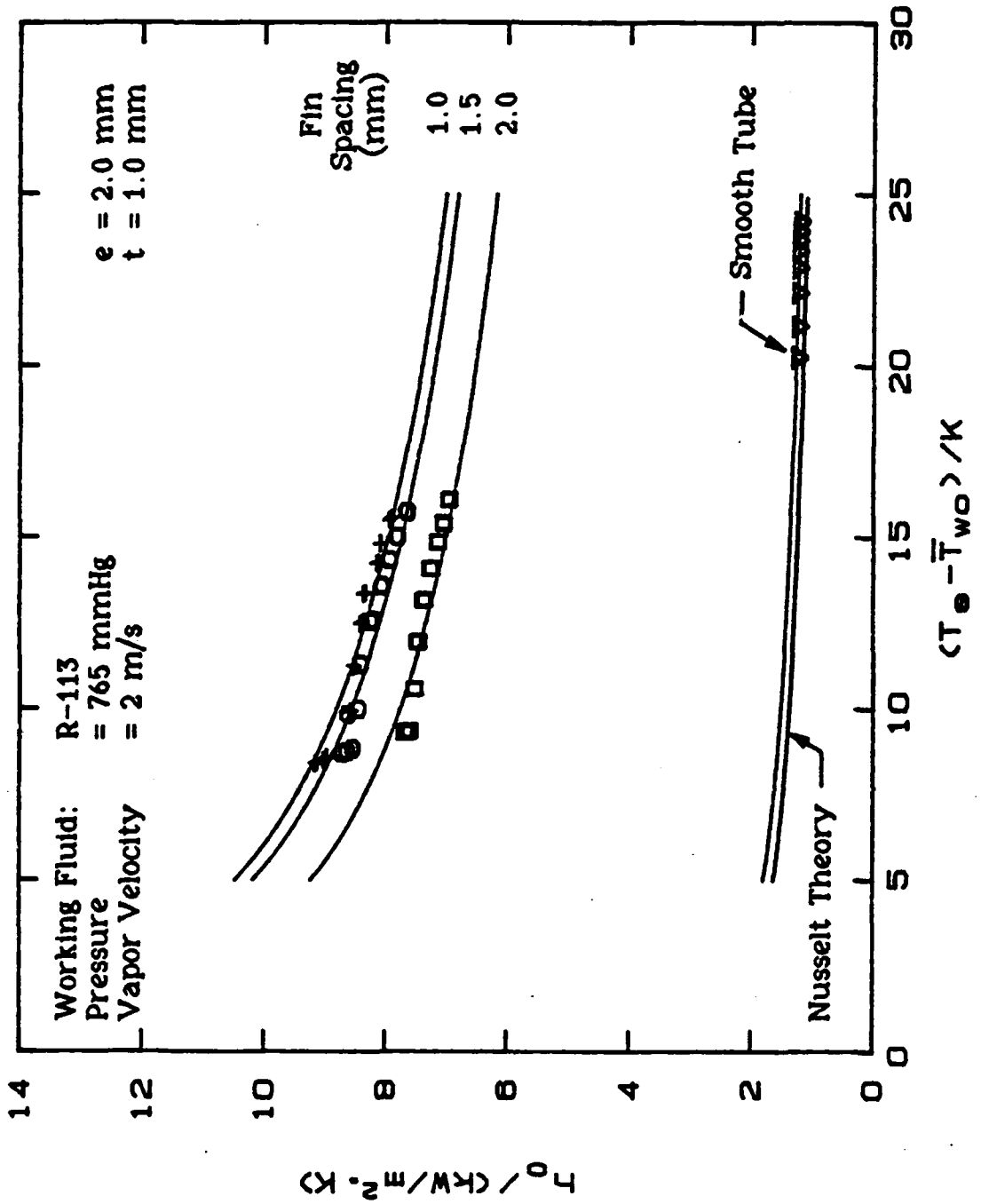

Figure 5.5 Effect of Fin Spacing on Vapor-Side Coefficient for Tubes with Fin Height of 2.0 mm and Fin Thickness of 1.0 mm.

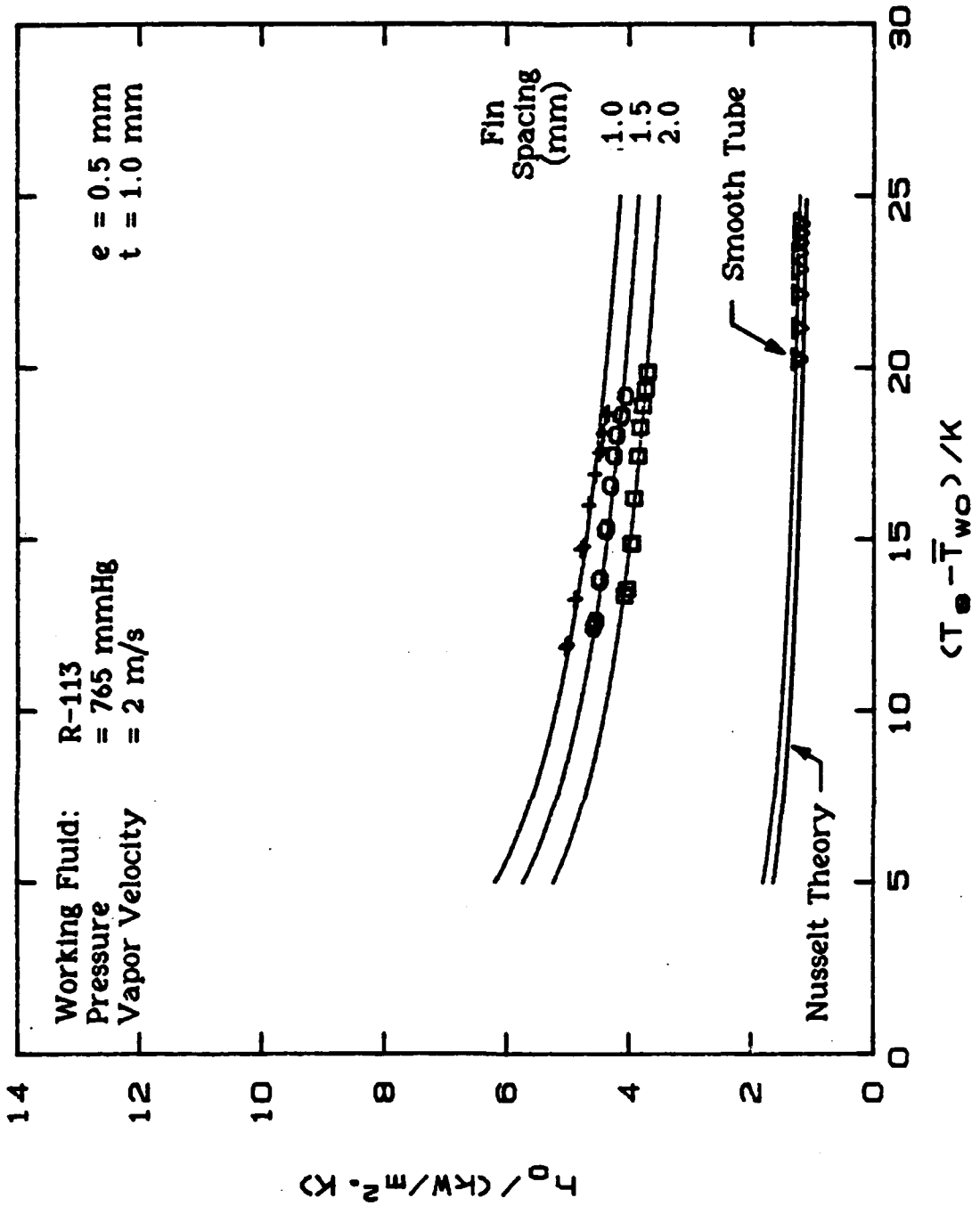

Figure 5.6 Effect of Fin Spacing on Vapor-Side Coefficient for Tubes with Fin Height of 0.5 mm and Fin Thickness of 1.0 mm.

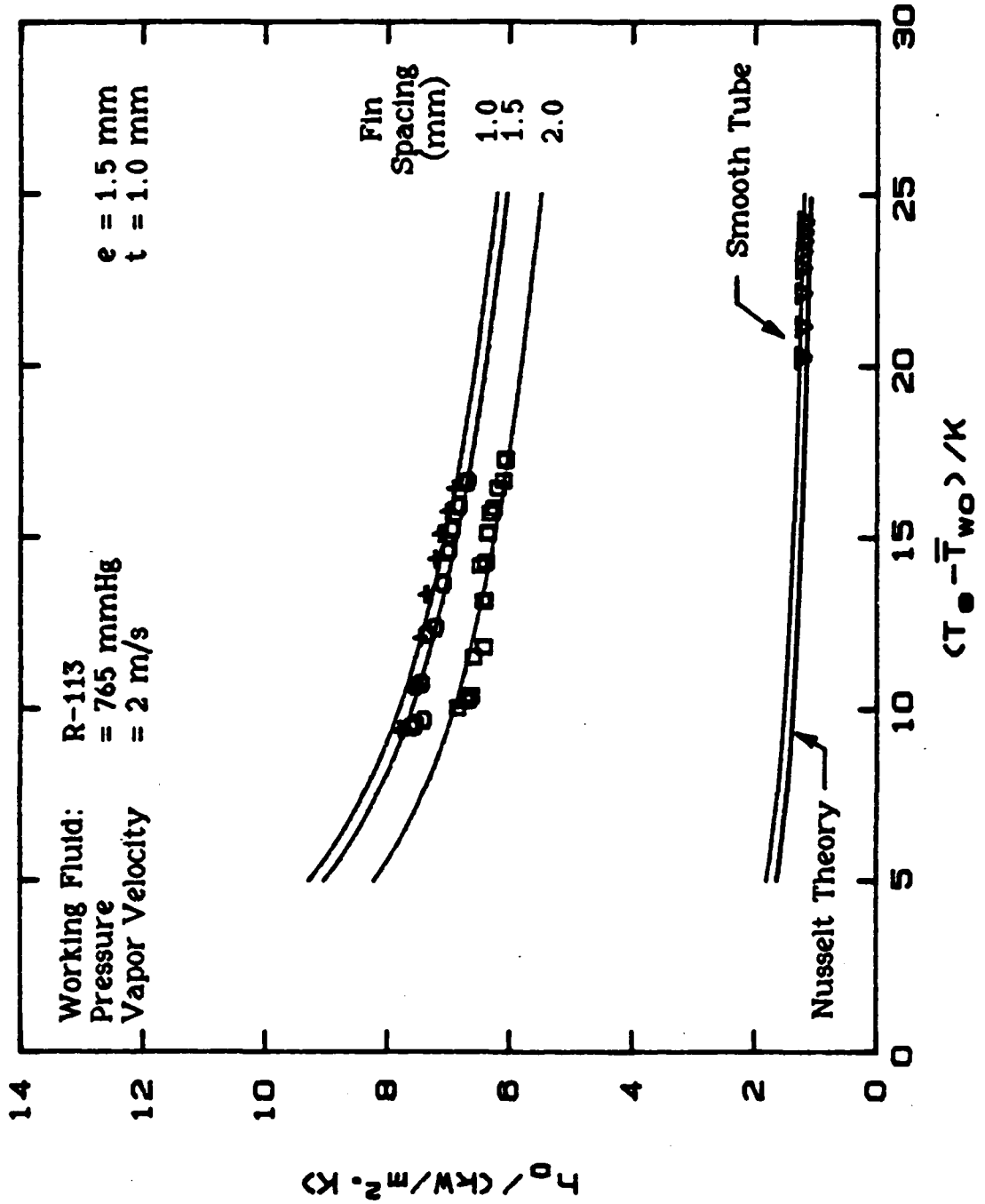

Figure 5.7 Effect of Fin Spacing on Vapor-Side Coefficient for Tubes with Fin Height of 1.5 mm and Fin Thickness of 1.0 mm.

The data presented in Figures 5.2, 5.5, 5.6, and 5.7 are replotted in Figure 5.8 on a different basis showing the fin height as a parameter. Notice that the ordinate represents the vapor-side enhancement ratio based on constant temperature drop across the condensate film ($\epsilon_{\Delta T}$) as defined below.

By definition,

$$q_f = h_f \, \Delta T_f \quad , \tag{5.3}$$

and

$$q_s = h_s \, \Delta T_s \quad . \tag{5.4}$$

From these equations:

$$h_f = a_f \, \Delta T_s^{-0.25} \tag{5.5}$$

and

$$h_s = a_s \, \Delta T_s^{-0.25} \quad . \tag{5.6}$$

$$\therefore \epsilon_{\Delta T} = \frac{h_f}{h_s} = \frac{a_f}{a_s} \left[\frac{\Delta T_s}{\Delta T_f} \right]^{0.25} \tag{5.7}$$

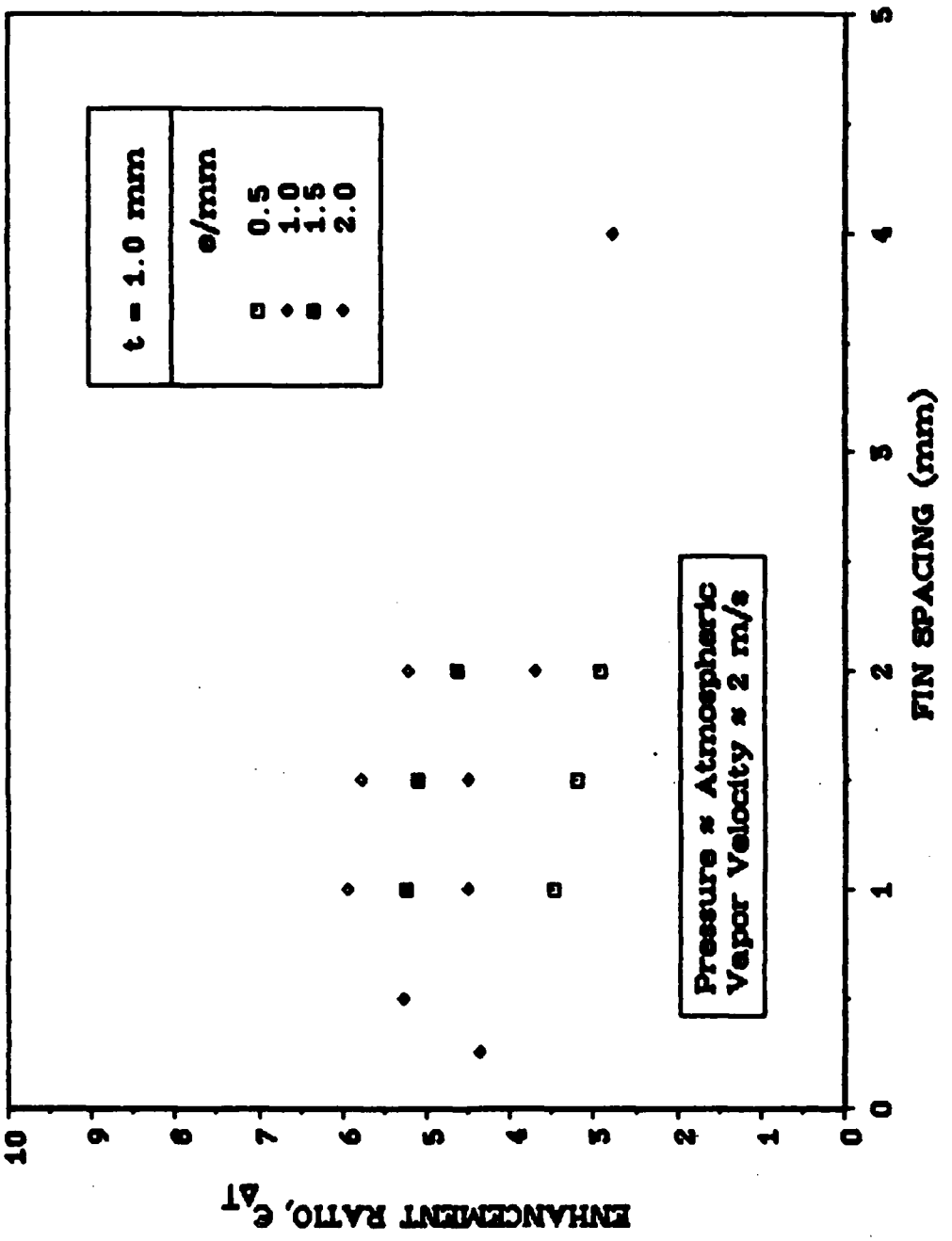

Figure 5.8 Effect of Fin Spacing on Vapor-Side Enhancement Ratio with Fin Height as a Parameter.

Thus, as proposed by Masuda and Rose [Ref. 15], for constant temperature drop across the condensate film (i.e., $\Delta T_f = \Delta T_s$),

$$\epsilon_{\Delta T} = \frac{a_f}{a_s} \tag{5.8}$$

On the other hand, for constant heat-flux conditions (i.e., $q_f = q_s$),

$$h_f \Delta T_f = h_s \Delta T_s \tag{5.9}$$

$$\epsilon_q = \frac{h_f}{h_s} = \frac{\Delta T_s}{\Delta T_f} \tag{5.10}$$

$$\frac{\Delta T_s}{\Delta T_f} = \left[\frac{a_f}{a_s}\right]^{4/3} \tag{5.11}$$

From equations (5.1) and (5.2),

$$\therefore \epsilon_q = \left[\frac{a_f}{a_s}\right]^{4/3} \tag{5.12}$$

$$\therefore \epsilon_q = \epsilon_{\Delta T}^{4/3} \tag{5.13}$$

According to Figure 5.8, for a given fin spacing, the performance increases monotonically with increasing fin height. Figure 5.9 shows a cross-plot of Figure 5.8, together with the area

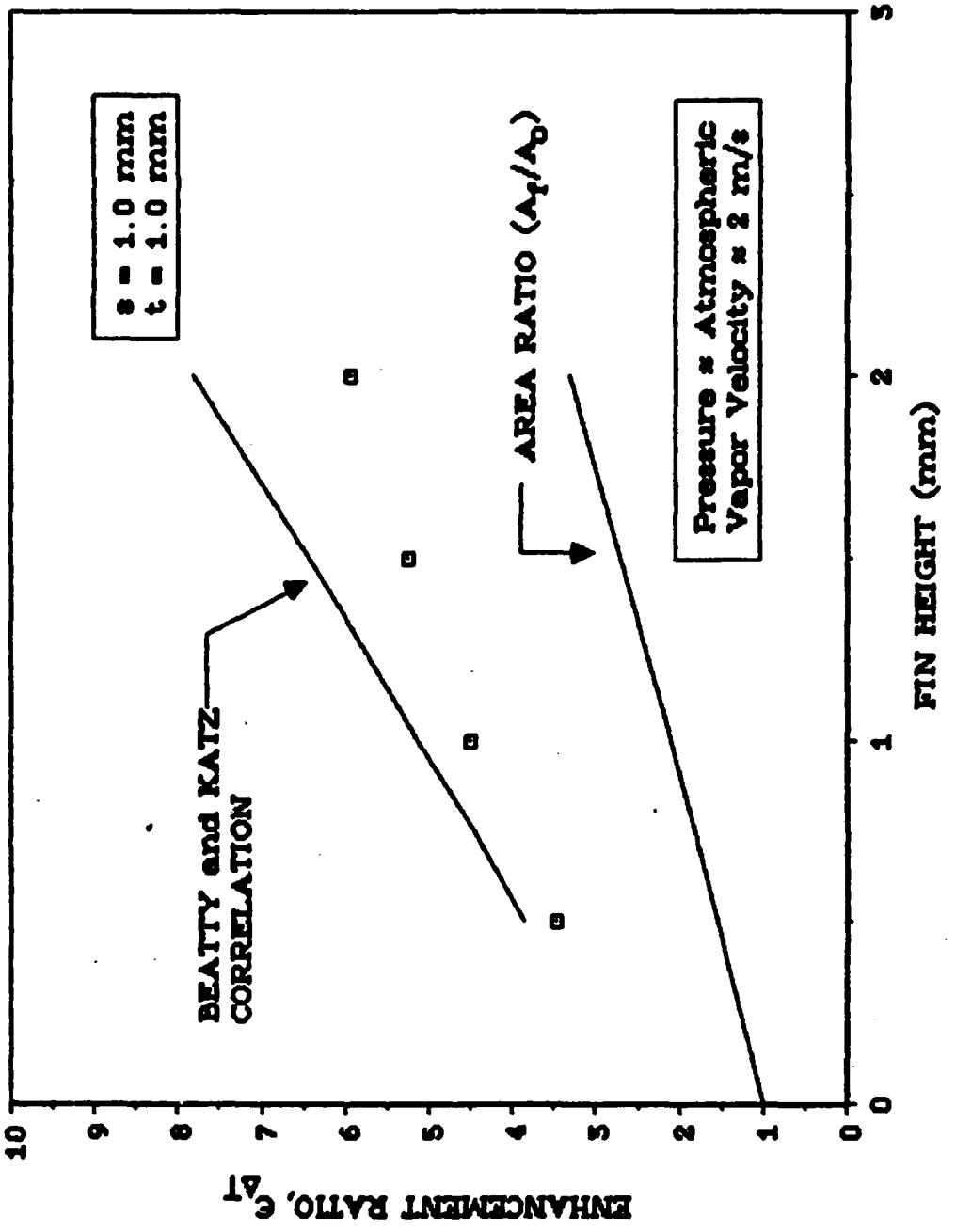

Figure 5.9 Effect of Fin Height on Vapor-Side Enhancement Ratio.

ratio and Beatty and Katz correlation [Ref. 7], for a fin spacing of 1.0 mm. Notice that when the fin height increases from 0.5 mm to 1.0 mm, the enhancement ratio increases by 29 percent and the area ratio increases by 37 percent. However, when the fin height is increased from 1.0 mm to 2.0 mm, the enhancement increases by only 33 percent, while the area ratio increases by 58 percent.

Figure 5.10 shows the variation of vapor-side enhancement ratio with the fin thickness as a parameter. As can be seen, for a given fin spacing, the tubes with a fin thickness of 1.0 mm show performance poorer than the tubes with smaller fin thicknesses. This observation can be easily explained by the decreasing area ratio with increasing fin thickness. However, a clear trend is not seen when comparing the performance of tubes with fin thicknesses of 0.5 mm and 0.75 mm. For example, for tubes with a fin spacing of 0.5 mm, the tubes with a fin thickness of 0.5 mm results in better performance than the tube with a fin thickness of 0.75 mm, which can be explained by the area ratio. On the other hand, for tubes with a spacing of 1.0 mm or more, the tubes with a fin thickness of 0.75 mm outperform the tubes with a fin thickness of 0.5 mm.

Notice that while the tube with a fin spacing of 0.25 mm outperforms the tube with a fin spacing of 0.5 mm in the set of tubes with a fin thickness of 0.5 mm, the trend is reversed in the set of tubes with a fin thickness of 1.0 mm. This observation may be explained by considering the condensate being fed by the fin tips

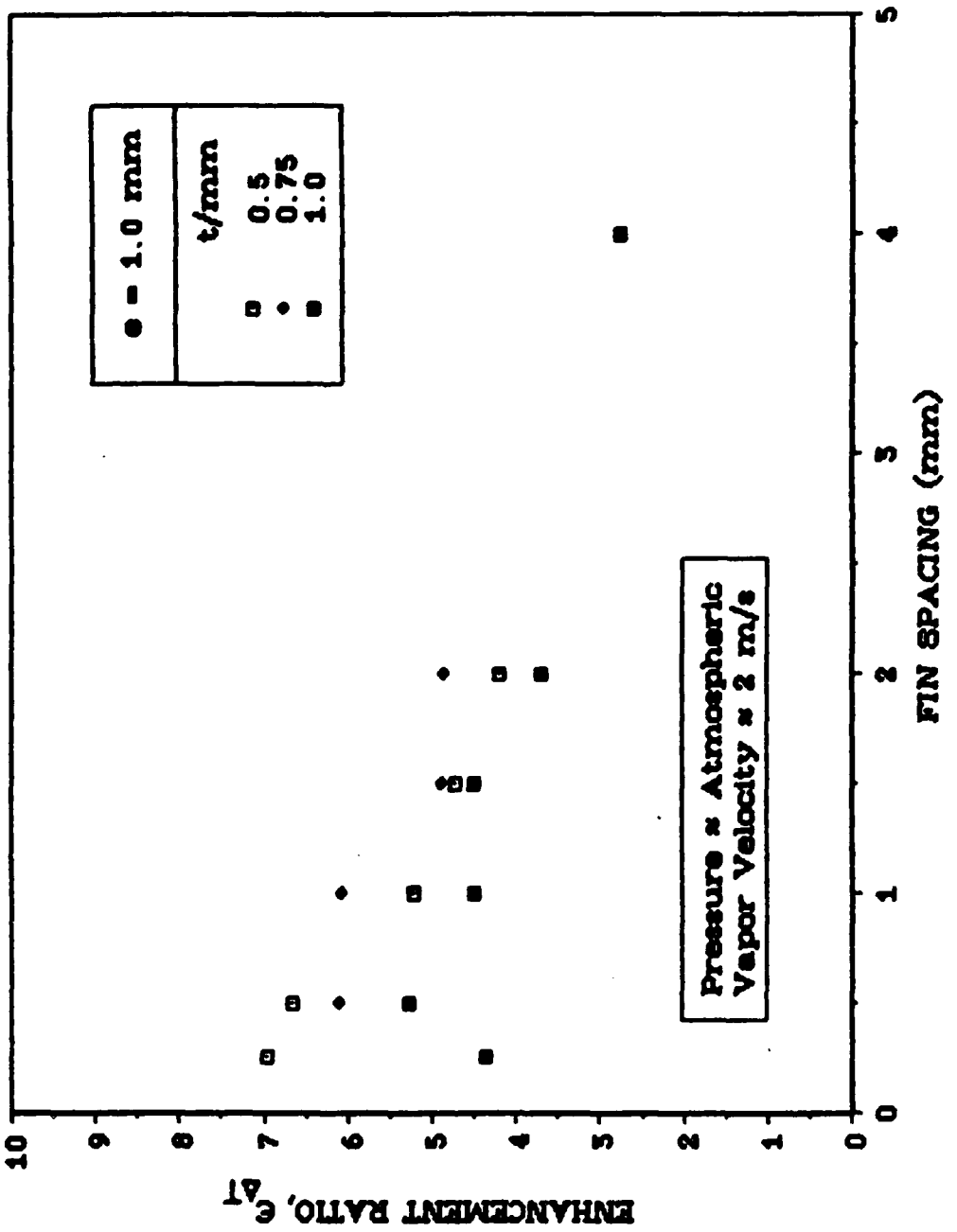

Figure 5.10 Effect of Fin Thickness on Vapor-Side Enhancement Ratio.

to the fin sides. Notice that as the fin thickness increases, the amount of condensate fed to the fin sides increases, thereby increasing the condensate film thickness on the sides. Thus, the heat-transfer performance decreases with increasing fin thickness while all other dimensions are held constant for small fin spacings.

3. Comparison of R-113 Data with Steam Data

Figures 5.11 through 5.16 present a direct comparison of vapor-side enhancement with steam data [Ref. 12, 13] for the six sets of tubes discussed in Section C above. Also, for comparison purposes, curves representing the area ratio (A_f/A_o) and the Beatty and Katz correlation [Ref. 7] ($\eta_f = 1.0$) are shown on these figures.

These figures show that, for any given tube, the enhancements for R-113 are always greater than that for steam. This is a direct result of significantly different surface tension values for these two fluids. Notice that water has surface tension values of 0.068 N/m at 48 °C (i.e., at a saturation pressure of 85 mmHg) and 0.059 N/m at 100 °C (i.e., at atmospheric pressure), while R-113 has a surface tension of 0.015 N/m at 48 °C. As listed in Table 5.2, the computed condensate retention angles are much lower for the case with R-113 than with steam. Since the heat-transfer performance through the flooded region is poorer than through the unflooded region, heat-transfer performance suffers significantly more when condensing steam than when condensing R-113.

Steam data show an optimum fin spacing of 1.5 mm (except Figure 5.16 which shows that the tube with a fin spacing of

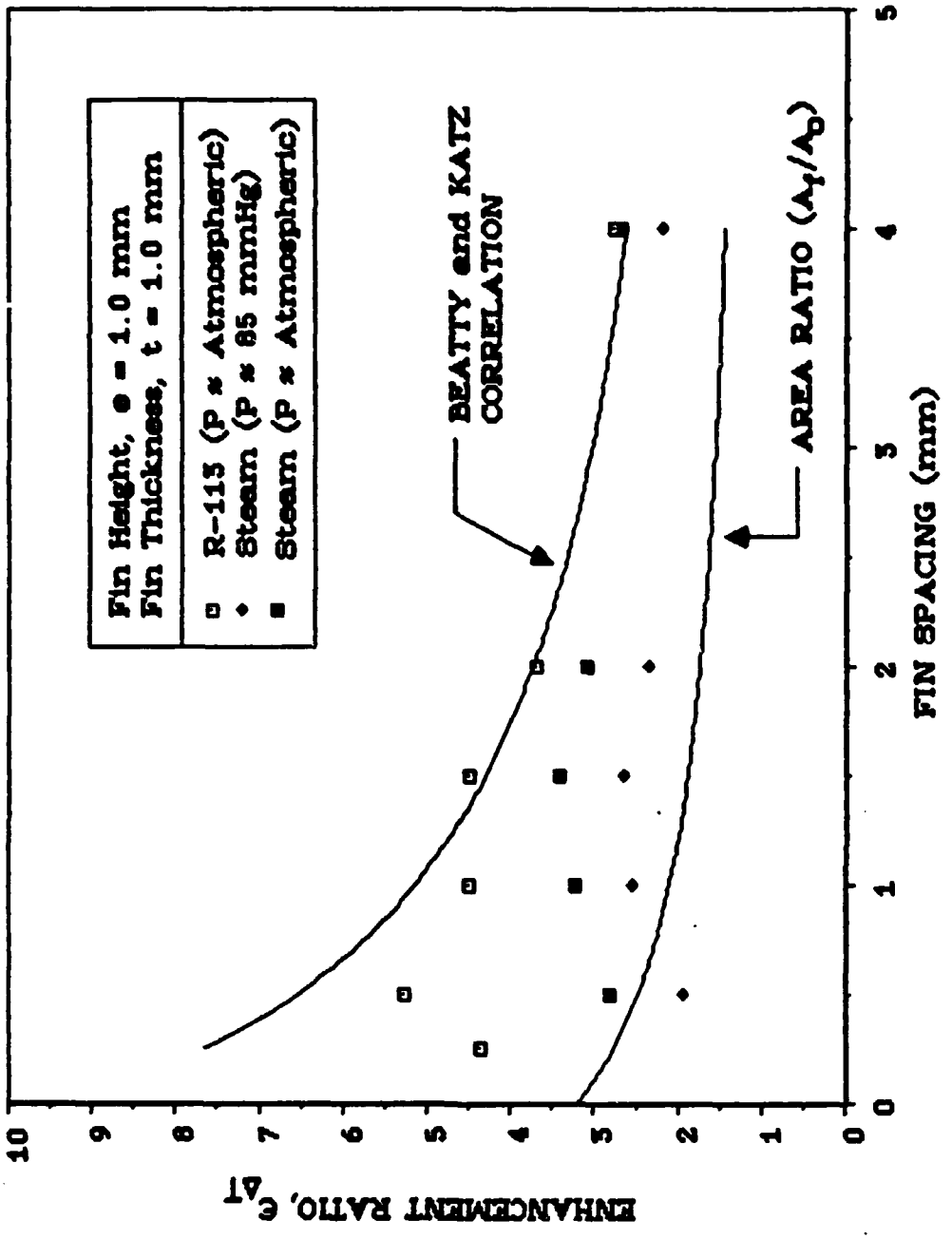

Figure 5.11 Comparison of R-113 Data with Steam Data [Ref. 12] and Beatty and Katz Correlation [Ref. 7] for Tubes with Fin Height of 1.0 mm and Fin Thickness of 1.0 mm.

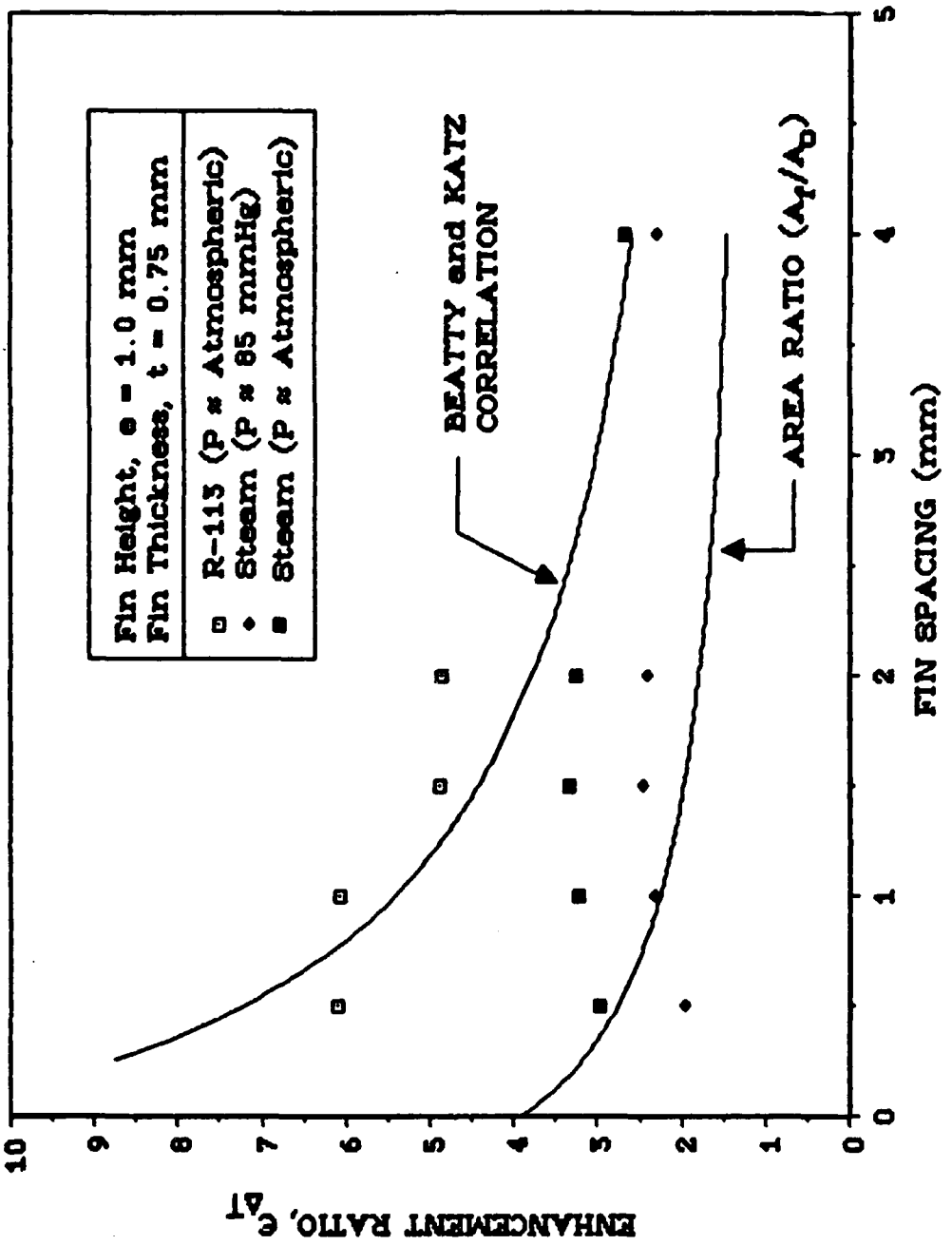

Figure 5.12 Comparison of R-113 Data with Steam Data [Ref. 12] and Beatty and Katz Correlation [Ref. 7] for Tubes with Fin Height of 1.0 mm and Fin Thickness of 0.75 mm.

AD-A185 383 CONDENSATION HEAT-TRANSFER MEASUREMENTS OF REFRIGERANTS ON EXTERNALLY ENHANCED TUBES(U) NAVAL POSTGRADUATE SCHOOL MONTEREY CA D S ZEBROWSKI JUN 87 2/2

UNCLASSIFIED F/G 13/1 NL

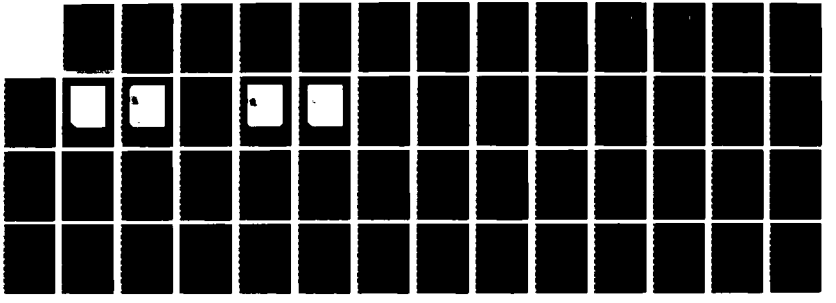

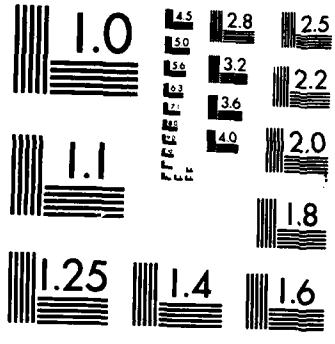

MICROCOPY RESOLUTION TEST CHART
NATIONAL BUREAU OF STANDARDS-1963-A

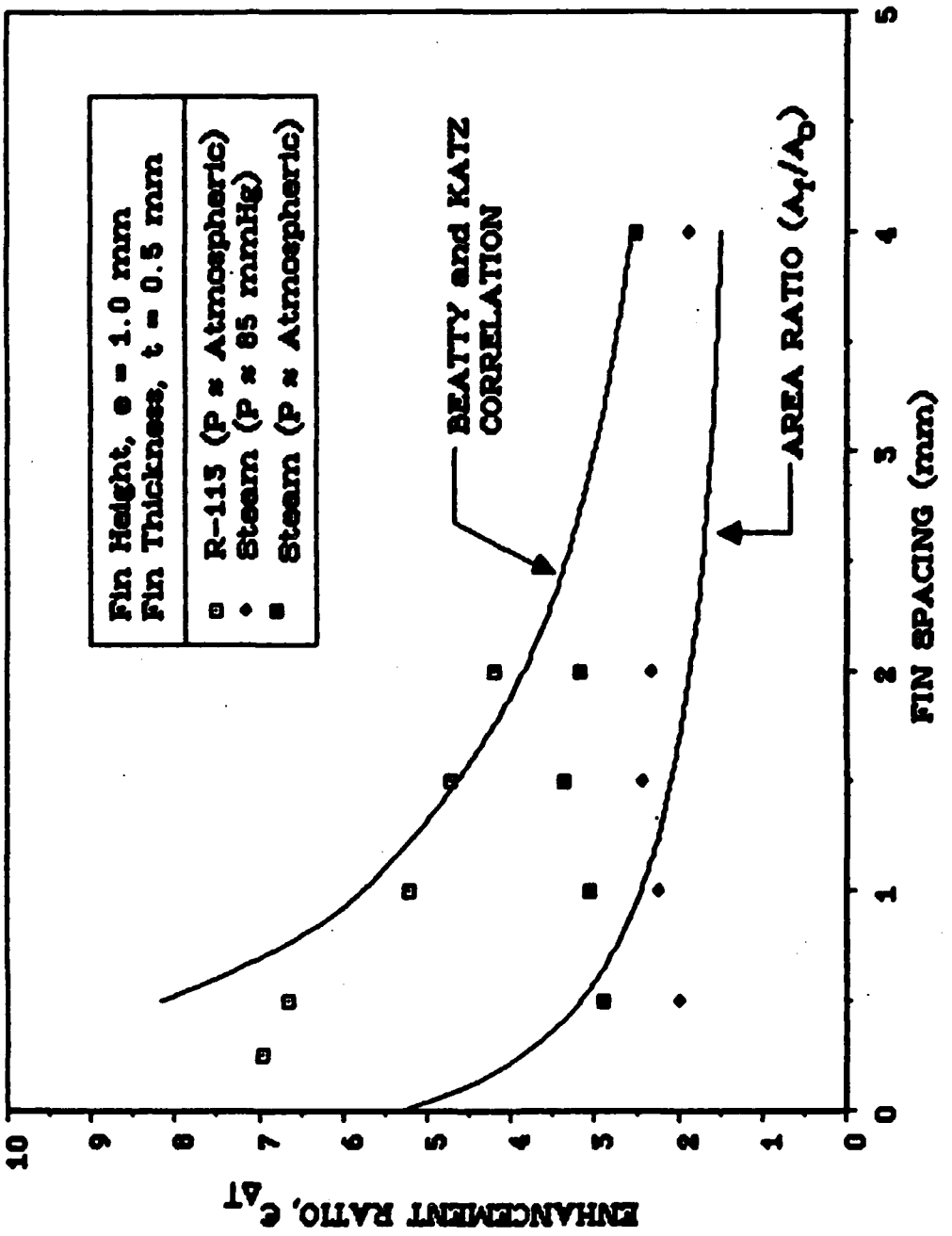

Figure 5.13 Comparison of R-113 Data with Steam Data [Ref. 12] and Beatty and Katz Correlation [Ref. 7] for Tubes with Fin Height of 1.0 mm and Fin Thickness of 0.5 mm.

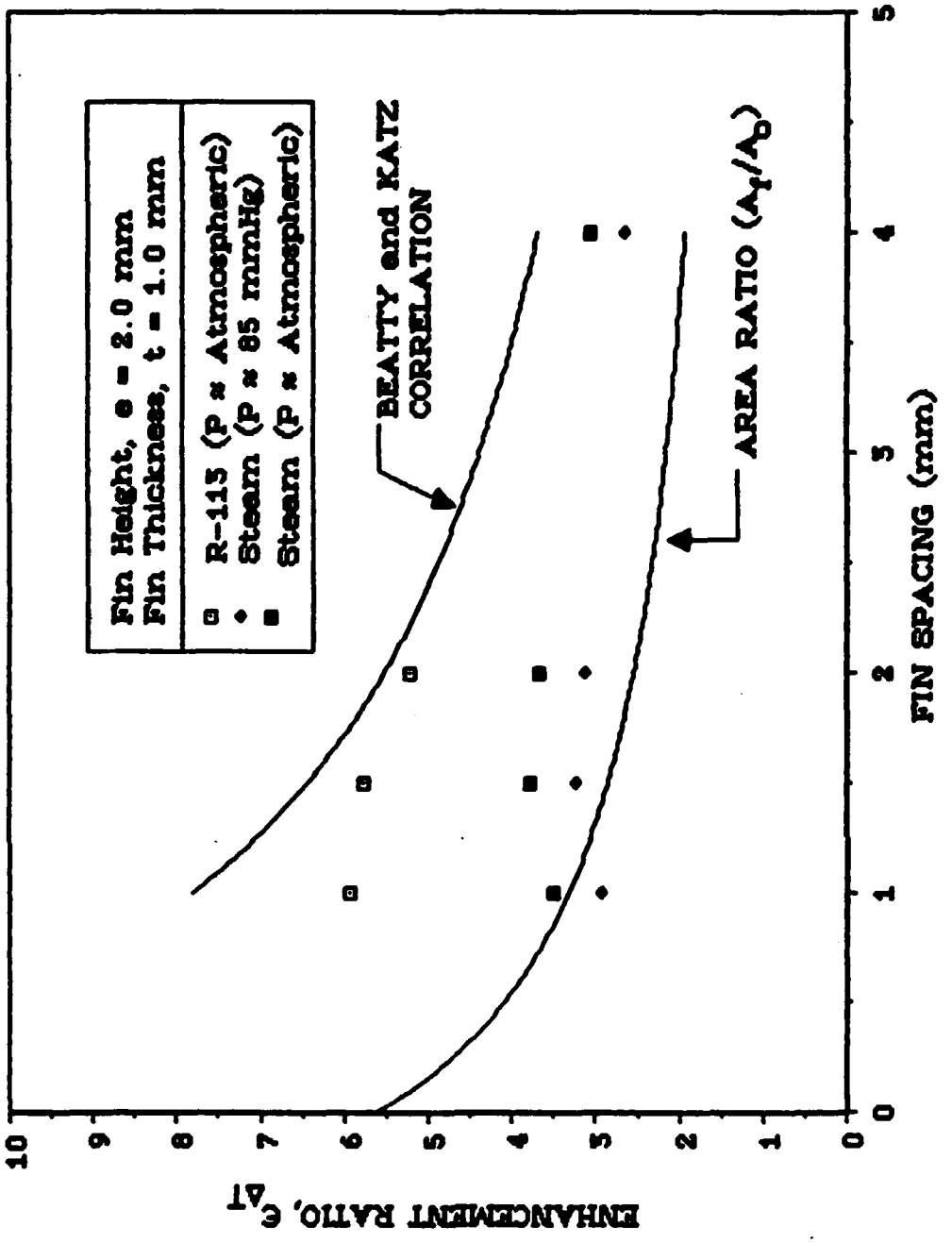

Figure 5.14 Comparison of R-113 Data with Steam Data [Ref. 12] and Beatty and Katz Correlation [Ref. 7] for Tubes with Fin Height of 2.0 mm and Fin Thickness of 1.0 mm.

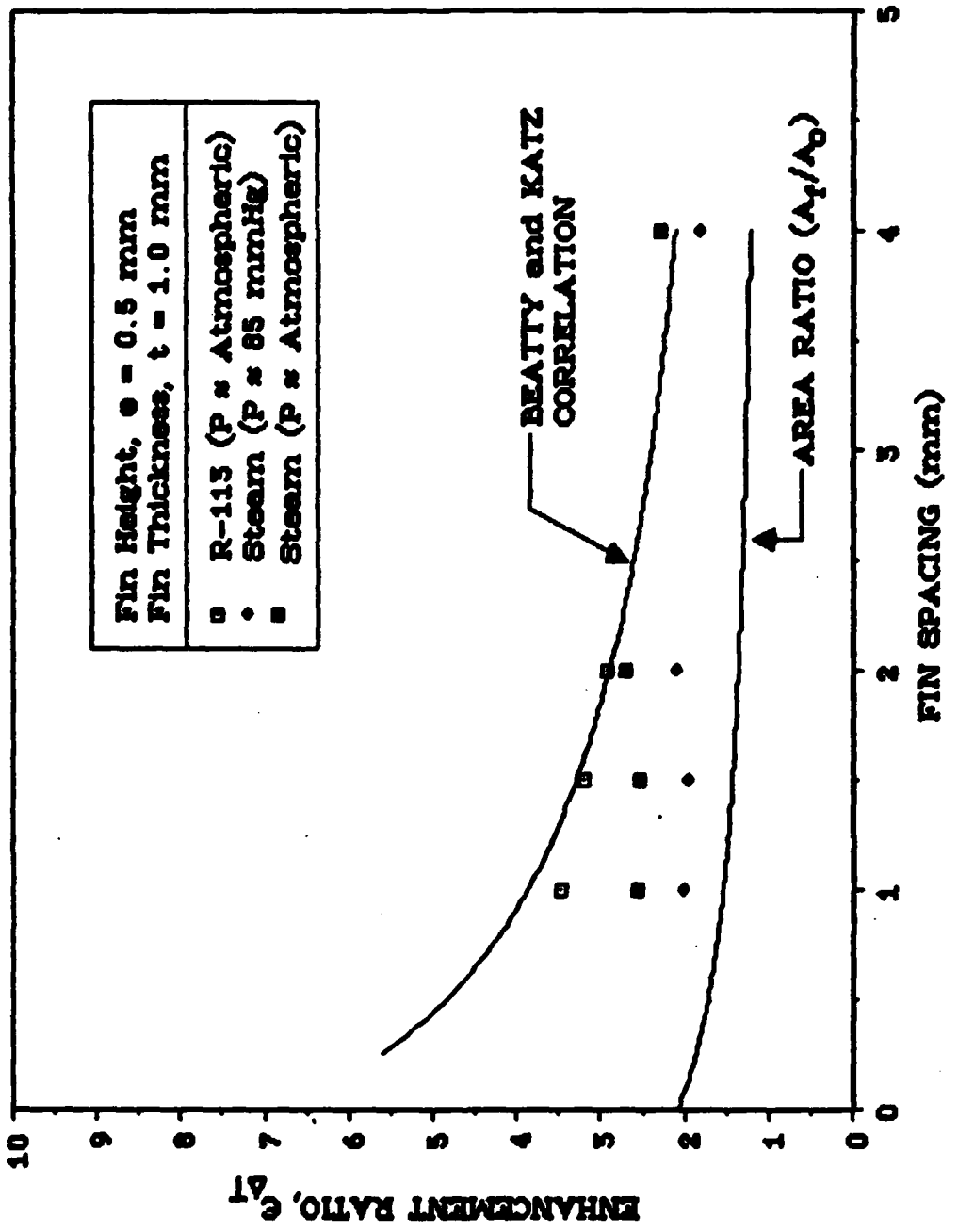

Figure 5.15 Comparison of R-113 Data with Steam Data [Ref. 13] and Beatty and Katz Correlation [Ref. 7] for Tubes with Fin Height of 0.5 mm and Fin Thickness of 1.0 mm.

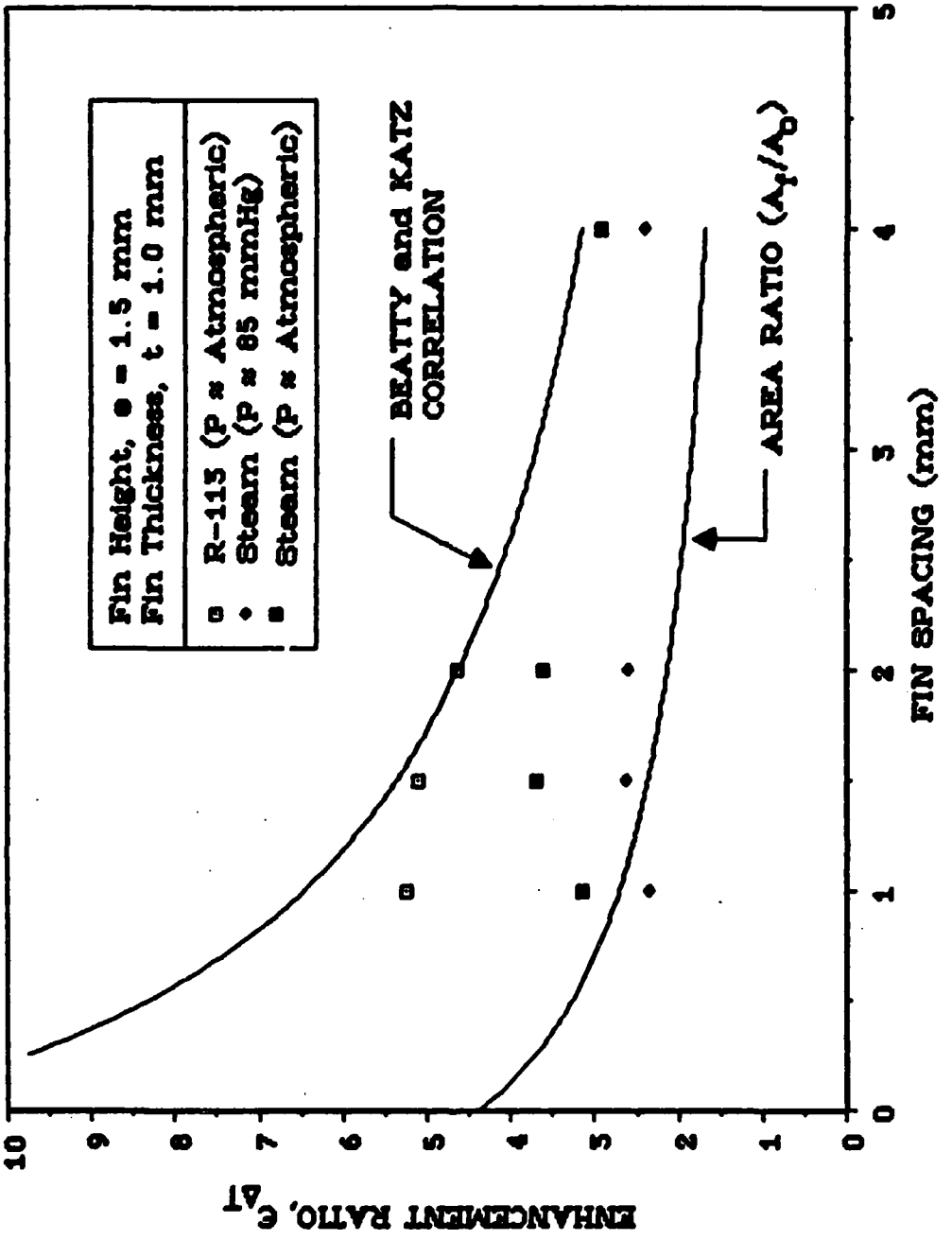

Figure 5.16 Comparison of R-113 Data with Steam Data [Ref. 13] and Beatty and Katz Correlation [Ref. 7] for Tubes with Fin Height of 1.5 mm and Fin Thickness of 1.0 mm.

TABLE 5.2
COMPUTED CONDENSATE RETENTION ANGLES FOR TUBES TESTED

Tube No.	Fin Height e (mm)	Fin Thickness t (mm)	Fin Spacing s (mm)	Condensate Retention Angle		
				Steam (85 mmHg)	Steam (Atm.)	R-113 (Atm.)
S01	-	-	-	-	-	-
D02	1.0	1.0	0.25	180	180	77
F04			0.5	180	180	52
F05			1.0	109	101	36
F06			1.5	84	78	29
F07			2.0	70	66	25
F08			4.0	48	45	18
F10	1.0	0.75	0.5	180	180	52
F11			1.0	109	101	36
F12			1.5	84	78	29
F13			2.0	70	66	25
D01	1.0	0.5	0.25	180	180	77
F15			0.5	180	180	52
F16			1.0	109	101	36
F17			1.5	84	78	29
F18			2.0	70	66	18
F22	2.0	1.0	1.0	103	95	34
F23			1.5	79	74	28
F24			2.0	67	63	24
F26	0.5	1.0	1.0	113	105	37
F27			1.5	86	81	30
F28			2.0	72	68	26
F30	1.5	1.0	1.0	106	98	35
F31			1.5	81	76	29
F32			2.0	69	64	25

2.0 mm slightly outperforms the tube with a fin spacing of 1.5 mm). However, R-113 data show an optimum fin spacing of less than 0.5 mm. Figure 5.11 shows that the performance of the tube with a fin spacing of 0.25 mm is less than that of the tube with a spacing of 0.5 mm. On the other hand, Figure 5.13 shows that the tube with a fin spacing of 0.25 mm slightly outperforms the tube with a fin spacing of 0.5 mm. This suggests that the optimum fin spacing may actually lie between 0.25 mm and 0.5 mm.

It is evident that the optimum fin spacing decreases and the optimum enhancement ratio increases with decreasing surface tension of the condensate. It appears that this phenomenon is controlled by the extent of flooding.

C. INDIRECT MEASUREMENT OF THE LOCAL AND AVERAGE HEAT-TRANSFER PERFORMANCE

1. Inside Heat-Transfer Coefficient

In contrast to the discussion provided in Section B.1 above for the case where the inside conditions were unchanged, the inside geometry varied with the extent of the internal insulation during the testing performed for this section. As shown in Figure 3.9, the internal insulation was held in place by a T-shaped device. Since only a portion of the circumference actually allowed heat transfer, the Sieder-Tate-type coefficient must vary with the angle of insulation.

Figure 5.17 shows the variation of C_i (based on the total inside area) with the half-angle of insulation. Also shown is the

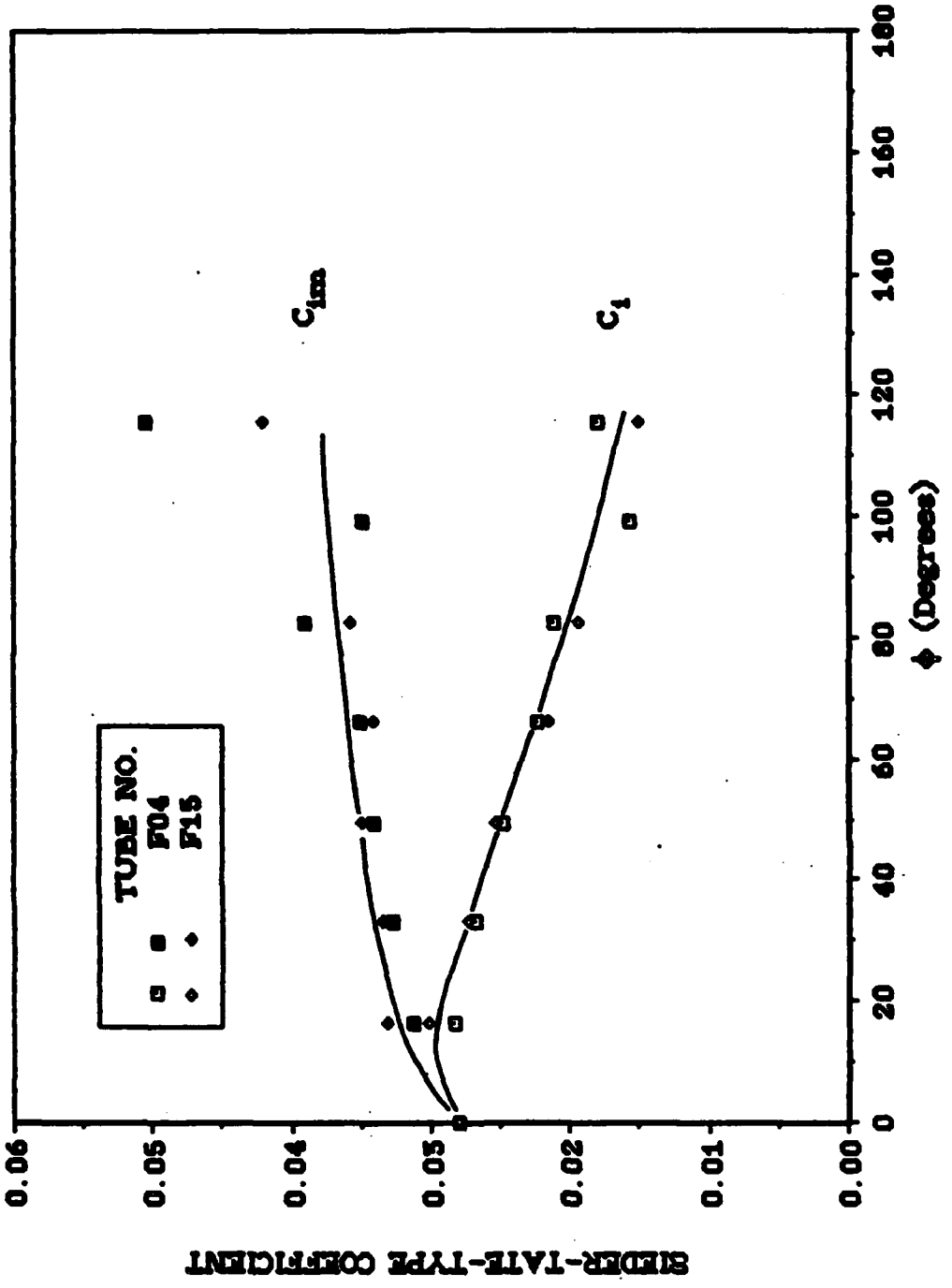

Figure 5.17 Effect of Insulating Tube Perimeter on Inside Heat-Transfer Performance.

modified value (i.e., C_{im}) obtained by correcting for the actual area of heat transfer. That is:

$$C_{im} = C_i \frac{180 - \phi}{180} \quad . \tag{5.14}$$

Notice that for both tubes (tube F04 and F15), C_i and C_{im} show similar trends. The presence of an unheated portion of the tube allows heat to be convected away from the heated portion across the tube cross-section. This turbulent convection decreases the apparent bulk mixture temperature within the heated portion, and the heat-transfer performance will be enhanced, as shown by the trend for C_{im}. While this argument provides a qualitative explanation for the experimental measurements, any quantitative explanation is beyond the scope of this investigation.

2. Indirect Measurement of Vapor-Side Heat-Transfer Coefficient

Figure 5.18 shows the variation of the vapor-side coefficient for tube No. F04 with the vapor-side temperature drop having the half angle of insulation as a parameter. Notice that the vapor-side coefficient which represents the average value for the uninsulated lower portion of the tube is computed based upon the total area of the corresponding smooth tube. Figure 5.19 shows similar data for tube No. F15. Using the analysis procedures of Lester [Ref. 30] (see Section 4.B.2.b), the average and local enhancement ratios were computed and are plotted in Figures 5.20

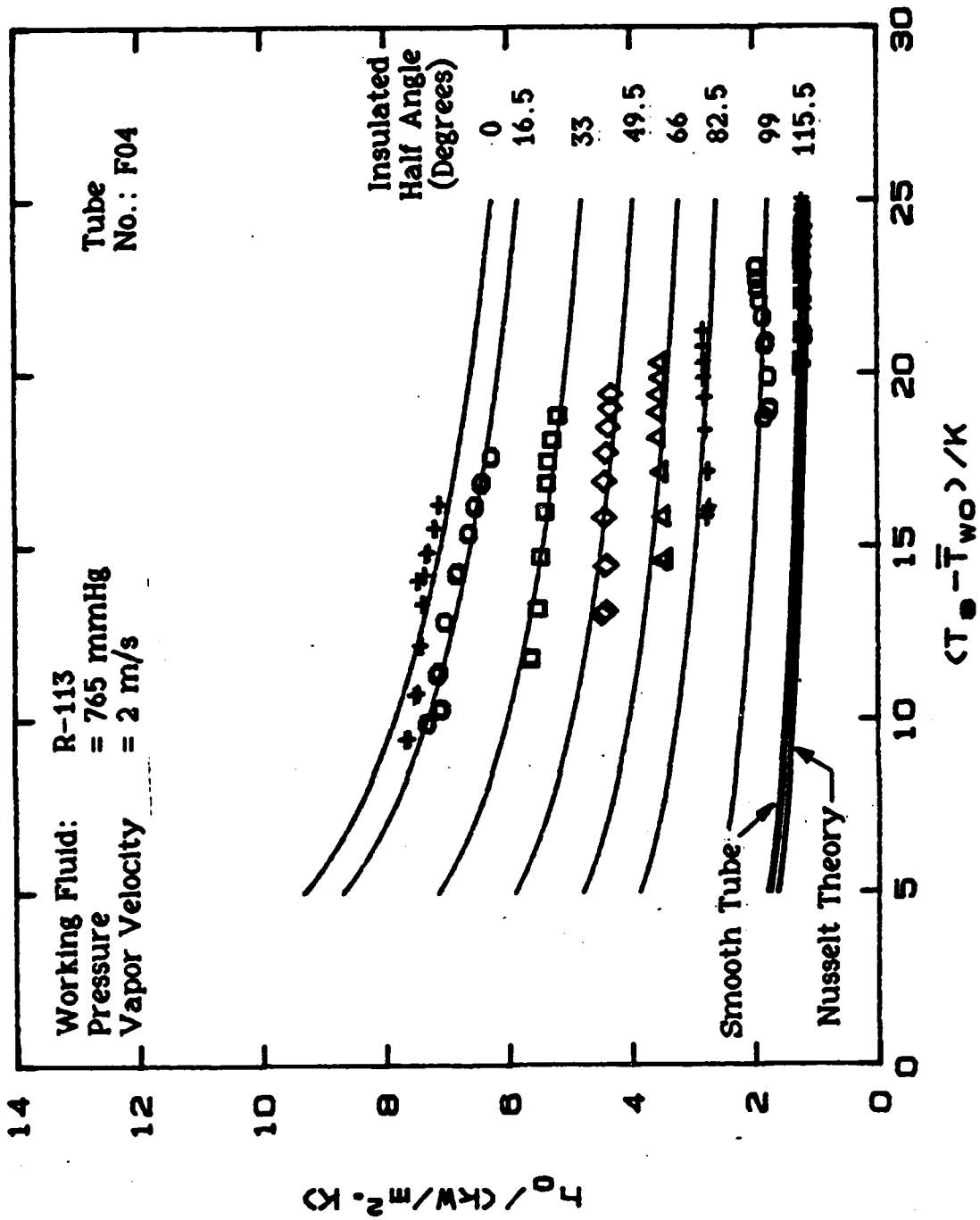

Figure 5.18 Effect of Insulating Tube Perimeter on Vapor-Side Coefficient for Tube F04.

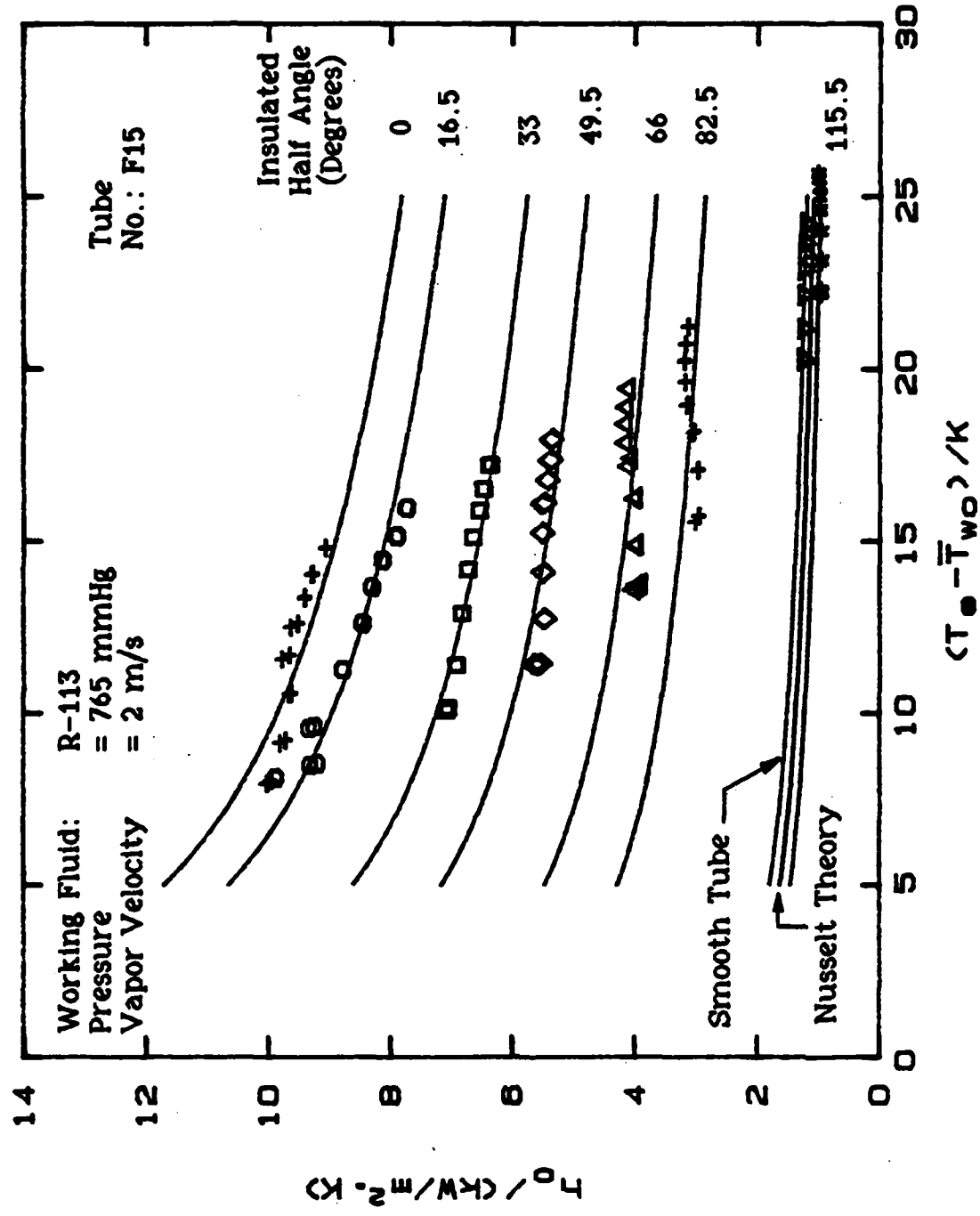

Figure 5.19 Effect of Insulating Tube Perimeter on Vapor-Side Coefficient for Tube F15.

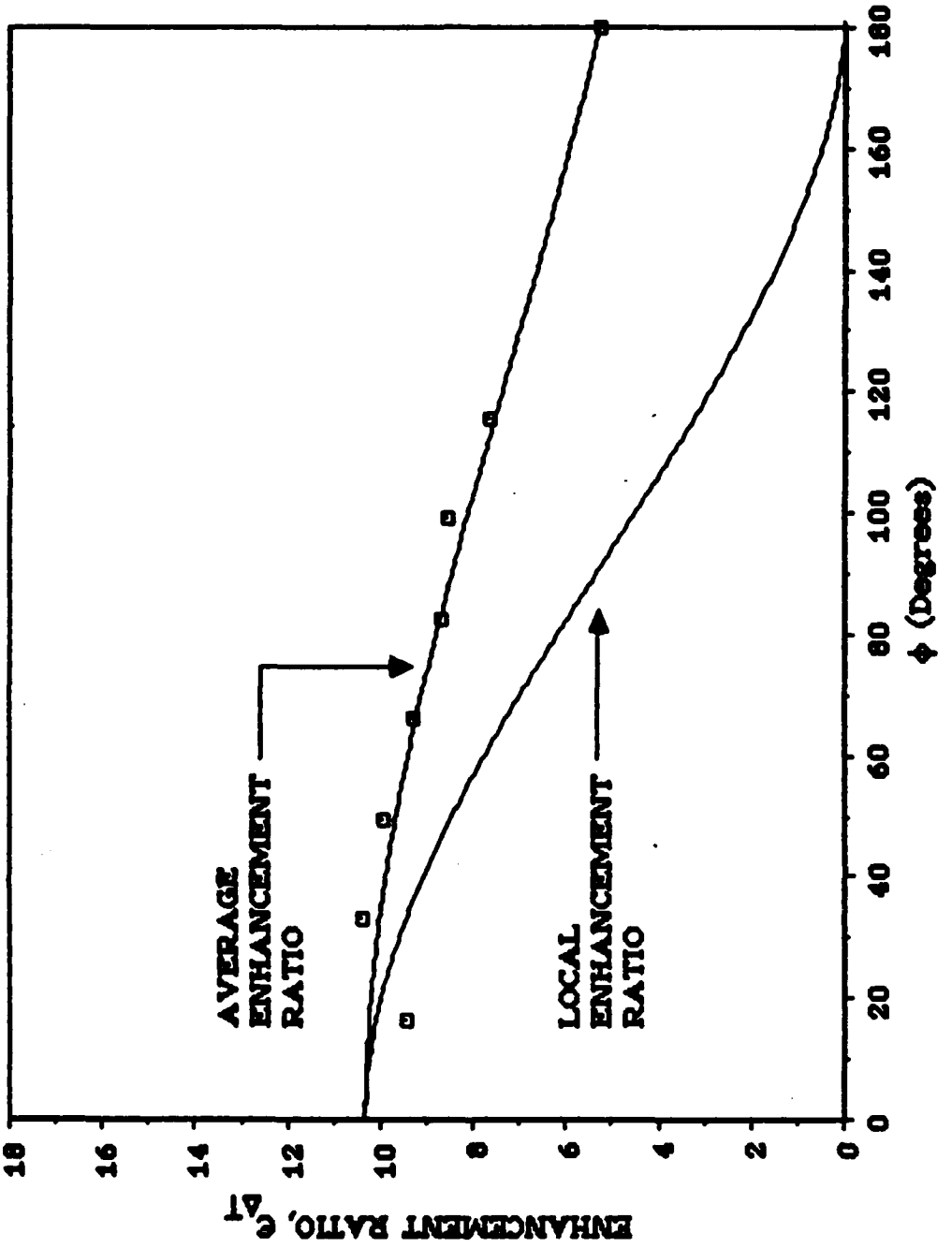

Figure 5.20 Variation of Third-Order-Polynomial-Based Local and Average Enhancement Ratios for Tube F04.

and 5.21 for tube F04 and F15 respectively. As can be seen, the local enhancement ratio at the top of the tube is approximately twice the average value for the entire tube

Notice that Figure 5.21 shows negative values for the local enhancement ratio for $\phi > 150°$, indicative of experimental uncertainties and the possible choice of an inappropriate form (third-order polynomial) to express the local enhancement ratio. For example, an improved representation might be possible by using a different form for the local enhancement ratio such as cosine functions. A more realistic form may also be guided by theoretical considerations. Foe example, an inflection point may be allowed at the computed condensate retention angle (i.e., $\epsilon_\phi" = 0$ at $\phi = \pi - \psi$) since the local heat-transfer coefficient is expected to undergo a significant variation at the flooding point.

D. VISUAL OBSERVATIONS

During the operation of the single-tube apparatus, photographs were taken of tubes F15 (fin height of 1.0 mm and fin spacing of 0.5 mm) and F08 (fin height of 1.0 mm and fin spacing of 4.0 mm). At all heat fluxes, tube F04 showed columns of condensate always forming at the fins. As can be seen in Figure 5.22, at low heat fluxes the columns of condensate were unsteady and broke off. At high heat fluxes, the columns became steady and continuous as seen in Figure 5.23.

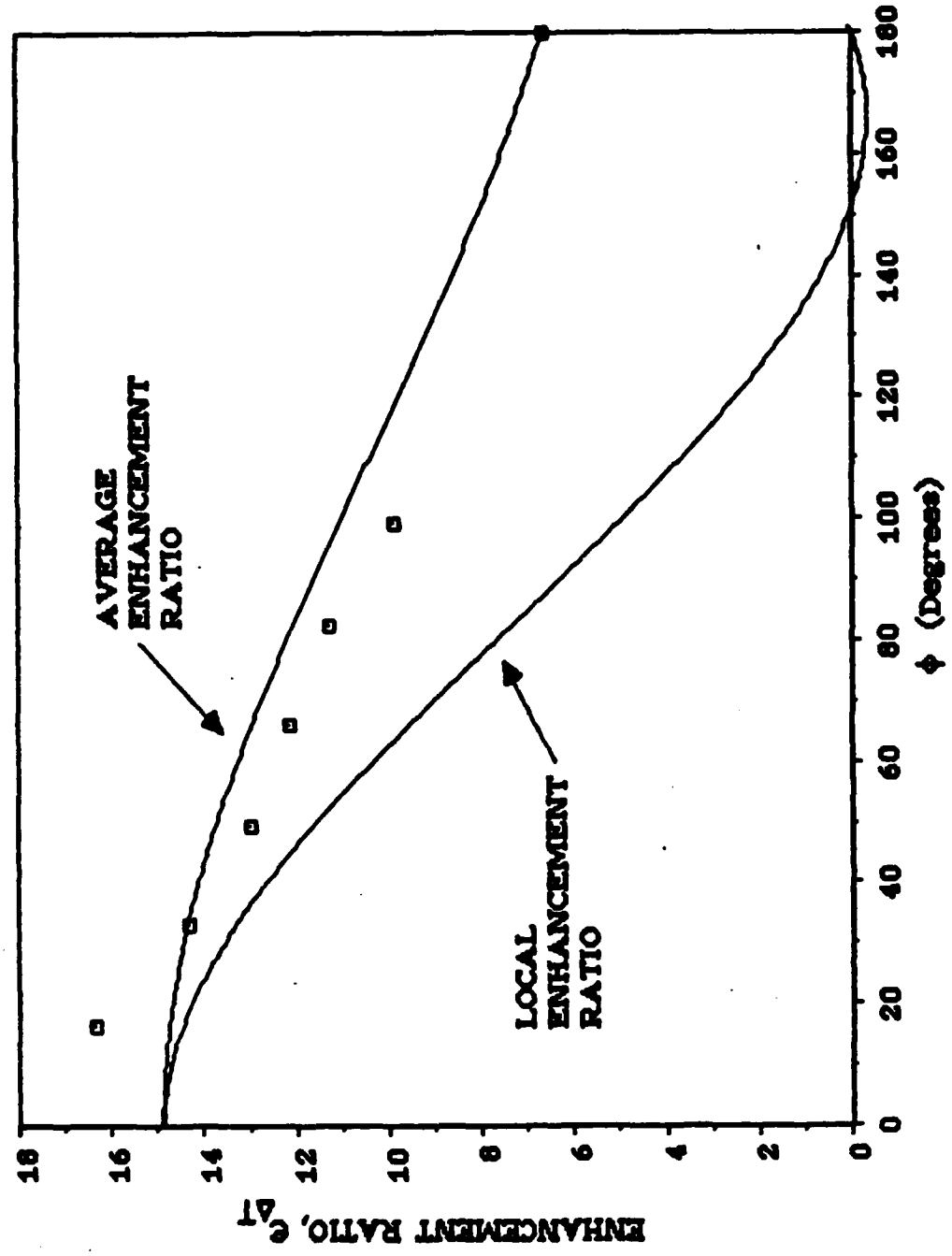

Figure 5.21 Variation of Third-Order-Polynomial-Based Local and Average Enhancement Ratios for Tube F15.

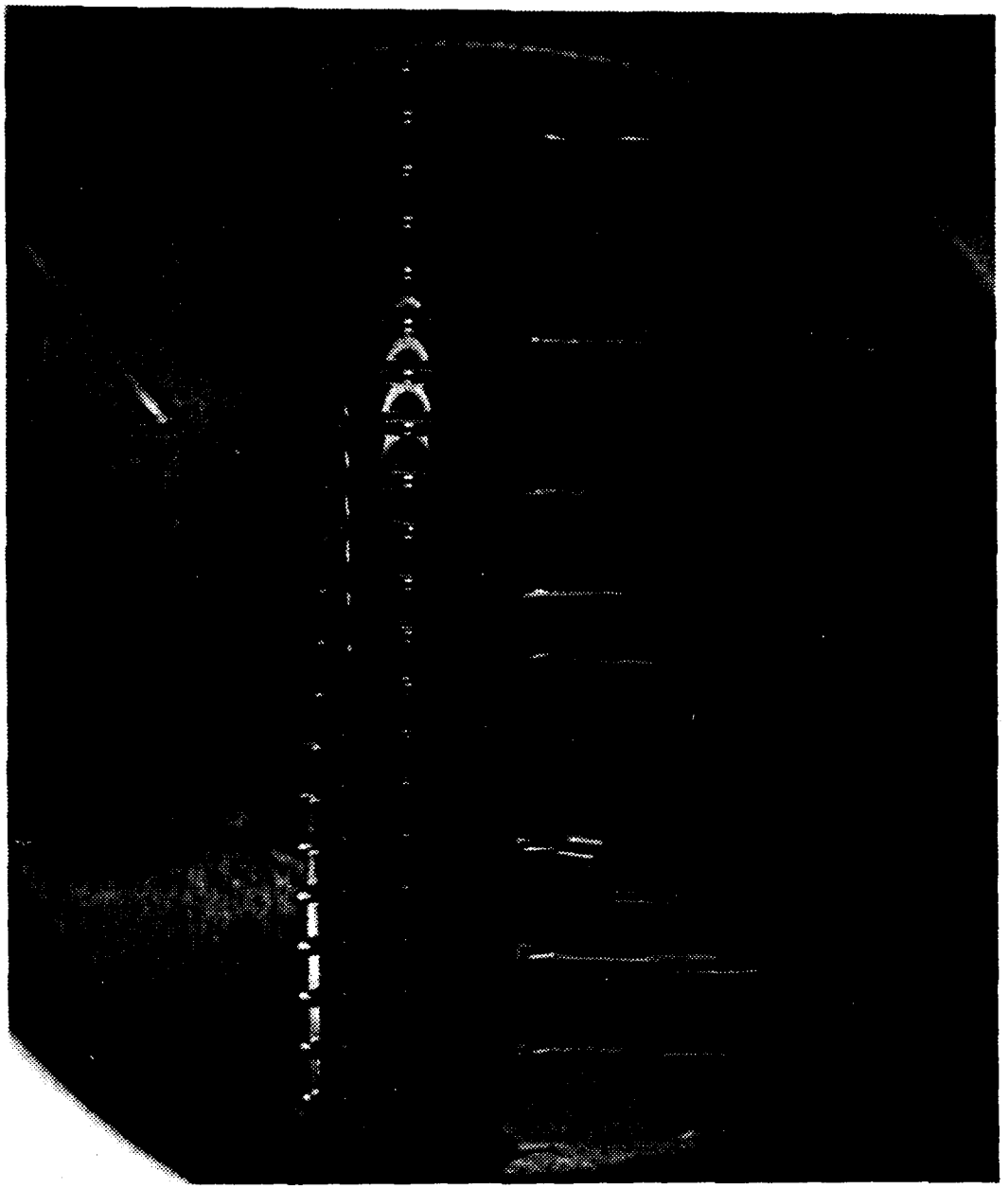

Figure 5.22 Photograph of Tube F08 Under Low Heat Flux.

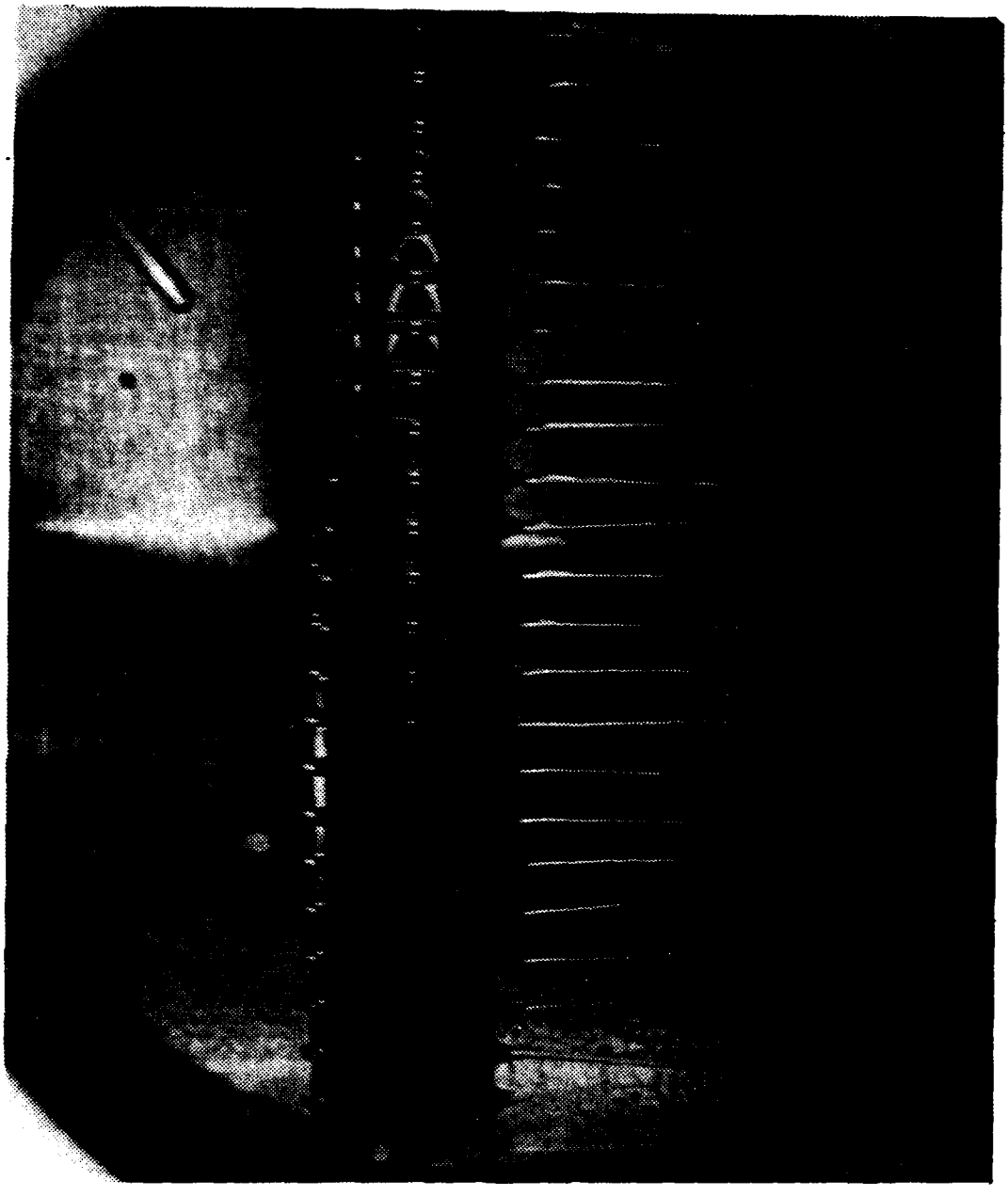

Figure 5.23 Photograph of Tube F08 Under High Heat Flux.

Figures 5.24 and 5.25 show tube F15 at low and high heat fluxes, respectively. As the heat flux increased, the distance between the columns decreased. At low heat fluxes the flow was nearly always steady, but an occasional perturbation could be seen.

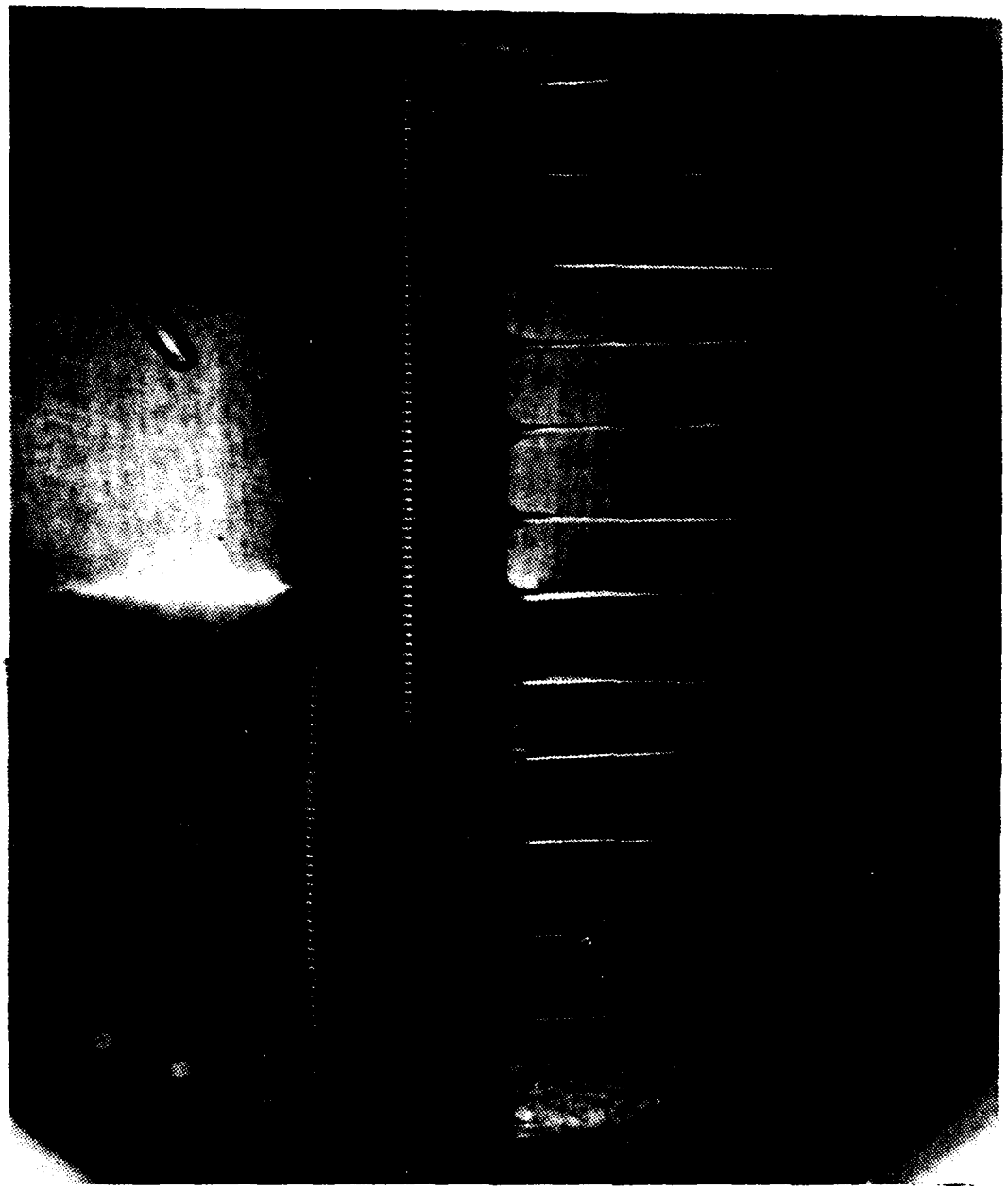

Figure 5.24 Photograph of Tube F15 Under Low Heat Flux.

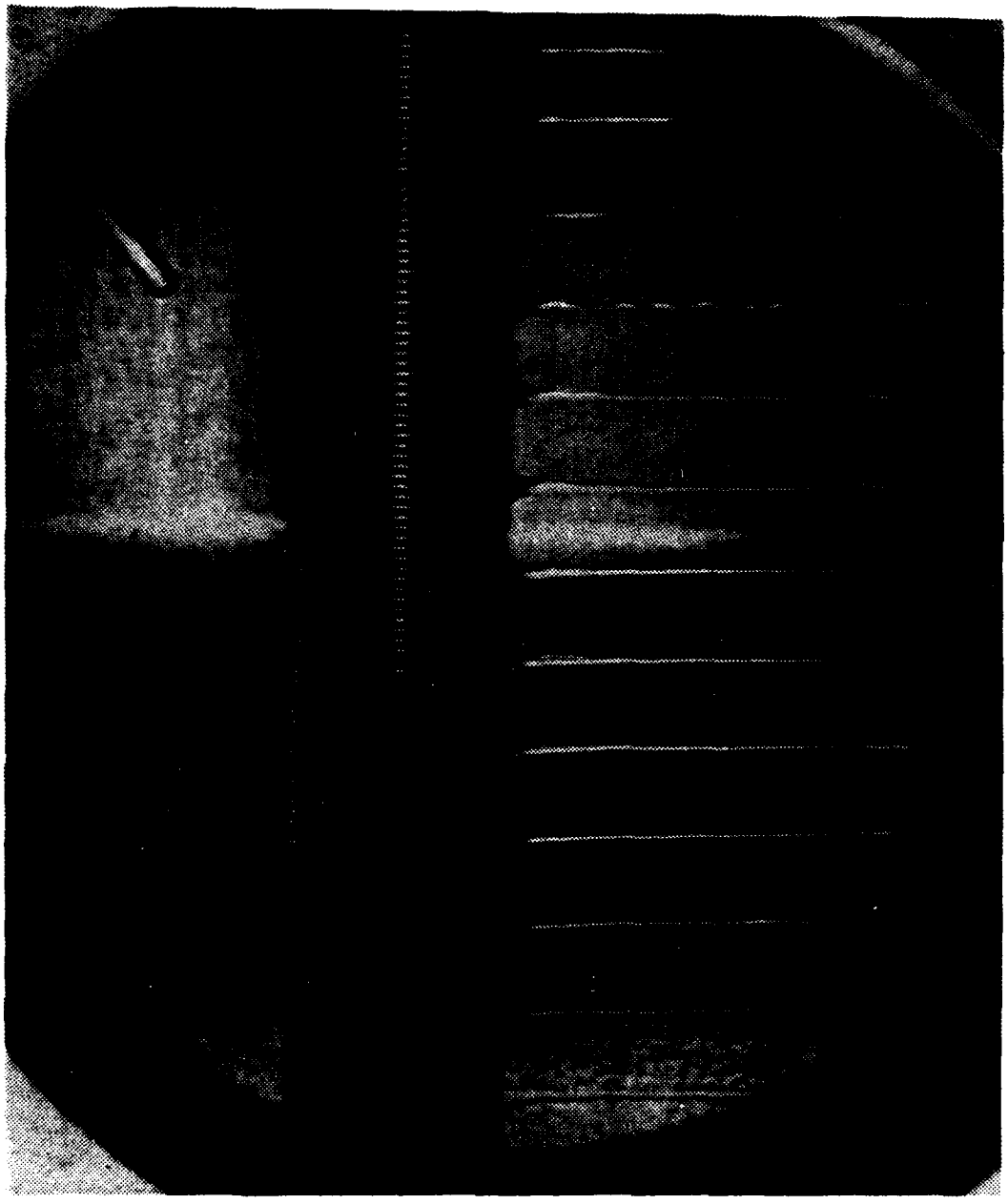

Figure 5.25 Photograph of Tube F15 Under High Heat Flux.

VI. CONCLUSIONS AND RECOMMENDATIONS

A. CONCLUSIONS

1. An apparatus has been designed and fabricated for testing of a 5-tube bundle with R-114 as the working fluid.

2. The data taken on tubes with rectangular-section fins show an optimum fin spacing of 0.25 mm to 0.5 mm for R-113 in contrast to a value of 1.5 mm for steam [Ref. 12].

3. Among the tubes with a 1.0 mm fin height, the tube with a fin spacing of 0.25 mm and a fin thickness of 0.5 mm outperformed the other tubes and showed a vapor-side enhancement ratio ($\epsilon_{\Delta T}$) of about 7.0. Thus, the optimum fin thickness appears to be 0.5 mm or less for R-113 compared to around 0.75 mm to 1.0 mm for steam [Ref. 12].

4. The vapor-side enhancement ratio increased with the fin height. However, the rate of increase in $\epsilon_{\Delta T}$ decreased with increasing fin height as also observed for steam [Ref. 13].

5. For tubes with fin spacings of 1.0 mm or more, the Beatty and Katz correlation [Ref. 7] showed agreement within ± 10 percent with R-113 data. However, for smaller fin spacings, this correlation overpredicted the data owing to the presence of condensate retention.

6. The indirect measurement of local condensing heat-transfer coefficient revealed a local value at the top of the tube that is approximately twice the average value for the entire tube.

B. RECOMMENDATIONS

1. Complete the installation and the instrumentation of the bundle test apparatus.

2. Test commercially available enhanced condensing surfaces, such as finned tubes, wire-wrapped tubes, and roped tubes in an attempt to obtain the best-performing tube geometry.

3. Manufacture new tubes for the single-tube test apparatus with smaller fin spacings in order to more precisely determine the optimum fin spacing for R-113.

4. Operate the single-tube to apparatus with ethylene-glycol as the working fluid to gather a systematic set of data to supplement data for R-113 and steam.

5. Continue taking data to determine the local vapor-side enhancement. Use other functions, such as cosine functions, to determine if a better representation can be found.

APPENDIX A
LISTING OF RAW DATA

This appendix contains the raw data for R-113 presented in this investigation.

File Name: S01A27
Pressure Condition: Atmospheric
Vapor Velocity: 2.0 (m/s)

Data #	Vw (m/s)	Tin (C)	Tout (C)	Ts (C)
1	1.16	21.84	22.17	47.97
2	1.16	21.84	22.16	47.90
3	1.49	21.65	21.91	47.89
4	1.49	21.63	21.90	47.92
5	1.97	21.44	21.65	47.96
6	1.97	21.44	21.65	47.96
7	2.51	21.31	21.48	47.98
8	2.51	21.31	21.48	48.01
9	3.00	21.23	21.38	48.03
10	3.00	21.23	21.38	48.03
11	3.43	21.17	21.30	48.01
12	3.43	21.18	21.30	47.99
13	3.86	21.13	21.25	48.00
14	3.86	21.13	21.25	47.97
15	4.40	21.09	21.19	48.01
16	4.40	21.09	21.19	47.97
17	1.16	21.81	22.15	48.00
18	1.16	21.82	22.15	47.94

File Name: F04A21
Pressure Condition: Atmospheric
Vapor Velocity: 2.0 (m/s)

Data #	Vw (m/s)	Tin (C)	Tout (C)	Ts (C)
1	1.16	22.15	23.08	47.92
2	1.16	22.15	23.09	47.97
3	1.49	21.95	22.77	48.00
4	1.49	21.94	22.76	48.03
5	1.97	21.74	22.43	48.05
6	1.97	21.74	22.43	48.04
7	2.51	21.61	22.20	48.04
8	2.51	21.61	22.20	48.03
9	3.00	21.52	22.05	47.86
10	3.00	21.52	22.04	47.96
11	3.43	21.46	21.94	47.88
12	3.43	21.46	21.94	47.90
13	3.86	21.41	21.85	48.01
14	3.86	21.41	21.85	47.96
15	4.40	21.37	21.76	48.05
16	4.40	21.37	21.76	48.05
17	1.16	22.11	23.05	47.90
18	1.16	22.11	23.05	47.89

File Name: F05A09
Pressure Condition: Atmospheric
Vapor Velocity: 2.0 (m/s)

Data #	Vw (m/s)	Tin (C)	Tout (C)	Ts (C)
1	1.16	21.97	22.86	48.00
2	1.16	21.99	22.87	47.92
3	1.49	21.96	22.73	48.00
4	1.49	21.99	22.76	48.08
5	1.97	21.95	22.58	48.01
6	1.97	21.96	22.60	47.97
7	2.51	21.91	22.44	47.88
8	2.51	21.93	22.46	47.80
9	3.00	21.89	22.36	47.81
10	3.00	21.90	22.37	47.86
11	3.43	21.88	22.29	47.90
12	3.43	21.88	22.30	47.83
13	3.86	21.88	22.26	47.94
14	3.86	21.88	22.26	47.96
15	4.40	21.86	22.20	47.89
16	4.40	21.87	22.21	47.96
17	1.16	22.66	23.54	47.93
18	1.16	22.67	23.54	47.87

File Name: F06A11
Pressure Condition: Atmospheric
Vapor Velocity: 2.0 (m/s)

Data #	Vw (m/s)	Tin (C)	Tout (C)	Ts (C)
1	1.16	22.59	23.47	48.02
2	1.16	22.59	23.46	48.07
3	1.48	22.35	23.10	47.97
4	1.48	22.34	23.09	47.93
5	1.97	22.11	22.74	47.87
6	1.97	22.11	22.74	47.85
7	2.51	21.96	22.49	47.92
8	2.51	21.95	22.48	47.91
9	3.00	21.85	22.32	47.92
10	3.00	21.85	22.32	47.86
11	3.43	21.78	22.20	47.95
12	3.43	21.78	22.20	47.95
13	3.86	21.72	22.10	47.91
14	3.86	21.72	22.10	47.85
15	4.40	21.66	22.00	47.92
16	4.40	21.66	22.00	47.95
17	1.16	22.40	23.27	47.90
18	1.16	22.40	23.27	47.95

File Name: F07A13
Pressure Condition: Atmospheric
Vapor Velocity: 2.0 (m/s)

Data #	Vw (m/s)	Tin (C)	Tout (C)	Ts (C)
1	1.16	21.94	22.73	47.80
2	1.16	21.94	22.74	47.85
3	1.49	21.74	22.42	47.84
4	1.49	21.74	22.42	47.83
5	1.97	21.55	22.12	47.89
6	1.97	21.55	22.12	47.89
7	2.51	21.43	21.90	47.95
8	2.51	21.43	21.90	47.93
9	3.00	21.35	21.77	47.93
10	3.00	21.35	21.77	47.91
11	3.43	21.31	21.68	47.91
12	3.43	21.31	21.68	47.89
13	3.86	21.27	21.61	47.89
14	3.86	21.27	21.61	47.87
15	4.40	21.23	21.53	47.83
16	4.40	21.23	21.54	47.86
17	1.16	21.97	22.78	48.04
18	1.16	21.98	22.78	48.09

File Name: F08A15
Pressure Condition: Atmospheric
Vapor Velocity: 2.0 (m/s)

Data #	Vw (m/s)	Tin (C)	Tout (C)	Ts (C)
1	1.16	22.54	23.20	47.96
2	1.16	22.54	23.21	47.91
3	1.48	22.34	22.91	47.86
4	1.48	22.34	22.91	47.83
5	1.97	22.16	22.62	47.95
6	1.97	22.16	22.62	48.00
7	2.51	22.03	22.41	48.04
8	2.51	22.03	22.41	48.07
9	2.99	21.96	22.29	48.01
10	2.99	21.96	22.29	48.01
11	3.43	21.91	22.21	47.91
12	3.43	21.91	22.21	47.91
13	3.86	21.87	22.14	47.87
14	3.86	21.87	22.14	47.85
15	4.40	21.84	22.07	47.82
16	4.40	21.84	22.07	47.83
17	1.16	22.60	23.27	47.98
18	1.16	22.60	23.27	47.98

File Name: F10A17
Pressure Condition: Atmospheric
Vapor Velocity: 2.0 (m/s)

Data #	Vw (m/s)	Tin (C)	Tout (C)	Ts (C)
1	1.16	22.81	23.78	47.92
2	1.16	22.81	23.79	47.94
3	1.48	22.62	23.47	47.86
4	1.48	22.61	23.47	47.86
5	1.97	22.43	23.16	47.87
6	1.97	22.43	23.16	47.91
7	2.51	22.30	22.93	47.96
8	2.51	22.30	22.93	47.98
9	2.99	22.23	22.79	47.96
10	2.99	22.22	22.79	47.95
11	3.43	22.17	22.68	47.93
12	3.43	22.18	22.69	47.93
13	3.86	22.13	22.60	47.87
14	3.86	22.13	22.60	47.84
15	4.40	22.09	22.51	47.83
16	4.40	22.09	22.51	47.83
17	1.16	22.83	23.82	48.03
18	1.16	22.84	23.81	47.96

File Name: F11A23
Pressure Condition: Atmospheric
Vapor Velocity: 2.0 (m/s)

Data #	Vw (m/s)	Tin (C)	Tout (C)	Ts (C)
1	1.16	21.79	22.71	47.84
2	1.16	21.79	22.71	47.91
3	1.49	21.59	22.39	47.84
4	1.49	21.59	22.39	47.85
5	1.97	21.39	22.06	47.87
6	1.97	21.39	22.06	47.90
7	2.51	21.26	21.83	47.93
8	2.51	21.26	21.83	47.96
9	3.00	21.18	21.69	47.91
10	3.00	21.18	21.68	47.96
11	3.43	21.12	21.57	47.90
12	3.43	21.12	21.58	47.86
13	3.86	21.08	21.49	47.93
14	3.86	21.08	21.49	47.90
15	4.40	21.04	21.41	47.97
16	4.40	21.04	21.41	47.92
17	1.16	21.75	22.69	48.03
18	1.16	21.77	22.70	48.01

File Name: F12A20
Pressure Condition: Atmospheric
Vapor Velocity: 2.0 (m/s)

Data #	Vw (m/s)	Tin (C)	Tout (C)	Ts (C)
1	1.16	22.48	23.39	47.87
2	1.16	22.48	23.38	47.83
3	1.48	22.25	23.04	47.93
4	1.48	22.25	23.03	47.93
5	1.97	22.05	22.71	47.92
6	1.97	22.05	22.71	47.92
7	2.51	21.91	22.47	48.00
8	2.51	21.91	22.47	48.04
9	3.00	21.82	22.32	48.05
10	3.00	21.82	22.31	48.02
11	3.43	21.75	22.20	48.00
12	3.43	21.75	22.20	48.05
13	3.86	21.69	22.10	47.98
14	3.86	21.69	22.10	47.94
15	4.40	21.64	22.00	47.88
16	4.40	21.64	22.00	47.84
17	1.16	22.38	23.28	47.97
18	1.16	22.38	23.28	47.96

File Name: F13A22
Pressure Condition: Atmospheric
Vapor Velocity: 2.0 (m/s)

Data #	Vw (m/s)	Tin (C)	Tout (C)	Ts (C)
1	1.16	21.82	22.66	47.95
2	1.16	21.82	22.66	47.95
3	1.49	21.60	22.33	47.90
4	1.49	21.60	22.32	47.91
5	1.97	21.40	22.00	47.93
6	1.97	21.40	22.00	47.87
7	2.51	21.27	21.77	47.89
8	2.51	21.26	21.77	47.94
9	3.00	21.18	21.63	47.94
10	3.00	21.18	21.63	47.82
11	3.43	21.12	21.52	47.86
12	3.43	21.12	21.52	47.85
13	3.86	21.08	21.44	47.90
14	3.86	21.07	21.44	47.85
15	4.40	21.03	21.35	47.81
16	4.40	21.03	21.35	47.88
17	1.16	21.76	22.60	48.05
18	1.16	21.76	22.61	47.99

File Name: F15A24
Pressure Condition: Atmospheric
Vapor Velocity: 2.0 (m/s)

Data #	Vw (m/s)	Tin (C)	Tout (C)	Ts (C)
1	1.16	21.81	22.85	47.81
2	1.16	21.81	22.85	47.82
3	1.49	21.60	22.51	47.80
4	1.49	21.60	22.51	47.89
5	1.97	21.42	22.20	47.93
6	1.97	21.41	22.19	47.94
7	2.51	21.29	21.96	47.92
8	2.51	21.29	21.96	47.85
9	3.00	21.21	21.81	47.83
10	3.00	21.21	21.81	47.90
11	3.43	21.15	21.71	47.97
12	3.43	21.16	21.71	47.94
13	3.86	21.11	21.62	48.01
14	3.86	21.11	21.62	48.00
15	4.40	21.07	21.52	47.99
16	4.40	21.06	21.52	48.01
17	1.16	21.80	22.85	48.04
18	1.16	21.81	22.85	47.97

File Name: F16A25
Pressure Condition: Atmospheric
Vapor Velocity: 2.0 (m/s)

Data #	Vw (m/s)	Tin (C)	Tout (C)	Ts (C)
1	1.16	21.84	22.79	47.87
2	1.16	21.84	22.79	47.87
3	1.49	21.63	22.45	47.83
4	1.49	21.62	22.45	47.89
5	1.97	21.43	22.13	47.83
6	1.97	21.43	22.13	47.93
7	2.51	21.30	21.89	47.91
8	2.51	21.30	21.89	47.91
9	3.00	21.22	21.75	47.96
10	3.00	21.22	21.74	47.92
11	3.43	21.17	21.64	47.91
12	3.43	21.17	21.64	47.95
13	3.86	21.13	21.56	47.93
14	3.86	21.13	21.56	47.90
15	4.40	21.08	21.47	47.93
16	4.40	21.08	21.47	47.95
17	1.16	21.83	22.79	48.06
18	1.16	21.84	22.79	48.05

File Name: F17A28
Pressure Condition: Atmospheric
Vapor Velocity: 2.0 (m/s)

Data #	Vw (m/s)	Tin (C)	Tout (C)	Ts (C)
1	1.16	21.76	22.67	47.88
2	1.16	21.76	22.67	47.88
3	1.49	21.57	22.35	47.87
4	1.49	21.57	22.35	47.84
5	1.97	21.38	22.04	47.89
6	1.97	21.38	22.04	47.88
7	2.51	21.26	21.82	47.91
8	2.51	21.26	21.82	47.88
9	3.00	21.18	21.67	47.93
10	3.00	21.18	21.67	47.92
11	3.43	21.13	21.57	47.91
12	3.43	21.13	21.58	47.91
13	3.86	21.09	21.49	47.95
14	3.86	21.09	21.49	47.98
15	4.40	21.05	21.41	47.99
16	4.40	21.05	21.41	47.99
17	1.16	21.78	22.70	47.98
18	1.16	21.78	22.70	48.00

File Name: F18A29
Pressure Condition: Atmospheric
Vapor Velocity: 2.0 (m/s)

Data #	Vw (m/s)	Tin (C)	Tout (C)	Ts (C)
1	1.16	21.85	22.71	47.88
2	1.16	21.85	22.71	47.92
3	1.49	21.64	22.38	47.94
4	1.49	21.64	22.38	47.94
5	1.97	21.46	22.07	47.90
6	1.97	21.46	22.07	47.89
7	2.51	21.34	21.85	47.88
8	2.51	21.34	21.85	47.87
9	3.00	21.26	21.72	47.94
10	3.00	21.26	21.72	48.00
11	3.43	21.21	21.62	48.02
12	3.43	21.21	21.62	48.01
13	3.86	21.16	21.53	48.06
14	3.86	21.16	21.53	48.03
15	4.40	21.12	21.45	47.92
16	4.40	21.11	21.45	48.00
17	1.16	21.84	22.70	47.87
18	1.16	21.84	22.70	47.89

File Name: F22A30
Pressure Condition: Atmospheric
Vapor Velocity: 2.0 (m/s)

Data #	Vw (m/s)	Tin (C)	Tout (C)	Ts (C)
1	1.16	21.97	22.97	47.86
2	1.16	21.98	22.97	47.85
3	1.49	21.77	22.64	47.91
4	1.49	21.77	22.64	47.93
5	1.97	21.60	22.33	47.89
6	1.97	21.59	22.33	47.86
7	2.51	21.47	22.10	47.89
8	2.51	21.47	22.10	47.94
9	3.00	21.40	21.96	47.85
10	3.00	21.40	21.96	47.86
11	3.43	21.34	21.85	48.01
12	3.43	21.34	21.85	48.03
13	3.86	21.31	21.78	47.94
14	3.86	21.31	21.78	47.98
15	4.40	21.27	21.69	47.95
16	4.40	21.27	21.69	47.92
17	1.16	21.99	22.99	48.00
18	1.16	22.00	23.01	47.84

File Name: F23A31
Pressure Condition: Atmospheric
Vapor Velocity: 2.0 (m/s)

Data #	Vw (m/s)	Tin (C)	Tout (C)	Ts (C)
1	1.16	22.13	23.11	47.96
2	1.16	22.13	23.11	48.00
3	1.49	21.93	22.79	47.88
4	1.49	21.92	22.78	47.94
5	1.97	21.75	22.47	47.90
6	1.97	21.75	22.47	47.91
7	2.51	21.62	22.24	47.85
8	2.51	21.62	22.24	47.85
9	3.00	21.55	22.10	47.93
10	3.00	21.55	22.10	47.94
11	3.43	21.50	22.00	47.98
12	3.43	21.50	22.00	47.98
13	3.86	21.46	21.91	47.99
14	3.86	21.46	21.91	48.02
15	4.40	21.42	21.83	48.02
16	4.40	21.42	21.83	48.01
17	1.16	22.13	23.11	47.96
18	1.16	22.15	23.13	47.96

File Name: F24A32
Pressure Condition: Atmospheric
Vapor Velocity: 2.0 (m/s)

Data #	Vw (m/s)	Tin (C)	Tout (C)	Ts (C)
1	1.16	22.46	23.39	47.88
2	1.16	22.46	23.39	47.96
3	1.48	22.26	23.07	48.00
4	1.48	22.25	23.06	47.97
5	1.97	22.07	22.75	47.94
6	1.97	22.07	22.75	47.96
7	2.51	21.95	22.53	47.95
8	2.51	21.95	22.53	47.93
9	3.00	21.88	22.39	47.96
10	3.00	21.88	22.39	47.91
11	3.43	21.83	22.30	48.04
12	3.43	21.83	22.30	48.01
13	3.86	21.79	22.21	47.86
14	3.86	21.79	22.21	47.94
15	4.40	21.75	22.14	47.96
16	4.40	21.75	22.14	47.93
17	1.16	22.49	23.42	47.93
18	1.16	22.49	23.42	47.87

File Name: F26A33
Pressure Condition: Atmospheric
Vapor Velocity: 2.0 (m/s)

Data #	Vw (m/s)	Tin (C)	Tout (C)	Ts (C)
1	1.16	22.59	23.36	47.99
2	1.16	22.58	23.36	48.01
3	1.48	22.38	23.04	48.00
4	1.48	22.38	23.04	48.03
5	1.97	22.20	22.73	48.00
6	1.97	22.19	22.73	47.98
7	2.51	22.06	22.51	47.97
8	2.51	22.06	22.51	47.96
9	2.99	21.98	22.37	47.95
10	2.99	21.98	22.37	47.95
11	3.43	21.92	22.27	47.95
12	3.43	21.92	22.27	47.91
13	3.86	21.87	22.18	47.91
14	3.86	21.87	22.18	47.88
15	4.40	21.82	22.10	47.83
16	4.40	21.82	22.10	47.85
17	1.16	22.54	23.32	48.01
18	1.16	22.54	23.32	48.06

File Name: F27A34
Pressure Condition: Atmospheric
Vapor Velocity: 2.0 (m/s)

Data #	Vw (m/s)	Tin (C)	Tout (C)	Ts (C)
1	1.16	22.48	23.22	47.83
2	1.16	22.47	23.22	47.93
3	1.48	22.27	22.90	47.91
4	1.48	22.27	22.90	47.88
5	1.97	22.08	22.59	47.89
6	1.97	22.07	22.58	47.82
7	2.51	21.93	22.36	47.92
8	2.51	21.93	22.36	47.95
9	3.00	21.85	22.22	47.97
10	3.00	21.85	22.22	47.96
11	3.43	21.79	22.13	47.96
12	3.43	21.79	22.12	47.93
13	3.86	21.75	22.04	47.93
14	3.86	21.74	22.04	47.90
15	4.40	21.69	21.96	47.91
16	4.40	21.69	21.96	47.90
17	1.16	22.41	23.15	48.05
18	1.16	22.41	23.15	48.03

File Name: F28A35
Pressure Condition: Atmospheric
Vapor Velocity: 2.0 (m/s)

Data #	Vw (m/s)	Tin (C)	Tout (C)	Ts (C)
1	1.16	22.06	22.77	47.83
2	1.16	22.06	22.77	47.92
3	1.49	21.84	22.44	48.04
4	1.49	21.84	22.44	48.05
5	1.97	21.65	22.14	47.86
6	1.97	21.65	22.14	47.88
7	2.51	21.52	21.93	47.91
8	2.51	21.52	21.93	47.91
9	3.00	21.45	21.80	47.95
10	3.00	21.45	21.80	47.96
11	3.43	21.39	21.71	47.97
12	3.43	21.39	21.71	47.98
13	3.86	21.35	21.63	47.94
14	3.86	21.35	21.63	47.92
15	4.40	21.30	21.55	47.88
16	4.40	21.30	21.56	47.87
17	1.16	22.00	22.71	48.06
18	1.16	22.01	22.72	48.05

File Name: F30A36
Pressure Condition: Atmospheric
Vapor Velocity: 2.0 (m/s)

Data #	Vw (m/s)	Tin (C)	Tout (C)	Ts (C)
1	1.16	22.01	22.96	47.84
2	1.16	22.01	22.96	47.90
3	1.49	21.81	22.63	47.87
4	1.49	21.81	22.63	47.85
5	1.97	21.63	22.32	47.84
6	1.97	21.63	22.32	47.84
7	2.51	21.50	22.09	47.87
8	2.51	21.50	22.09	47.90
9	3.00	21.42	21.95	47.98
10	3.00	21.42	21.94	47.98
11	3.43	21.37	21.84	48.04
12	3.43	21.37	21.84	48.03
13	3.86	21.32	21.76	48.01
14	3.86	21.32	21.76	48.04
15	4.40	21.28	21.67	48.01
16	4.40	21.28	21.67	47.96
17	1.16	21.99	22.94	48.04
18	1.16	21.99	22.94	48.01

File Name: F31A37
Pressure Condition: Atmospheric
Vapor Velocity: 2.0 (m/s)

Data #	Vw (m/s)	Tin (C)	Tout (C)	Ts (C)
1	1.16	22.02	22.95	47.82
2	1.16	22.01	22.95	47.91
3	1.49	21.81	22.63	47.81
4	1.49	21.81	22.63	47.81
5	1.97	21.63	22.32	47.84
6	1.97	21.63	22.31	47.98
7	2.51	21.51	22.09	47.99
8	2.51	21.50	22.08	47.96
9	3.00	21.43	21.94	47.97
10	3.00	21.43	21.94	48.06
11	3.43	21.38	21.84	47.89
12	3.43	21.38	21.84	47.97
13	3.86	21.34	21.76	48.00
14	3.86	21.33	21.76	47.95
15	4.40	21.29	21.67	47.96
16	4.40	21.29	21.67	47.98
17	1.16	21.99	22.93	47.79
18	1.16	22.00	22.93	47.89

File Name: F32A38
Pressure Condition: Atmospheric
Vapor Velocity: 2.0 (m/s)

Data #	Vw (m/s)	Tin (C)	Tout (C)	Ts (C)
1	1.16	22.09	22.98	47.67
2	1.16	22.09	22.98	47.87
3	1.49	21.88	22.65	48.12
4	1.49	21.88	22.65	47.86
5	1.97	21.69	22.34	48.06
6	1.97	21.69	22.33	48.03
7	2.51	21.57	22.12	47.91
8	2.51	21.56	22.11	47.93
9	3.00	21.49	21.97	47.86
10	3.00	21.48	21.97	47.92
11	3.43	21.43	21.87	47.77
12	3.43	21.43	21.87	47.90
13	3.86	21.39	21.79	48.06
14	3.86	21.39	21.79	47.87
15	4.40	21.35	21.70	48.05
16	4.40	21.35	21.70	48.10
17	1.16	22.07	22.96	47.89
18	1.16	22.07	22.96	48.04

File Name: D01A42
Pressure Condition: Atmospheric
Vapor Velocity: 2.0 (m/s)

Data #	Vw (m/s)	Tin (C)	Tout (C)	Ts (C)
1	1.16	21.79	22.89	48.02
2	1.16	21.77	22.88	48.09
3	1.49	21.51	22.45	47.90
4	1.49	21.51	22.43	47.83
5	1.97	21.28	22.08	47.91
6	1.97	21.28	22.07	47.92
7	2.51	21.14	21.83	47.92
8	2.51	21.14	21.82	47.91
9	3.00	21.05	21.66	47.89
10	3.00	21.05	21.66	47.89
11	3.43	20.97	21.53	47.99
12	3.43	20.97	21.53	48.04
13	3.86	20.90	21.41	48.04
14	3.86	20.90	21.41	47.99
15	4.40	20.81	21.27	47.99
16	4.40	20.80	21.27	47.95
17	1.16	21.52	22.62	47.86
18	1.16	21.52	22.62	47.86

File Name: D02A45
Pressure Condition: Atmospheric
Vapor Velocity: 2.0 (m/s)

Data #	Vw (m/s)	Tin (C)	Tout (C)	Ts (C)
1	1.16	20.99	21.90	47.89
2	1.16	20.99	21.90	48.06
3	1.49	20.77	21.56	48.05
4	1.49	20.77	21.55	48.07
5	1.97	20.59	21.23	48.05
6	1.97	20.59	21.23	47.99
7	2.52	20.46	21.00	47.82
8	2.52	20.45	21.00	47.86
9	3.00	20.38	20.86	48.03
10	3.00	20.38	20.86	48.07
11	3.43	20.32	20.75	48.01
12	3.43	20.32	20.75	47.95
13	3.87	20.28	20.67	47.83
14	3.87	20.28	20.67	47.88
15	4.41	20.24	20.58	47.83
16	4.41	20.24	20.58	47.87
17	1.16	20.97	21.88	47.89
18	1.16	20.98	21.89	47.90

File Name: F04B44
Pressure Condition: Atmospheric
Vapor Velocity: 2.0 (m/s)

Data #	Vw (m/s)	Tin (C)	Tout (C)	Ts (C)
1	1.16	21.54	22.48	47.85
2	1.16	21.45	22.39	47.82
3	1.49	21.19	22.01	47.95
4	1.49	21.16	21.98	48.07
5	1.97	20.92	21.60	47.96
6	1.97	20.91	21.59	47.90
7	2.51	20.72	21.30	47.84
8	2.51	20.71	21.29	47.92
9	3.00	20.60	21.11	48.04
10	3.00	20.59	21.11	48.01
11	3.43	20.49	20.96	48.02
12	3.43	20.49	20.95	48.00
13	3.87	20.42	20.84	48.01
14	3.87	20.41	20.83	47.97
15	4.41	20.35	20.73	47.96
16	4.41	20.34	20.72	47.96
17	1.16	21.06	22.00	47.98
18	1.16	21.05	21.99	48.00

File Name: F04C46
Pressure Condition: Atmospheric
Vapor Velocity: 2.0 (m/s)

Data #	Vw (m/s)	Tin (C)	Tout (C)	Ts (C)
1	1.16	21.04	21.89	47.86
2	1.16	21.03	21.89	47.90
3	1.49	20.82	21.56	48.02
4	1.49	20.82	21.56	48.02
5	1.97	20.63	21.25	48.02
6	1.97	20.63	21.24	48.02
7	2.52	20.49	21.01	47.99
8	2.52	20.49	21.01	48.01
9	3.00	20.41	20.87	47.93
10	3.00	20.41	20.87	47.91
11	3.43	20.36	20.77	47.89
12	3.43	20.36	20.77	47.86
13	3.87	20.31	20.68	47.90
14	3.87	20.31	20.68	47.89
15	4.41	20.27	20.60	47.92
16	4.41	20.27	20.60	47.93
17	1.16	21.01	21.87	48.00
18	1.16	21.01	21.87	48.01

File Name: F04D48
Pressure Condition: Atmospheric
Vapor Velocity: 2.0 (m/s)

Data #	Vw (m/s)	Tin (C)	Tout (C)	Ts (C)
1	1.16	21.57	22.32	47.86
2	1.16	21.57	22.32	47.88
3	1.49	21.34	21.98	47.99
4	1.49	21.34	21.98	47.97
5	1.97	21.15	21.69	48.04
6	1.97	21.15	21.68	48.03
7	2.51	21.02	21.47	47.86
8	2.51	21.02	21.47	47.86
9	3.00	20.94	21.33	47.83
10	3.00	20.94	21.33	47.83
11	3.43	20.89	21.24	47.98
12	3.43	20.89	21.24	47.99
13	3.86	20.85	21.17	48.01
14	3.86	20.85	21.17	48.00
15	4.40	20.80	21.09	47.84
16	4.40	20.80	21.09	47.83
17	1.16	21.55	22.31	47.84
18	1.16	21.55	22.31	47.86

File Name: F04E50
Pressure Condition: Atmospheric
Vapor Velocity: 2.0 (m/s)

Data #	Vw (m/s)	Tin (C)	Tout (C)	Ts (C)
1	1.16	21.71	22.36	47.82
2	1.16	21.72	22.37	47.83
3	1.49	21.51	22.07	47.92
4	1.49	21.51	22.07	47.94
5	1.97	21.33	21.78	47.93
6	1.97	21.33	21.78	47.95
7	2.51	21.20	21.59	47.93
8	2.51	21.20	21.59	47.92
9	3.00	21.13	21.47	47.93
10	3.00	21.13	21.47	47.91
11	3.43	21.08	21.38	47.87
12	3.43	21.08	21.38	47.89
13	3.86	21.04	21.31	47.87
14	3.86	21.04	21.31	47.84
15	4.40	21.00	21.24	47.83
16	4.40	21.00	21.25	47.81
17	1.16	21.75	22.41	47.92
18	1.16	21.75	22.41	47.95

File Name: F04F52
Pressure Condition: Atmospheric
Vapor Velocity: 2.0 (m/s)

Data #	Vw (m/s)	Tin (C)	Tout (C)	Ts (C)
1	1.16	22.04	22.61	47.87
2	1.16	22.04	22.60	47.92
3	1.49	21.81	22.28	48.01
4	1.49	21.81	22.29	48.02
5	1.97	21.61	22.00	48.04
6	1.97	21.61	22.00	48.03
7	2.51	21.47	21.80	47.97
8	2.51	21.47	21.79	47.94
9	3.00	21.39	21.67	47.88
10	3.00	21.39	21.67	47.86
11	3.43	21.33	21.58	47.83
12	3.43	21.33	21.58	47.79
13	3.86	21.28	21.51	47.86
14	3.86	21.28	21.51	47.90
15	4.40	21.23	21.44	47.92
16	4.40	21.23	21.44	47.93
17	1.16	21.97	22.54	48.07
18	1.16	21.97	22.54	48.10

File Name: F04G54
Pressure Condition: Atmospheric
Vapor Velocity: 2.0 (m/s)

Data #	Vw (m/s)	Tin (C)	Tout (C)	Ts (C)
1	1.16	21.58	22.00	47.99
2	1.16	21.57	21.99	48.02
3	1.49	21.35	21.70	47.96
4	1.49	21.35	21.70	47.93
5	1.97	21.16	21.45	47.91
6	1.97	21.15	21.44	47.96
7	2.51	21.02	21.26	47.95
8	2.51	21.02	21.26	47.97
9	3.00	20.94	21.15	47.96
10	3.00	20.94	21.15	47.98
11	3.43	20.88	21.07	47.97
12	3.43	20.88	21.06	47.96
13	3.86	20.83	21.00	47.94
14	3.86	20.83	21.00	47.96
15	4.40	20.78	20.93	47.94
16	4.40	20.78	20.93	47.91
17	1.16	21.52	21.95	48.00
18	1.16	21.52	21.96	48.00

File Name: F04H56
Pressure Condition: Atmospheric
Vapor Velocity: 2.0 (m/s)

Data #	Vw (m/s)	Tin (C)	Tout (C)	Ts (C)
1	1.16	21.27	21.59	47.91
2	1.16	21.26	21.57	47.95
3	1.49	21.04	21.30	48.01
4	1.49	21.03	21.30	48.04
5	1.97	20.77	20.98	47.97
6	1.97	20.77	20.97	47.95
7	2.52	20.54	20.70	47.83
8	2.52	20.53	20.70	47.83
9	3.00	20.44	20.58	47.92
10	3.00	20.44	20.58	47.93
11	3.43	20.36	20.49	47.91
12	3.43	20.35	20.48	47.95
13	3.87	20.30	20.41	47.90
14	3.87	20.29	20.40	47.91
15	4.41	20.22	20.32	47.92
16	4.41	20.21	20.32	47.93
17	1.16	20.93	21.26	47.96
18	1.16	20.93	21.26	47.94

File Name: F15B47
Pressure Condition: Atmospheric
Vapor Velocity: 2.0 (m/s)

Data #	Vw (m/s)	Tin (C)	Tout (C)	Ts (C)
1	1.16	21.67	22.70	47.88
2	1.16	21.67	22.70	47.93
3	1.49	21.45	22.35	47.99
4	1.49	21.45	22.35	47.99
5	1.97	21.26	22.01	47.98
6	1.97	21.25	22.01	47.98
7	2.51	21.11	21.75	47.86
8	2.51	21.11	21.75	47.83
9	3.00	21.03	21.59	47.98
10	3.00	21.02	21.59	47.98
11	3.43	20.95	21.47	48.00
12	3.43	20.95	21.47	47.96
13	3.86	20.90	21.37	47.88
14	3.86	20.90	21.37	47.88
15	4.40	20.85	21.28	48.00
16	4.40	20.85	21.27	47.99
17	1.16	21.59	22.61	47.95
18	1.16	21.59	22.60	47.87

File Name: F15C49
Pressure Condition: Atmospheric
Vapor Velocity: 2.0 (m/s)

Data #	Vw (m/s)	Tin (C)	Tout (C)	Ts (C)
1	1.16	21.61	22.54	47.84
2	1.16	21.61	22.54	47.86
3	1.49	21.40	22.20	47.88
4	1.49	21.40	22.20	47.85
5	1.97	21.20	21.87	47.93
6	1.97	21.20	21.87	47.91
7	2.51	21.07	21.64	47.91
8	2.51	21.07	21.64	47.90
9	3.00	20.98	21.49	47.91
10	3.00	20.98	21.49	47.91
11	3.43	20.93	21.38	47.95
12	3.43	20.93	21.38	47.97
13	3.86	20.88	21.30	47.99
14	3.86	20.88	21.30	47.97
15	4.40	20.83	21.21	47.97
16	4.40	20.83	21.21	47.97
17	1.16	21.57	22.50	47.99
18	1.16	21.58	22.51	48.01

File Name: F15D51
Pressure Condition: Atmospheric
Vapor Velocity: 2.0 (m/s)

Data #	Vw (m/s)	Tin (C)	Tout (C)	Ts (C)
1	1.16	22.02	22.84	47.84
2	1.16	22.02	22.85	47.86
3	1.49	21.80	22.51	47.88
4	1.49	21.80	22.51	47.90
5	1.97	21.62	22.21	47.87
6	1.97	21.62	22.21	47.89
7	2.51	21.48	21.99	47.87
8	2.51	21.48	21.99	47.88
9	3.00	21.40	21.85	47.90
10	3.00	21.40	21.84	47.90
11	3.43	21.34	21.74	47.87
12	3.43	21.34	21.74	47.87
13	3.86	21.30	21.66	47.86
14	3.86	21.30	21.66	47.88
15	4.40	21.25	21.58	47.92
16	4.40	21.25	21.58	47.92
17	1.16	21.99	22.82	48.04
18	1.16	21.99	22.83	48.04

File Name: F15E53
Pressure Condition: Atmospheric
Vapor Velocity: 2.0 (m/s)

Data #	Vw (m/s)	Tin (C)	Tout (C)	Ts (C)
1	1.16	21.95	22.64	47.91
2	1.16	21.94	22.65	47.97
3	1.49	21.73	22.33	47.99
4	1.49	21.72	22.33	48.00
5	1.97	21.53	22.03	48.03
6	1.97	21.53	22.02	48.01
7	2.51	21.40	21.82	48.19
8	2.51	21.40	21.82	47.97
9	3.00	21.31	21.68	47.91
10	3.00	21.31	21.68	47.90
11	3.43	21.25	21.58	47.89
12	3.43	21.25	21.58	47.89
13	3.86	21.20	21.50	47.87
14	3.86	21.20	21.50	47.84
15	4.40	21.15	21.42	47.86
16	4.40	21.15	21.42	47.82
17	1.16	21.87	22.58	47.99
18	1.16	21.88	22.59	47.89

File Name: F15F55
Pressure Condition: Atmospheric
Vapor Velocity: 2.0 (m/s)

Data #	Vw (m/s)	Tin (C)	Tout (C)	Ts (C)
1	1.16	21.48	22.09	47.83
2	1.16	21.48	22.08	47.90
3	1.49	21.24	21.76	48.09
4	1.49	21.23	21.75	48.08
5	1.97	21.04	21.47	47.99
6	1.97	21.04	21.46	47.97
7	2.51	20.91	21.27	47.90
8	2.51	20.91	21.27	47.90
9	3.00	20.82	21.13	47.88
10	3.00	20.82	21.13	47.86
11	3.43	20.76	21.05	47.96
12	3.43	20.76	21.05	48.02
13	3.87	20.72	20.97	48.01
14	3.87	20.72	20.97	48.03
15	4.41	20.67	20.90	47.98
16	4.41	20.67	20.90	47.99
17	1.16	21.42	22.02	47.83
18	1.16	21.42	22.02	47.86

File Name: F15H57
Pressure Condition: Atmospheric
Vapor Velocity: 2.0 (m/s)

Data #	Vw (m/s)	Tin (C)	Tout (C)	Ts (C)
1	1.16	20.69	20.96	47.85
2	1.16	20.68	20.96	47.83
3	1.49	20.45	20.68	48.00
4	1.49	20.45	20.68	47.95
5	1.98	20.26	20.44	48.04
6	1.98	20.26	20.43	48.00
7	2.52	20.12	20.26	48.02
8	2.52	20.12	20.26	48.06
9	3.00	20.04	20.16	48.06
10	3.00	20.03	20.16	48.08
11	3.44	19.98	20.09	48.04
12	3.44	19.98	20.09	48.06
13	3.87	19.93	20.03	48.07
14	3.87	19.93	20.02	48.03
15	4.41	19.88	19.97	47.94
16	4.41	19.88	19.96	47.96
17	1.16	20.64	20.91	47.96
18	1.16	20.64	20.91	47.93

APPENDIX B
UNCERTAINTY ANALYSIS

Uncertainties are always associated with any measurement. These uncertaities are dependent on the accuracy and calibration of the measuring device and the operator's experience. Numerical data collected during this investigation were used together with theoretical formulations, so the final vapor-side heat-transfer coefficients may be distorted due to the propagation of errors during calculations. The uncertainty of a computation may be determined using the following equation proposed by Kline and McClintok [Ref. 32]:

$$w_r = \left\{\left[\frac{\delta R}{\delta x_1} w_1\right]^2 + \left[\frac{\delta R}{\delta x_1} w_1\right]^2 + \cdots + \left[\frac{\delta R}{\delta x_n} w_n\right]^2\right\}^{1/2} \qquad (B.1)$$

where:

R is the result of the calculation,

w_r is the uncertainty of the result R,

$x_1, x_2, \ldots, x_n$ are the measured independent variables, and

$w_1, w_2, \ldots, w_n$ are the uncertainties in the measured variables.

The uncertainty analysis program used in this investigation is given by Mitrou [Ref. 14]. Samples of the results of the uncertainty analysis are presented here.

DATA FOR THE UNCERTAINTY ANALYSIS:

File Name:	S01A27	
Pressure Condition:	Atmospheric (101 kPa)	
Vapor Temperature	= 47.97	(Deg C)
Water Flow Rate (%)	= 20.00	
Water Velocity	= 1.16	(m/s)
Heat Flux	= 2.535E+04	(W/m^2)
Tube-metal thermal conduc.	= 385.0	(W/m.K)
Sieder-Tate constant	= 0.0280	

UNCERTAINTY ANALYSIS:

VARIABLE	PERCENT UNCERTAINTY
Mass Flow Rate, Md	3.00
Reynolds Number, Re	3.10
Heat Flux, q	3.71
Log-Mean-Tem Diff, LMTD	2.15
Wall Resistance, Rw	2.67
Overall H.T.C., Uo	4.29
Water-Side H.T.C., Hi	3.08
Vapor-Side H.T.C., Ho	5.63

DATA FOR THE UNCERTAINTY ANALYSIS:

File Name:	S01A27	
Pressure Condition:	Atmospheric (101 kPa)	
Vapor Temperature	= 47.97	(Deg C)
Water Flow Rate (%)	= 80.00	
Water Velocity	= 4.40	(m/s)
Heat Flux	= 2.943E+04	(W/m^2)
Tube-metal thermal conduc.	= 385.0	(W/m.K)
Sieder-Tate constant	= 0.0280	

UNCERTAINTY ANALYSIS:

VARIABLE	PERCENT UNCERTAINTY
Mass Flow Rate, Md	0.79
Reynolds Number, Re	1.10
Heat Flux, q	7.07
Log-Mean-Tem Diff, LMTD	7.01
Wall Resistance, Rw	2.67
Overall H.T.C., Uo	9.96
Water-Side H.T.C., Hi	2.03
Vapor-Side H.T.C., Ho	11.10

DATA FOR THE UNCERTAINTY ANALYSIS:

File Name:	F04A21	
Pressure Condition:	Atmospheric (101 kPa)	
Vapor Temperature	= 47.92	(Deg C)
Water Flow Rate (%)	= 20.00	
Water Velocity	= 1.16	(m/s)
Heat Flux	= 7.204E+04	(W/m^2)
Tube-metal thermal conduc.	= 385.0	(W/m.K)
Sieder-Tate constant	= 0.0280	

UNCERTAINTY ANALYSIS:

VARIABLE	PERCENT UNCERTAINTY
Mass Flow Rate, Md	3.00
Reynolds Number, Re	3.10
Heat Flux, q	3.12
Log-Mean-Tem Diff, LMTD	.76
Wall Resistance, Rw	2.67
Overall H.T.C., Uo	3.22
Water-Side H.T.C., Hi	3.08
Vapor-Side H.T.C., Ho	10.71

DATA FOR THE UNCERTAINTY ANALYSIS:

File Name:	F04A21	
Pressure Condition:	Atmospheric (101 kPa)	
Vapor Temperature	= 48.05	(Deg C)
Water Flow Rate (%)	= 80.00	
Water Velocity	= 4.40	(m/s)
Heat Flux	= 1.154E+05	(W/m^2)
Tube-metal thermal conduc.	= 385.0	(W/m.K)
Sieder-Tate constant	= 0.0280	

UNCERTAINTY ANALYSIS:

VARIABLE	PERCENT UNCERTAINTY
Mass Flow Rate, Md	0.79
Reynolds Number, Re	1.10
Heat Flux, q	2.00
Log-Mean-Tem Diff, LMTD	1.79
Wall Resistance, Rw	2.67
Overall H.T.C., Uo	2.69
Water-Side H.T.C., Hi	2.03
Vapor-Side H.T.C., Ho	4.65

DATA FOR THE UNCERTAINTY ANALYSIS:

File Name:	F05A09	
Pressure Condition:	Atmospheric (101 kPa)	
Vapor Temperature	= 48.00	(Deg C)
Water Flow Rate (%)	= 20.00	
Water Velocity	= 1.16	(m/s)
Heat Flux	= 6.810E+04	(W/m^2)
Tube-metal thermal conduc.	= 385.0	(W/m.K)
Sieder-Tate constant	= 0.0280	

UNCERTAINTY ANALYSIS:

VARIABLE	PERCENT UNCERTAINTY
Mass Flow Rate, Md	3.00
Reynolds Number, Re	3.10
Heat Flux, q	3.13
Log-Mean-Tem Diff, LMTD	.80
Wall Resistance, Rw	2.67
Overall H.T.C., Uo	3.24
Water-Side H.T.C., Hi	3.08
Vapor-Side H.T.C., Ho	9.53

DATA FOR THE UNCERTAINTY ANALYSIS:

File Name:	F05A09	
Pressure Condition:	Atmospheric (101 kPa)	
Vapor Temperature	= 47.96	(Deg C)
Water Flow Rate (%)	= 80.00	
Water Velocity	= 4.40	(m/s)
Heat Flux	= 9.904E+04	(W/m^2)
Tube-metal thermal conduc.	= 385.0	(W/m.K)
Sieder-Tate constant	= 0.0280	

UNCERTAINTY ANALYSIS:

VARIABLE	PERCENT UNCERTAINTY
Mass Flow Rate, Md	0.79
Reynolds Number, Re	1.11
Heat Flux, q	2.27
Log-Mean-Tem Diff, LMTD	2.08
Wall Resistance, Rw	2.67
Overall H.T.C., Uo	3.08
Water-Side H.T.C., Hi	2.03
Vapor-Side H.T.C., Ho	4.85

DATA FOR THE UNCERTAINTY ANALYSIS:

File Name:	F06A11	
Pressure Condition:	Atmospheric (101 kPa)	
Vapor Temperature	= 48.02	(Deg C)
Water Flow Rate (%)	= 20.00	
Water Velocity	= 1.16	(m/s)
Heat Flux	= 6.726E+04	(W/m^2)
Tube-metal thermal conduc.	= 385.0	(W/m.K)
Sieder-Tate constant	= 0.0280	

UNCERTAINTY ANALYSIS:

VARIABLE	PERCENT UNCERTAINTY
Mass Flow Rate, Md	3.00
Reynolds Number, Re	3.10
Heat Flux, q	3.14
Log-Mean-Tem Diff, LMTD	.81
Wall Resistance, Rw	2.67
Overall H.T.C., Uo	3.24
Water-Side H.T.C., Hi	3.08
Vapor-Side H.T.C., Ho	9.65

DATA FOR THE UNCERTAINTY ANALYSIS:

File Name:	F06A11	
Pressure Condition:	Atmospheric (101 kPa)	
Vapor Temperature	= 47.95	(Deg C)
Water Flow Rate (%)	= 80.00	
Water Velocity	= 4.40	(m/s)
Heat Flux	= 1.004E+05	(W/m^2)
Tube-metal thermal conduc.	= 385.0	(W/m.K)
Sieder-Tate constant	= 0.0280	

UNCERTAINTY ANALYSIS:

VARIABLE	PERCENT UNCERTAINTY
Mass Flow Rate, Md	0.79
Reynolds Number, Re	1.11
Heat Flux, q	2.24
Log-Mean-Tem Diff, LMTD	2.06
Wall Resistance, Rw	2.67
Overall H.T.C., Uo	3.04
Water-Side H.T.C., Hi	2.03
Vapor-Side H.T.C., Ho	4.81

DATA FOR THE UNCERTAINTY ANALYSIS:

File Name:	F07A13	
Pressure Condition:	Atmospheric (101 kPa)	
Vapor Temperature	= 47.80	(Deg C)
Water Flow Rate (%)	= 20.00	
Water Velocity	= 1.16	(m/s)
Heat Flux	= 6.137E+04	(W/m^2)
Tube-metal thermal conduc.	= 385.0	(W/m.K)
Sieder-Tate constant	= 0.0280	

UNCERTAINTY ANALYSIS:

VARIABLE	PERCENT UNCERTAINTY
Mass Flow Rate, Md	3.00
Reynolds Number, Re	3.10
Heat Flux, q	3.16
Log-Mean-Tem Diff, LMTD	.89
Wall Resistance, Rw	2.67
Overall H.T.C., Uo	3.28
Water-Side H.T.C., Hi	3.08
Vapor-Side H.T.C., Ho	8.27

DATA FOR THE UNCERTAINTY ANALYSIS:

File Name:	F07A13	
Pressure Condition:	Atmospheric (101 kPa)	
Vapor Temperature	= 47.86	(Deg C)
Water Flow Rate (%)	= 80.00	
Water Velocity	= 4.40	(m/s)
Heat Flux	= 8.835E+04	(W/m^2)
Tube-metal thermal conduc.	= 385.0	(W/m.K)
Sieder-Tate constant	= 0.0280	

UNCERTAINTY ANALYSIS:

VARIABLE	PERCENT UNCERTAINTY
Mass Flow Rate, Md	0.79
Reynolds Number, Re	1.10
Heat Flux, q	2.50
Log-Mean-Tem Diff, LMTD	2.34
Wall Resistance, Rw	2.67
Overall H.T.C., Uo	3.42
Water-Side H.T.C., Hi	2.03
Vapor-Side H.T.C., Ho	5.02

DATA FOR THE UNCERTAINTY ANALYSIS:

File Name:	F08A15	
Pressure Condition:	Atmospheric (101 kPa)	
Vapor Temperature	= 47.96	(Deg C)
Water Flow Rate (%)	= 20.00	
Water Velocity	= 1.16	(m/s)
Heat Flux	= 5.112E+04	(W/m^2)
Tube-metal thermal conduc.	= 385.0	(W/m.K)
Sieder-Tate constant	= 0.0280	

UNCERTAINTY ANALYSIS:

VARIABLE	PERCENT UNCERTAINTY
Mass Flow Rate, Md	3.00
Reynolds Number, Re	3.10
Heat Flux, q	3.21
Log-Mean-Tem Diff, LMTD	1.07
Wall Resistance, Rw	2.67
Overall H.T.C., Uo	3.39
Water-Side H.T.C., Hi	3.08
Vapor-Side H.T.C., Ho	6.95

DATA FOR THE UNCERTAINTY ANALYSIS:

File Name:	F08A15	
Pressure Condition:	Atmospheric (101 kPa)	
Vapor Temperature	= 47.83	(Deg C)
Water Flow Rate (%)	= 80.00	
Water Velocity	= 4.40	(m/s)
Heat Flux	= 6.961E+04	(W/m^2)
Tube-metal thermal conduc.	= 385.0	(W/m.K)
Sieder-Tate constant	= 0.0280	

UNCERTAINTY ANALYSIS:

VARIABLE	PERCENT UNCERTAINTY
Mass Flow Rate, Md	0.79
Reynolds Number, Re	1.11
Heat Flux, q	3.10
Log-Mean-Tem Diff, LMTD	2.96
Wall Resistance, Rw	2.67
Overall H.T.C., Uo	4.28
Water-Side H.T.C., Hi	2.03
Vapor-Side H.T.C., Ho	5.73

LIST OF REFERENCES

1. Wanniarachchi, A. S., Marto, P. J., and Reilly, T. J., "The Effect of Oil Contamination on the Nucleate Pool-Boiling Performance of R-114 from a Porous-Coated Surface," *ASHRAE Transactions 1986*, Vol. 92, Pt. 2, pp. 525-538.

2. Helmick, R. L., Unkel, B. G., Cromis, R. A., and Hershey, A. L., "Development of an Advanced air conditioning Plant for DDG-51 Class Ships," *Naval Engineers Journal*, Vol. 99, No. 3, pp. 112-123, May 1987.

3. Katz, D. L., Hope, R. E., and Dasko, S. C., *Liquid Retention on Finned Tubes*, Dept. of Engr. Research, University of Michigan, Ann Arbor, Michigan, Project M 592, 1946.

4. Rudy, T. M., and Webb, R. L., "Condensate Retention of Horizontal Integral-Finned Tubing," *Advances in Enhanced Heat Transfer*, HTD-Vol. 18, pp. 35-41, 20th National Heat Transfer Conference, Milwaukee, Wisconsin, August 1981.

5. Honda, H., Nozu, S., and Mitsumori, K., "Augmentation of Condensation on Horizontal Finned Tubes by Attaching Porous Drainage Plates," *Proceedings of the ASME-JSME Thermal Engineering Conference*, pp. 289-295, Honolulu, 1983.

6. Yau, K. K., Cooper, J. R., and Rose, J. W., 'Effects of Drainage Strips and Fin Spacing on Heat Transfer and Condensate Retention for Horizontal Finned and Plain Condenser Tubes," *Fundamentals of Phase Change: Boiling and Condensation*, C. T. Avedisian and T. M. Rudy (Eds.), ASME, pp. 151-156, 1984.

7. Beatty, K. T., Jr., and Katz, D. L., "Condensation of Vapors on Outside of Finned Tubes," *Chemical Engineering Progress*, Vol. 44, No. 1, pp. 55-77, January 1948.

8. Heat Transfer Research, Inc., HTRI Project 2439-300, *Comparison of Condensation of steam on Plain and Turbotec Spirally Grooved Tubes in a Baffled Shell-and-Tube Condenser*, by J. Palen, B. Cham, and J. Taborek, January 1971.

9. Karkhu, V. A., and Borovkov, V. P., "Film Condensation of Vapor at Finely-Finned Horizontal Tubes," *Heat Transfer-Soviet Research*, Vol. 3, No. 2, pp. 183-191, March-April 1971.

10. Carnavos, T. C., "An Experimental Study: Condensation of R-11 on Augmented Tubes," ASME Paper No. 80-HT-54, Nineteenth National Heat Transfer conference, Milwaukee, August 1981.

11 Poole, W. M., *Filmwise Condensation of Steam on Externally-Finned Horizontal Tubes*, M.S. Thesis, Naval Postgraduate School, Monterey, California, December 1983.

12. Georgiadis, I. V., *Filmwise Condensation of Steam on Low Integral-Finned Tubes*, M.S. Thesis, Naval Postgraduate School, Monterey, California, September 1984.

13. Flook, F. V., *Filmwise Condensation of Steam on Low Integral-Finned Tubes*, M.S. Thesis, Naval Postgraduate School, Monterey, California, March 1985.

14. Mitrou, E. S., *Film Condensation of Steam on Externally Enhanced Horizontal Tubes*, M.S. Thesis, Naval Postgraduate School, Monterey, California, March 1986.

15 Masuda, H., and Rose, J. W., "An Experimental Study of Condensation of Refrigerant 113 on Low Integral-fin Tubes," *Proceedings of the International Symposium on Heat Transfer*, Vol. 2, Paper 32, Beijing, PRC.

16. Union Carbide Corporation, *Union Carbide Thin Film Condensing Promoter for Submarine Steam Condensers, Final Report*, by A. M. Czikk, H. D. Fricke, A. C. Grant, and E. G. Ragi, August 1982.

17. Marto, P. J., and Wanniarachchi, A. S., "The Use of Wire-Wrapped Tubing to Enhance Steam Condensation in Tube Bundles," *Heat Transfer in Heat Rejection Systems*, HTD-Vol. 37, S. Sengupta and Y. Mussalli (Eds.), ASME, 1984.

18. Sethumadhavan, R., and Rao, M. R., "Condensation of Steam on Single Start and Multistart Spiral Wire-Wound Horizontal Tubes," *Ind. Eng. Chem. Process Des. Dev.*, Vol. 24, No. 3, pp. 783-787, 1985.

19. Rifert,V. G., "Steam Condensation on Profiled Surfaces," *Heat and Mass-Transfer Processes in Porous Media With Phase Transformation*, Academy of Science, BSSR, A. B. Lykov (Ed.), pp. 373-378, Minsk, 1982.

20. Rudy, T. M., and Webb, R. L., "An Analytical Model to Predict Condensate Retention on Horizontal, Integral-Fin Tubes," *Proceedings of the ASME-JSME Thermal Engineering Conference*, Vol. 1, pp. 373-378, Hawaii, 1983.

21. Rudy, T. M., and Webb, R. L., "An Analytical Model to Predict Condensation Retention on Horizontal Integral-Finned Tubes," *Journal of Heat Transfer*, Vol. 107, pp. 361-368, May 1985.

22. Masuda, H., and Rose, J. W., *Static Configuration of Liquid Films on Horizontal Tubes With Low Radial Fins: Implications for Condensation Heat Transfer*, paper to be published in Proceedings of the Royal Society, London.

23. Gregorig, R., "Hautkondesation an feingewellten Oberflachen bei Beerucksichtigung der Oberfdachenspannungen," *Zeitschrift fur angewandte Mathemetik und Physik*, Vol. V, 1954, pp. 36-48. Translated by D. K. Edwards.

24. Webb, R. L., Rudy, T. M., and Kedzierski, M. A., "Prediction of the Condensation Coefficient on Horizontal Integral-Fin Tubes," *Journal of Heat Transfer*, Vol. 107, pp. 369-376, May 1985.

25. Wanniarachchi, A. S., Marto, P. J., and Rose, J. W., "Film Condensation of Steam on Horizontal Finned Tubes: Effect of Fin Spacing," *Journal of Heat Transfer*, Vol. 108, pp. 960-966, November 1986.

26. Honda, H., and Nozu, S.,"A Prediction for Heat Transfer During Film Condensation on Horizontal Low Integral-Fin Tubes," *Fundamentals of Phase Change: Boiling and Condensation*, HTD-Vol. 38, pp. 107-114, C. T. Avedisian and T. M. Rudy (eds), ASME, 1984.

27. Honda, H., Nozu, S., and Uchima, B., "A Generalized Prediction Method for Heat Transfer During Film Condensation on a Horizontal Low Finned Tube," *Proceedings of the 1987 ASME-JSME Thermal Engineering Conference*, Vol. 4, pp. 385-392. Hawaii, 1987.

28. Murphy, T. J., M.S. Thesis, Naval Postgraduate School, Monterey, California, September 1987 (in preparation).

29. Krohn, R. L., *An Experimental Apparatus to Study Enhanced Condensaation Heat-Transfer of Steam on Horizontal Tubes*, M.S. Thesis, Naval Postgraduate School, Monterey, California, June, 1983.

30. Graber, K. A., *Condensation Heat Transfer of Steam on a Single Horizontal Tube*, M.S. Thesis, Naval Postgraduate School, Monterey, California, June 1983.

31. Lester, D., M.S. Thesis, Naval Postgraduate School, Monterey, California, September 1987 (in preparation).

32. Kline, S. J., and McClintok, F. A., "Describing Uncertainties in Single-Sample Experiments," *Mechanical Engineering*, Vol. 74, pp. 3-8, January, 1953

INITIAL DISTRIBUTION

		No. Copies
1.	Defense Technical Information Center Cameron Station Alexandria, Virginia 22304-6145	2
2.	Library, Code 0142 Naval Postgraduate School Monterey, California 93943-5002	2
3.	Chairman, Code 69He Mechanical Engineering Department Naval Postgraduate School Monterey, California 93943-5000	1
4.	Professor P. J. Marto, Code 69Mx Mechanical Engineering Department Naval Postgraduate School Monterey, California 93943-5000	5
5.	Professor A. S. Wanniarachchi, Code 69Wa Mechanical Engineering Department Naval Postgraduate School Monterey, California 93943-5000	5
6.	Professor John W. Rose Department of Mechanical Engineering Queen Mary College London E1 4NS England	1
7.	LCDR D. S. Zebrowski 4116 N. LeClaire Avenue Chicago, Illinois 60641	10
8.	Mr. R. Helmick, Code 2722 David W. Taylor Naval Ship Research and Development Center Annapolis, Maryland 21402	1

9. Mr. J. Sherman, Code 2759 — 1
David W. Taylor Naval Ship Research
and Development Center
Annapolis, Maryland 21402

10. Mr. B. Unkle, Navsea 56Y15 — 1
Naval Sea Systems Command
Washington, DC 20362-5101

11. Mr. A. Smookler, Navsea 05R32 — 1
Naval Sea Systems Command
Washington, DC 20362-5101

END

11-87

DTIC